

國立交通大學

光電工程研究所

博士論文

以分離式螢光粉波長轉換機制所形成的平面光源
之研究

**Study on Planar Lighting Systems Using Remote
Phosphor Wavelength Conversion**

研究生：黃信道

指導教授：蔡娟娟 教授

黃乙白 副教授

中華民國一〇〇年一月

以分離式螢光粉波長轉換機制所形成的平面光源
之研究

**Study on Planar Lighting Systems Using Remote
Phosphor Wavelength Conversion**

研究生: 黃信道

Student: Hsin-Tao Huang

指導教授: 蔡娟娟

Advisor: Dr. Chuang-Chuang Tsai

黃乙白

Dr. Yi-Pai Huang



國立交通大學 電機學院
光電工程研究所
博士論文

A Thesis

Submitted to Institute of Electro-Optical
Engineering National Chiao Tung
University

in partial Fulfillment of the
Requirements for the

Degree of

Doctorate of Philosophy

in

Electro-Optical Engineering

January 2011

Hsinchu, Taiwan, Republic of China



以分離式螢光粉波長轉換機制所形成的平面光源 之研究

博士研究生：黃信道

指導教授：蔡娟娟 教授
黃乙白 副教授

國立交通大學 光電工程研究所

摘 要

本論文研製之螢光粉波長轉換機制所形成的平面光源技術，主要專注於解決目前 LED 發光二極體做為平面光源應用時在光學與色彩表現上不均勻的問題，以及進一步提升發光模組的光學效益之研究。雖然 LED 光源具有綠色環保以及節能減碳之技術優勢，但因 LED 屬於點光源，故傳統 LED 在形成面光源之後，在發光效益、光源特性以及發光品質仍有待進一步的改善。因此關於本論文的研究，從 LED 發光二極體的螢光粉封裝進行研討，再深入至 LED 發光模組的研究，最後再將相關研究結論應用於雙面顯示之系統。研究中發展了一種新的"螢光粉沿晶塗佈(Conformal Phosphor Coating, CPC)技術"以及另一種"分離式螢光粉塗層(Remote Phosphor Coating, RPC)技術"，並分別以該兩種技術研究改善 LED 光源的顏色不均以及發光不均等問題，並進一步提升 LED 面光源模組的發光效率。

由本論文研究結果顯示，使用脈衝式的 CPC 技術，螢光粉可以沿著 LED 晶片外緣

形成一理想的螢光層塗層厚度，而有效降低了 LED 在不同視角之下的顏色不均勻問題，同時採用物理原理的脈衝式 CPC 技術又具有環保無化學污染的技術優勢。而採用 RPC 技術則具有高發光效益之特性，但該技術應用在平面光源模組之相關研究卻是非常稀少。研究結果顯示利用 RPC 技術經最佳化參數設計之後，可以兼具低色偏以及高發光效益之特性，同時 RPC 技術因為兼具波長轉換機制以及光擴散機制之二重效果，所以以 RPC 技術可以輕易的形成均勻發光之平面光源模組。研究結果顯示採用 RPC 技術的 TFT-LCD 背光源模組或是照明模組，其光學與色彩表現結果皆優於採用傳統白光 LED 的光源模組。

本論文除了研究以波長 457 nm 的藍光，激發分離式的黃色螢光粉塗層而形成平面光源之外，另採用波長 254 nm 的 UV 光源，激發 R/G/B 三色螢光粉混合塗層的平面光源技術。因為 UV LED 尚未發展成熟，本論文採用 UV CCFL 作為本研究的基礎光源。由於作為一次光源的 UV 光本身為不可見光，並不參與波長轉換之後的混光行為，當 R/G/B 螢光粉的激發頻譜經最佳化之後，以這樣的光源技術作為 TFT-LCD 背光源模組使用，可以達成高色彩飽和度之光學表現，同時並避免了混光不均所造成的色偏問題；若作為照明使用，又能達成高演色性的高品質光源需求。因為這樣的平面光源技術具有雙面對稱且均勻發光之光學特性，因此預期本技術所完成的雙面顯示系統將具有作為數位電子看板或是促進新應用之潛力。

本研究從 LED 元件的螢光粉封裝技術出發，再至 LED 發光模組的色彩分析與光學研究，最後結合熱傳模擬與熱輻射分析並應用於雙面顯示之數位電子看板系統。由樣品實測結果顯示，本研究具有低色偏、高發光效益且兼具薄型化之機構特性，同時又無化學污染等問題，因此本成果將完成一個新階段的 LED 光源系統之發展。

Study on Planar Lighting Systems Using Remote Phosphor Wavelength Conversion

Ph.D. student : Hsin-Tao Huang

Advisors : Dr. Chuang-Chuang Tsai
Dr. Yi-Pai Huang

Institute of Electro-Optical Engineering
National Chiao Tung University

ABSTRACT

This study investigates planar lighting that is based on remote phosphor conversion to solve the problems of color deviation, non-uniform light distribution and low luminance efficiency of LED lighting. The LED is an emerging solid state light source that could potentially replace traditional light sources, and the interest in the use of LEDs for general illumination has been rapidly increasing. The point-type lighting of LEDs demands a focus on illumination performance, and understanding of the features of uniformity, light distribution and efficiency when LEDs are used in planar lighting. Conventional white LEDs is not simultaneously satisfactory in all these respects. This study focuses on LED devices using "conformal phosphor coating, CPC" and LED lighting module using "remote phosphor coating, RPC" method. Eventually, a dual-sided display system was produced to realize the color and optics performance as compared to conventional planar lighting systems.

The results of this study reveal that the placement and arrangement of phosphors critically determine both the luminous efficiency and the color deviation. Since the phosphor in a conventional LED package is in contact with the LED die, a significant fraction of the

blue light is backscattered by the phosphor and lost by absorption by the LED chips. Additionally, the high temperature of an operating wLEDs causes thermal quenching, reducing the light radiation efficiency of the phosphor and InGaN blue LEDs. Therefore, the placing of phosphor remote to the LED chip has been explored to analyze the luminous efficiency and color deviation of lighting module.

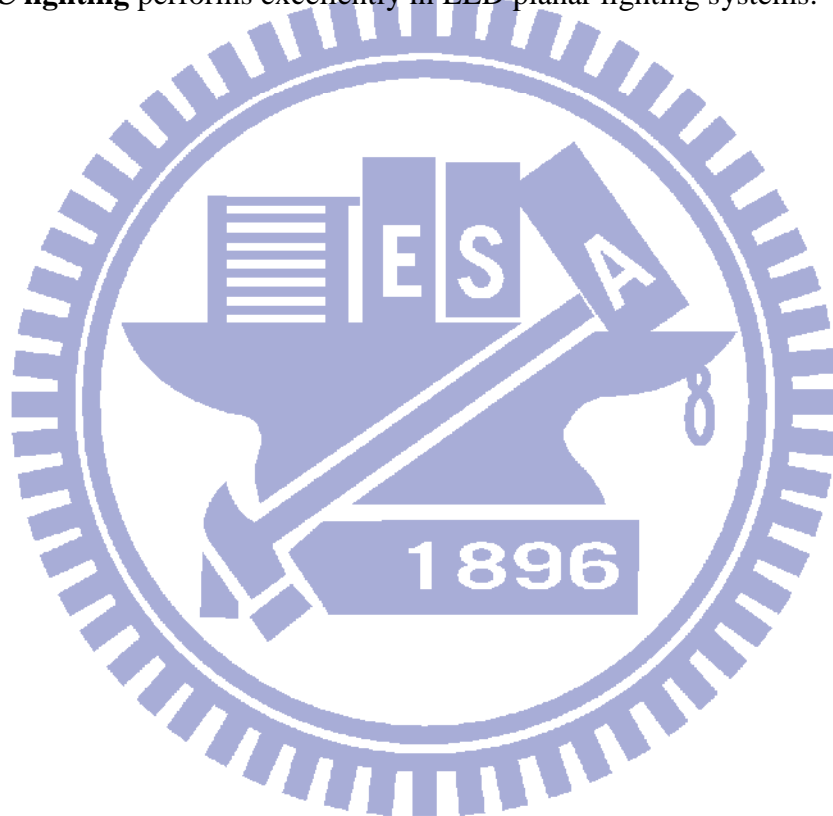
The study of CPC by the pulsed spray (PS) method to an array of blue LED devices is investigated. PS can yield a wide range of color temperatures (T_c) from 2500 K to 9500 K with high color accuracy. Unlike other coating approaches, PS is a mechanical spray-based, environmentally friendly method that does not produce harmful ionic pollution in chemical reactions.

In an investigation of RPC, a planar lighting module of blue LEDs was utilized to excite a yellow phosphor film. The phosphor film herein acts simultaneously as a wavelength converter and a light diffuser simultaneously. The proposed configuration yields a lower color deviation than a conventional wLEDs lighting system, and a uniform luminous distribution, from an ultra-slim structure. Most importantly, the configuration does not include a conventional diffuser plate or light guide plate (LGP). Accordingly, an RPC lighting system with excellent optical performance can be realized in a compact module.

Hence, an ultraviolet (UV)-excited flat lighting (UFL) system, comprising a RPC is examined. An R/G/B trichromatic RPC is excited using a 254 nm UV light to achieve high color rendering and high luminous backlighting in a slim TFT-LCD display. A UFL system provides symmetrical dual-sided illumination without conventional optical reflectors. Furthermore, UFL exploits the thermal radiation mechanism to release the large amount of heat that is produced by the illumination system, preventing thermal accumulation. These characteristics of the UFL scheme were studied and compared with those of conventional lighting. A dual-sided display based on UFL lighting has potential for use in digital signage or

public information displays, for example.

This present investigation provides clear evidence of the low color deviation of LED devices. The color analysis and optics of an LED lighting module are studied. The findings are important since they suggest that a dual-sided display system with thermal radiation was low color deviation, high luminous efficiency and a compact mechanism design. The RPC scheme is environmentally friendly that does not involve chemical reactions that generate pollution. **RPC lighting** performs excellently in LED planar lighting systems.



誌謝

真誠感恩生命中的貴人，我才能完成博士學業。

在交通大學的博士論文研究期間，最感謝指導教授蔡娟娟教授以及黃乙白博士在研究工作與論文撰寫上的指導；同時也感謝金益世公司(KISmart Corporation)包含簡學仁董事長、林澄鋒副董事長、簡偉隆總經理、張文吉副總經理以及其他同仁等等的體恤，方便我在工作中亦能兼顧學校的修課與研究的進行，使我能在三年半的時間內，順利完成四篇國際學術期刊論文(SCI)、十篇國際研討會議論文(Oral Presentation Paper)的發表以及最後的博士論文。

在工作十年之後選擇再攻讀博士學位，真的是一個很大的挑戰，感謝自己的雙親黃錦雲先生與許月華女士默默的支持著我，更感謝我的另一半香嬪無怨無悔的支撐著家，讓我在工作、家庭與學業的多方煎熬當中，仍能讓兩個寶貝兒子和田與和闖幸福成長，我的岳父、岳母吳榮華先生與吳曾淑英女士也不時的鼓勵著我，因為擁有這麼多親人的愛，我才能有足夠的意志熬到今天。

同時，口試委員紀國鐘教授、謝漢萍教授、郭浩中教授、電控系趙昌博教授、中興大學材料系武東星教授、台大光電所黃建璋教授以及中央大學光電系張正陽教授在論文口試時的指正，讓我的論文邏輯更加完整。另外，台灣禪宗佛教會的師兄師姐們在精神上的鼓勵，以及悟覺妙天師父的身心靈引導，讓我能在千頭萬緒的研究中，看見一線金光乍現，精神專注如山，靈感如山泉般湧至。而前瞻光學實驗室的建翔、博文、智清等也在我的研究上給予我很多的協助。再次，我發自內心真誠的感謝。

陳之藩先生說：要謝的人太多，就謝天吧！而我，卻要跟生命中所有的貴人一一真誠感恩、道謝！

Table of Contents

摘要	iii
Abstract	v
致謝	viii
Table of Contents.....	ix
List of Tables.....	xii
Figure Caption.....	xiii

Chapter 1

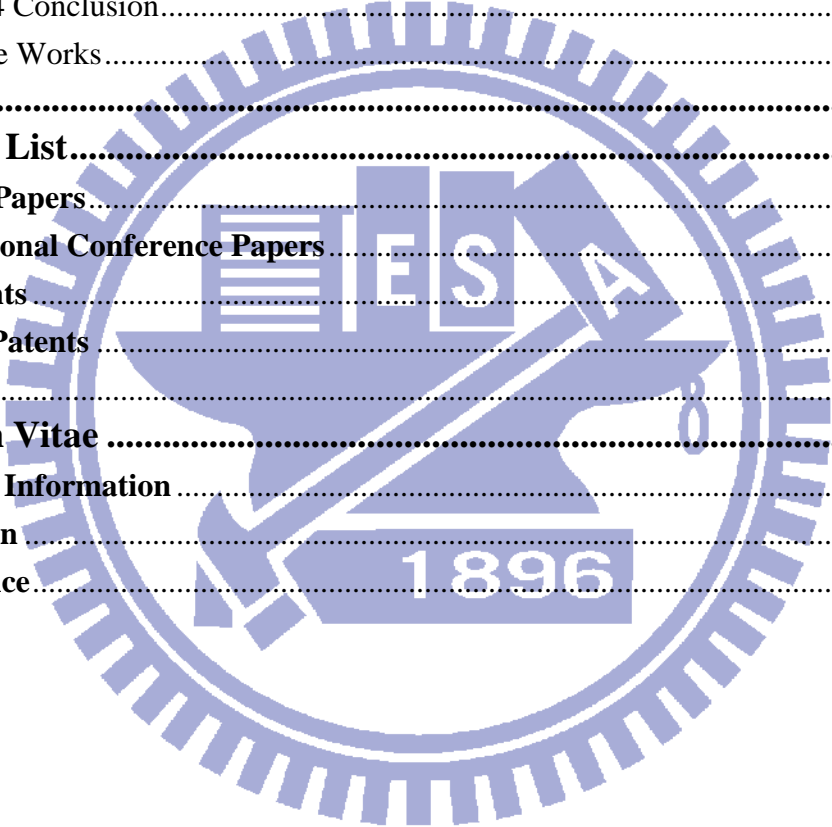
Introduction	1
1.1 Preface	1
1.2 Issues of Current wLEDs Phosphor Distribution.....	4
1.2.1 Conformal Phosphor Coating.....	5
1.2.2 Remote Phosphor Coating.....	7
1.3 Motivation and Objectives	11
1.4 Organization of This Thesis	13

Chapter 2

Theoretical Backgrounds.....	16
2.1 Radiometry and Photometry.....	16
2.1.1 Spectral Power Distribution	18
2.1.2 Eye Sensitivity Functions.....	19
2.1.3 Solid Angle.....	20
2.1.4 Luminous Intensity.....	21
2.1.5 Luminous Flux	21
2.1.6 Luminance.....	21
2.1.7 Illuminance.....	22
2.1.8 Lambert's Cosine Law and Lambertian Surface	22
2.2 Ray Tracing	23
2.2.1 Law of Refraction (Snell's Law)	23
2.2.2 Law of Reflection.....	24
2.2.3 Fresnel's Equations.....	24
2.3 Bidirectional scattering distribution functions (BSDFs).....	25
2.4 Light and Vision.....	28
2.4.1 Full-width at half-maximum (FWHM)	28
2.4.2 Glare	29
2.4.3 Haze.....	29
2.4.4 Mura	30
2.5 Colorimetry and CIE Chromaticity Diagram	31

2.5.1 Tristimulus Values	32
2.5.2 CIE Chromaticity Coordinates	33
2.5.3 Color Difference.....	35
2.5.4 Color Temperature	36
2.5.5 Correlated Color Temperature	37
2.5.6 Color Saturation	39
2.5.7 Color Rendering Index	41
Chapter 3	
Experimental Details.....	44
3.1 Phosphor.....	44
3.2 Remote Phosphor Converter.....	47
3.3 Optical Materials.....	49
3.4 Experiment Process.....	50
Chapter 4	
Low Color Deviation LED Devices using Conformal Phosphor Coating....	52
4.1 Why Conformal Phosphor.....	52
4.2 Color Distribution Analysis	53
4.3 Color Temperature Range	55
4.4 Environmental Influence.....	57
4.5 Summary	59
Chapter 5	
High Efficiency LED Lighting Module using Remote Phosphor Scheme ...	60
5.1 Why Remote Phosphor.....	60
5.2 Sample Preparation	61
5.3 RPC Light-emission Measurement	63
5.4 Theoretical Modeling	65
5.5 Optimized Configuration and Luminous Uniformity.....	68
5.6 Color Temperature	69
5.7 Angular Color Deviation.....	72
5.8 Summary	74
Chapter 6	
Ultra Slim Dual-sided Display System using UV-excited Fluorescent	
Lighting (UFL).....	76
6.1 Why Dual-sided Display	76
6.2 What UV-excited Flat Lighting (UFL)	77
6.3 Experimental Indices Definition	78
6.4 Sample Preparation	80
6.5 Luminous Uniformity Analysis.....	81

6.6 Dual-sided Displays	83
6.7 Thermal Releasing Analysis.....	86
6.8 Summary	89
Chapter 7	
Conclusion and Future Works	90
7.1 Conclusion.....	90
7.1.1 Part I: LED Devices	90
7.1.2 Part II: LED Lighting Module.....	91
7.1.3 Part III: Dual-sided Display System.....	95
7.1.4 Conclusion.....	97
7.2 Future Works.....	100
References	105
Publication List.....	114
Journal Papers.....	114
International Conference Papers.....	114
US Patents	115
Taiwan Patents	116
Awards.....	117
Curriculum Vitae	118
Personal Information	118
Education	118
Experience.....	118



LIST OF TABLES

TABLE 1-1 COMPARISON OF DIFFERENT BL SYSTEMS.....	10
TABLE 2-1 SI PHOTOMETRY UNITS.....	18
TABLE 3-1 OPTICAL CHARACTERISTICS OF RPC.	48
TABLE 4-1. OPTICAL COMPARISON BETWEEN CONVENTIONAL DISPENSING AND CPC BY PS ^A	55
TABLE 5-1 OPTICAL COMPARISON BETWEEN CONVENTIONAL LIGHTING AND RPC LIGHTING. ^{A,B}	74
TABLE 6-1 THE COMPARISON OF DIFFERENT DUAL-SIDED DISPLAY.	84
TABLE 6-2 COMPARISON OF MEASURED TEMPERATURE OF CONVENTIONAL SINGLE-SIDED DISPLAY WITH UFL UFL DUAL-SIDED DISPLAY. ^A	88
TABLE 7-1 THE EFFICIENCY PREDICTION OF RPC BACKLIGHTING.	104

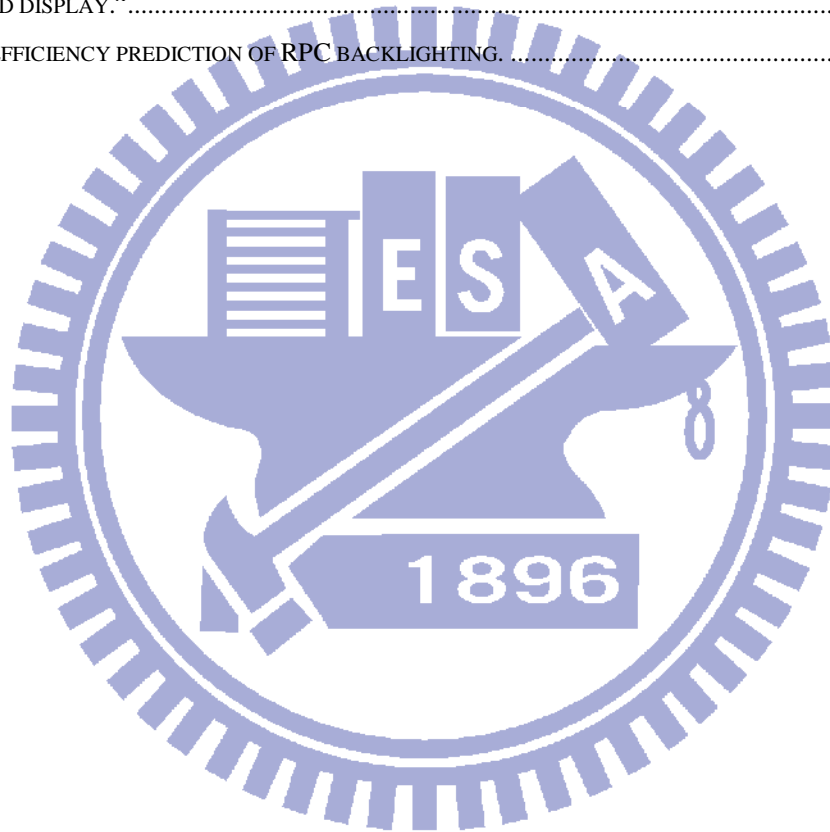


FIGURE CAPTION

FIG. 1-1 TFT-LCD DISPLAYS ARE BECOMING THE MAIN CHOICE FOR GREAT DIVERSITY NEW APPLICATIONS.....	1
FIG. 1-2 FOURTH GENERATION OF THE FPD INDUSTRY.....	2
FIG. 1-3 THE PROPOSED REMOTE PHOSPHOR CONVERTER (RPC) LIGHTING SYSTEM IN THIS DISSERTATION.....	3
FIG. 1-4 A NEW GROWTH APPLICATIONS OF DUAL-SIDED DISPLAY IN PRIVATE OR PUBLIC SCENES.	4
FIG. 1-5 PHOSPHOR PLACEMENTS IN LED. (A) PROXIMATE PHOSPHOR DISTRIBUTION BY CONVENTIONAL DISPENSING. (B) PROXIMATE CONFORMAL PHOSPHOR DISTRIBUTION. (C) REMOTE PHOSPHOR DISTRIBUTION [39].	5
FIG. 1-6 SCHEMATIC DIAGRAM OF THE SLURRY COATING PROCESS [44].	6
FIG. 1-7 CCT VS. VIEWING ANGLE FOR LEDs WITH CONFORMAL PHOSPHOR LAYER SHOWING IMPROVEMENT IN UNIFORMITY COMPARED TO TRADITIONAL WHITE LED [41].	7
FIG. 1-8 (A) UNIFORM DISTRIBUTION OF THIN LAYER ABOVE LED CHIPS (REMOTE PHOSPHOR). (B) REMOTE PHOSPHOR DISTRIBUTION IN DIFFUSE REFLECTOR [49].	8
FIG. 1-9 COMPARED WITH TYPICAL WLEDs LIGHTING, REMOTE PHOSPHOR REVEALS HIGHER LIGHT OUTPUT AND EFFICACY [53].	8
FIG. 1-10 CROSS-SECTIONAL VIEWS OF SEVERAL PCLED PACKAGES. (A) CONFORMAL PHOSPHOR COATING; (B) REMOTE PHOSPHOR WITH SCATTERED PHOTON EXTRACTION; (C) REMOTE PHOSPHOR WITH HEMISPHERICAL DOME; AND (D) ELIXIR [50].	9
FIG. 1-11 AMBIENT TEMPERATURE DEPENDENCE OF RELATIVE RADIANT EFFICIENCY OF YAG PHOSPHOR AND INGAN BLUE LED [52].	10
FIG. 1-12 THREE PARTS IN THIS THESIS.	11
FIG. 1-13 THE ORGANIZATION OF THIS INVESTIGATION.	13
FIG. 2-1 WAVELENGTHS OF ELECTROMAGNETIC RADIATION AND LIGHT [2].	16
FIG. 2-2 DEFINITION OF RADIOMETRIC AND PHOTOMETRIC QUANTITIES [3].	17
FIG. 2-3 EXAMPLE OF A TYPICAL SPECTRAL POWER DISTRIBUTION (SPD) [6].	18
FIG. 2-4 EYE SENSITIVITY FUNCTION OF TWO TYPES OF VISION CAN BE DESCRIBED BY PHOTOPIC AND SCOTOPIC RESPONSE CURVES [3].	20
FIG. 2-5 THE DEFINITION OF SOLID ANGLE [7].	20
FIG. 2-6 LAMBERT'S COSINE LAW [7-8].	22
FIG. 2-7 LAMBERTIAN SURFACE [7-8].	22
FIG. 2-8 BSDFs IS A SUPERSET AND THE GENERALIZATION OF THE BTDFs AND BRDFs [15].	26
FIG. 2-9 SCHEMATIC MEASUREMENT SETUP OF BSDFs [13].	26
FIG. 2-10 PHOTOMETRIC AND GEOMETRIC QUANTITIES IN THE SPHERICAL COORDINATE SYSTEM [16].	27
FIG. 2-11 FUALL WIDTH AT HALF MAXIMUM (FWHM) [17].	28
FIG. 2-12 THE CONFIGURATION OF HAZE MEASUREMENT.	30
FIG. 2-13 THE MEASURED POINT OF LIGHT DISTRIBUTION UNIFORMITY.	31
FIG. 2-14 CIE 1931 COLOR MATCHING FUNCTIONS [20].	32
FIG. 2-15 COMPUTATION PROCEDURE OF TRISTIMULUS XYZ [3].	33

FIG. 2-16 CIE 1931 (x,y) CHROMATICITY DIAGRAM. MONOCHROMATIC COLORS ARE LOCATED ON THE PERIMETER AND WHITE LIGHT IS LOCATED IN THE CENTER OF THE DIAGRAM [22].	34
FIG. 2-17 CIE 1976 (u',v') UNIFORM CHROMATICITY DIAGRAM CALCULATED USING THE CIE 1931 (2° STANDARD OBSERVER). THE CHROMATICITY DIFFERENCE IS DIRECTLY PROPORTIONAL TO THE GEOMETRIC DISTANCE [22].	35
FIG. 2-18 COLOR TEMPERATURE CHART OF GENERAL LIGHT SOURCES [23].	37
FIG. 2-19 PLANCKIAN LOCUS (THICK LINE) AND ISO-TEMPERATURE LINES (FINE LINES) [3].	38
FIG. 2-20 SPECTRAL PROPERTIES OF THE CCFL LIGHTING VERSUS RGB-LED LIGHTING WHEN MATCHING WITH THE SPECTRAL TRANSMITTANCE FACTOR OF COLOR FILTER [25].	39
FIG. 2-21 THE TRIANGLE IS THE GAMUT AVAILABLE TO A TYPICAL COMPUTER MONITOR, IT DOES NOT COVER THE ENTIRE SPACE. THE CORNERS OF THE TRIANGLE ARE THE PRIMARY COLORS FOR THIS GAMUT [30].	40
FIG. 2-22 THE HIGHER CRI PROVIDES RICHER AND FULLER LOOKING SURFACES, MERCHANDISE AND FOOD [38].	41
FIG. 2-23 CIE TEST COLOR SAMPLES USED TO CALCULATE THE GENERAL COLOR RENDERING INDEX (RA) (CIE 13.3 -1995) [22].	42
FIG. 2-24 CIE TEST COLOR SAMPLES USED TO CALCULATE THE SPECIAL COLOR RENDERING INDICES CRI ₉ -CRI ₁₄ [22].	43
FIG. 3-1 (A) YAG PHOSPHOR POWDER [124]. (B) SEM MORPHOLOGY OF YAG:Ce ³⁺ PHOSPHOR. (C) THE SIZE DISTRIBUTION OF PHOSPHOR PARTICLES. (D) THE SPECTRAL PROPERTIES OF THE BLUE EXCITATION AND YELLOW EMISSION. (E) BLUE LIGHT EXCITATION.	45
FIG. 3-2 THE SPECTRAL PROPERTIES OF THE PHOSPHOR VERSUS THE SPECTRAL TRANSMITTANCE FACTOR OF CF (PHOSPHOR PHOTO CITED FROM [124]).	46
FIG. 3-3 THE SCHEME OF COATING PROCESS IN THIS RESEARCH.	47
FIG. 3-4 (A) THE REMOTE PHOSPHOR CONVERTER (RPC); (B) THE COATED PET FILMS WITH TRICHROMATIC PHOSPHOR.	48
FIG. 3-5 VIEWS OF YAG PHOSPHOR FILM. (A) APPEARANCE. (B) SEM MICROGRAPH.	48
FIG. 3-6 THE SCHEME REVEALS THE EFFECTIVE FUNCTION OF BEF AND PCF MATERIALS [67].	49
FIG. 3-7 MECHANICAL STRUCTURE OF PULSED-SPRAY COATER.	50
FIG. 3-8 SCHEMATICALLY DEPICTS THE SIMPLIFIED PROCESS OF SLOT-DIE COATING.	51
FIG. 3-9 MECHANICAL STRUCTURE OF SLOT-DIE COATER.	51
FIG. 4-1 PHOSPHOR COATING USING PS SCHEME. (A) AN ARRAY OF BLUE LED CHIPS ON BOARD (COB); (B) THE MAGNIFICATION OF INDIVIDUAL LED.	53
FIG. 4-2 CIE 1976 CHROMATICITY INDICES VERSUS ANGULAR DISTRIBUTION OF LED WHEN THE LIGHT IS EMITTED AT ANGLES FROM -60° TO +60°. (A) CONVENTIONAL DISPENSING; (B) CONFORMAL COATING USING PS.	54
FIG. 4-3 RELATIONSHIP BETWEEN PHOSPHOR LOADING (MG/CM ²) AND COLOR TEMPERATURE (TC).	55
FIG. 4-4 CIE 1931 CHROMATICITY INDICES VERSUS ANGULAR DISTRIBUTION OF LED AT Tc CENTRE AROUND 9500 K. (A) CONVENTIONAL DISPENSING; (B) CONFORMAL COATING USING PS.	56
FIG. 4-5 (A) CONOSCOPIC MEASURED POINT AND RANGE FROM +60° ~ 0° ~ -60°. (B) COLOR TEMPERATURE (TC)-ANGULAR DISTRIBUTION.	56

FIG. 4-6 THE CIE 1931 CHROMATICITY DIAGRAM. RED TRIANGLE DENOTES THE WHITE POINT WITH DIFFERENT COLOR TEMPERATURE (TC).	57
FIG. 4-7 SEM MICROGRAPHS OF PHOSPHOR COATING USING PS. (A) TOP VIEW; (B) CROSS-SECTIONAL VIEW; (C) ILLUMINATED LIGHTING MODULE WITH PHOSPHOR COATED BY PS.	58
FIG. 5-1 SCHEMATICALLY DEPICTS THE PACKING METHOD OF LED. (A) THE PACKAGE OF DISPENSING PHOSPHOR; (B) THE PACKAGE OF REMOTE PHOSPHOR.	61
FIG. 5-2 THE PROPOSED LIGHT-EMISSION SYSTEM CONSTRUCTED BY RPC.	61
FIG. 5-3 THE SEM PICTURE OF THE PLASTIC SUBSTRATE WITH MICRO LINE LENTICULAR (MLL) ARRAYS. (PITCH: 80 μm , HEIGHT: 80 μm).	62
FIG. 5-4 (A) THE LIGHTING MODULE INTEGRATES AN ARRAY OF BLUE LEDs WITH YAG RPC LAYER; (B) THE OBVERSE VIEW OF RPC COUPLED WITH TWO SHEETS OF MICRO LINE LENTICULAR (MLL) ARRAY (ARROW MARKED THE STRUCTURAL DIRECTION ON MLL).	63
FIG. 5-5 MEASURED BTDFs RESULT OF (A) DIFFUSED BLUE LIGHT, (B) UP CONVERTED YELLOW LIGHT; (C) LIGHT-EMITTING MECHANISM OF RPC LIGHTING SYSTEM; MEASURED BRDFs RESULT OF (D) REFLECTED BLUE LIGHT, (E) DOWN CONVERTED YELLOW LIGHT.	64
FIG. 5-6 THE COMPARISON OF LUMINANCE IN ANGULAR DISTRIBUTION, BETWEEN CONVENTIONAL LIGHTING AND RPC LIGHTING.	65
FIG. 5-7 THE DEFINITION OF PHOTOMETRIC IN THIS THEORETICAL CALCULATION.	66
FIG. 5-8 THE COMPARISON OF LUMINOUS UNIFORMITY (U_{PL}) WITH (H/P) RATIO.	68
FIG. 5-9 THE COMPARISON OF LUMINOUS UNIFORMITY (U_{PL}) AT (H)= 5 MM AND (P)= 12 MM. (A) CONVENTIONAL WLEDs LIGHTING, (B) RPC LIGHTING INTEGRATED WITH MLL SHEETS.	69
FIG. 5-10 THE CIE 1931 CHROMATICITY DIAGRAM. RED CROSS-MARK DENOTES THE WHITE POINT WITH DIFFERENT COLOR TEMPERATURE (TC).	70
FIG. 5-11 RELATIONSHIP BETWEEN TC AND (A) PHOSPHOR THICKNESS, (B) LED DRIVING CURRENT, (C) LED GAP. (D) THE RELATIONSHIP OF LUMINOUS FLUX WITH LED GAP.	71
FIG. 5-12 (A) THE MEASUREMENT OF OPTICAL CHARACTERISTICS BY CONOSCOPIC APPROACH. THE COLOR DISTRIBUTION OF (B) CONVENTIONAL WLEDs LIGHTING SYSTEM, (C) RPC LIGHTING SYSTEM WHEN VIEW ANGLE VARIES FROM $\theta=0^\circ$ TO $\theta=60^\circ$ AT FIXED $\phi=0^\circ$. (D) THE SPECTRAL PROPERTIES OF BOTH CONVENTIONAL AND RPC LIGHTING AT VIEW POINT OF $\theta=0^\circ$, $\phi=0^\circ$. THE SPECTRAL PROPERTIES OF (E) CONVENTIONAL WLEDs LIGHTING SYSTEM, (F) RPC LIGHTING SYSTEM AT $\theta=60^\circ$, $\phi=0^\circ$.	73
FIG. 6-1 DUAL-SIDED APPLICATION CONSTRUCTED BY (A) A CONVENTIONAL PAIR OF SINGLE-SIDED DISPLAY APPLIED BACK-TO-BACK; (B) UFL DUAL-SIDED DISPLAY.	77
FIG. 6-2 SCHEMATIC RELATIONS BETWEEN THE INCLUDED ANGLE (Δ) AND LUMINOUS DISTRIBUTION IN THE ENTIRE ILLUMINATION AREA.	79
FIG. 6-3 THE RELATIONSHIP BETWEEN (Δ) AND (U_{PL}) ACCORDING TO UFL AND CONVENTIONAL DIRECT-EMISSION BL SYSTEM.	79
FIG. 6-4 (A) MEASUREMENT CONSTRUCTION OF ANGULAR-LUMINANCE DISTRIBUTION. (B) & (C): RAY TRACING AND LUMINOUS DISTRIBUTION OF FLs DUAL-SIDED ILLUMINATION. (D) & (E): RAY TRACING AND LUMINOUS	

DISTRIBUTION OF UFL ILLUMINATION.	81
FIG. 6-5 THE LUMINOUS UNIFORMITY SIMULATION RESULT.	82
FIG. 6-6 THE BL LUMINANCE IN SPATIAL DISTRIBUTION, RAY TRACING AND LUMINOUS UNIFORMITY OF THE EXPERIMENTAL SAMPLES AT $\Delta= 135^\circ$, $I= 6.5$ MA. (A), (B) AND (C) REPRESENT CONVENTIONAL DIRECT-EMISSION BL; (D), (E) AND (F) REPRESENT UFL BL.	83
FIG. 6-7 LUMINOUS DISTRIBUTION OF DUAL-SIDED ILLUMINATION (A) FLS LIGHTING; (B) UFL LIGHTING, (C) UFL FRONT VIEW, (D) UFL BACK VIEW.	85
FIG. 6-8 ULTRA-SLIM DUAL-SIDED BACKLIGHTING MODULE (28.8 MM THICKNESS).	86
FIG. 6-9 THERMAL SIMULATION BY FLOTHERM [®]	87
FIG. 6-10 THERMAL DISTRIBUTION MEASUREMENT BY FLOTHERM [®] REGARDING (A) FLS DUAL-SIDED BL; (B) UFL DUAL-SIDED BL.	88
FIG. 7-1 CONFORMAL COATING TECHNOLOGY COMPARISON.	91
FIG. 7-2 CORRELATIONS BETWEEN LIGHTING MODULE THICKNESS AND LUMINOUS EFFICIENCY IN DIFFERENT PLANAR LIGHTING MODULES.	92
FIG. 7-7 ULTRA-SLIM DUAL-SIDED DISPLAY SYSTEM USING UFL LIGHTING BY RPC SCHEME.	95
FIG. 7-8 INEFFECTIVE APPLICATIONS OF TWO CONVENTIONAL SETS OF SINGLE-SIDED LCDS INSTALLED BACK-TO-BACK.	95
FIG. 7-9 DUAL-SIDED LIGHTING TECHNOLOGY COMPARISON.	96
FIG. 7-13 THE ACCOMPLISHMENT OF OBJECTIVES IN THIS INVESTIGATION.	99
FIG. 7-14 THE APPLICATIONS MEET THE REQUIREMENT OF ASYMMETRY DUAL-SIDED DISPLAY.	100
FIG. 7-15 THE ENVIRONMENTAL ILLUMINATION AFFECTS THE DEMAND OF DISPLAY LUMINANCE.	101
FIG. 7-16 THE FUTURE WORKS OF RPC SCHEME IN DUAL-SIDED DISPLAY SYSTEM. FROM PICTURE (A) TO (B), IT ILLUSTRATES THE CURRENT ACCOMPLISHMENT; WHEREAS, FROM PICTURE (B) TO (C) TO (D), THESE SUGGEST PROPOSAL OF ASYMMETRY ILLUMINATION AND BLUE LED LIGHT SOURCE IN FUTURE WORKS.	101
FIG. 7-17 TO VERIFY THE COLOR VARIATION OF RPC SCHEME USING TFT-LCD DISPLAY SYSTEM WITH LOCAL DIMMING FUNCTION. (A) SMALL AREA ON PATTERN, AND (B) SMALL AREA DIMMING PATTERN.	102
FIG. 7-18 THE PROPOSAL OF RPC SCHEME ASSOCIATED WITH COLOR FILTER LESS TO INCREASE LUMINANCE EFFICIENCY. (A) CONVENTIONAL TFT-LCD MODULE; (B) PHILIPS PRESENTATION; (C) NCTU PROPOSAL (PARTLY INFORMATION CITED FROM [122]).....	103
FIG. 7-19 EVOLUTION OF LUMINOUS EFFICACY PERFORMANCE OF WHITE LIGHT SOURCES. COMMERCIALY AVAILABLE HIGH-POWER LED PERFORMANCE IS INDICATED BY THE POINTS ALONG THE SOLID BLUE CURVE. THE U.S. DEPARTMENT OF ENERGY (DOE) PROJECTIONS IS INDICATED BY THE DASHED PURPLE LINE [125]. THE EFFICIENCY PREDICTION OF RPC BACKLIGHTING IN THIS INVESTIGATION IS INDICATED BY BACK DASH LINE.	104

Chapter 1

Introduction

1.1 Preface

This investigation considers a compact lighting module with a uniform and planar distribution of bright light for use in TFT-LCD backlighting applications. LCD displays are rapidly becoming the technology of choice for a wide range of new applications [Fig. 1-1], including outdoor advertising, electrical signage and displays that can be read in the sunlight. As Fig. 1-2 shows, these new applications of flat panel display (FPD) following the Third generation of LCD represent the Fourth generation of the FPD industry.



Fig. 1-1 TFT-LCD displays are becoming the main choice for great diversity new applications.

Backlighting requires high brightness, a uniform light distribution and accurate color distribution through the display area. A conventional lighting module that is constructed from

fluorescent tubes or solid-state light emitting diodes (LEDs) as light source converts electrical energy into light, but does not satisfy the optical, color, efficient and mechanical requirements of future displays. This investigation seeks to address this issue by developing a novel optical mechanism of a planar light radiation system from a compact device that satisfies the requirements of display with significantly improved efficiency, uniformity, and thermal characteristics over those of a conventional backlighting system.

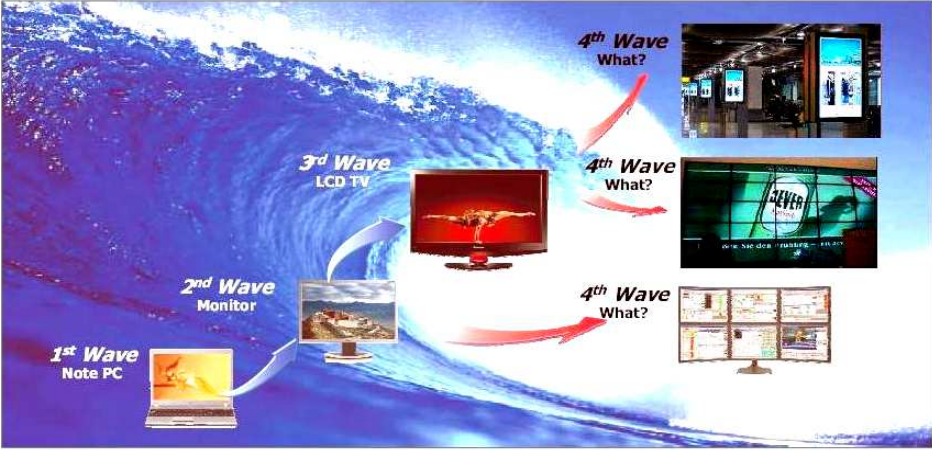


Fig. 1-2 Fourth generation of the FPD industry.

In particular, since the development of planar lighting, LEDs are being used more as TFT-LCD backlights or for general lighting. LEDs have the potential to reduce pollution considerably, save energy, save financial resources, and add functions to various applications. However, point-typed LEDs are difficult to achieve a uniform and planar illumination [1]. This investigation develops a novel lighting system that uses an array of blue LEDs to excite a yellow phosphor remotely, yielding a high luminous efficiency with uniform and planar light emission. Herein, the remote phosphor simultaneously acts as a wavelength converter and a light diffuser. The optical properties of the proposed lighting system, the angular color deviation, the locations of the phosphor and the light-emitting uniformity, are explored. A thin lighting module with high light-emitting uniformity but without a conventional diffuser plate or light guiding plate (LGP) is demonstrated. A low color deviation was achieved.

Accordingly, the proposed lighting system offers superior optical performance using a compact module [Fig. 1-3].

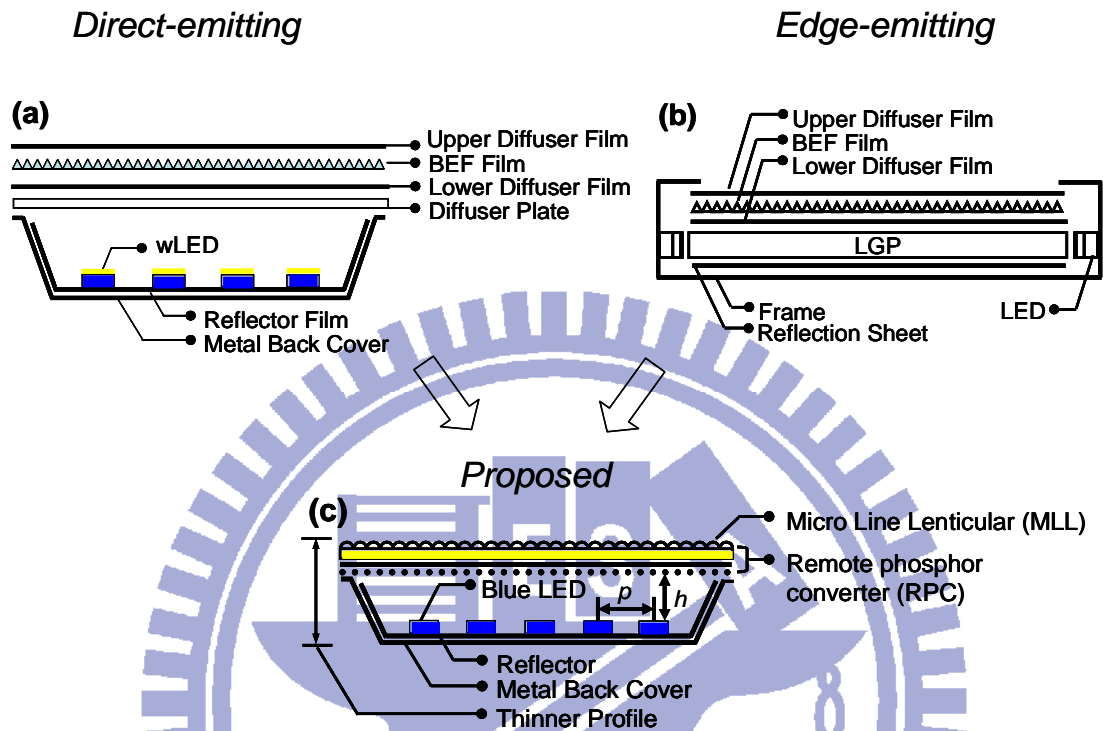


Fig. 1-3 The proposed remote phosphor converter (RPC) lighting system in this dissertation.

In addition, planar lighting system using the UV-excited flat lighting (UFL) approach is investigated herein. It involves the use of a remote phosphor film to convert the wavelength of ultraviolet light to visible light, and has high brightness as well as planar and uniform illumination. In particular, a compact UFL system with low power consumption that provides symmetrical dual-sided illumination is developed. Since future display applications will be very diverse, including digital signage and public information displays, they cannot all be based on single-sided LCD. These characteristics of the UFL approach motivate new-aged applications in TFT-LCD backlighting [Fig. 1-4]. For instance, dual-sided displays can add value to public spaces by enabling two displays to be operated simultaneously.



Fig. 1-4 A new growth applications of dual-sided display in private or public scenes.

1.2 Issues of Current wLEDs Phosphor Distribution

The LED is an emerging solid state light source that has the potential to replace traditional light sources, and interest in the use of LEDs for TFT-LCD backlighting and general illumination has been rapidly increasing. However, in conventional phosphor-based wLEDs, the phosphor absorbs the short-wavelength emission from the primary LED chip and down-converts it to a longer-wavelength emission. For example, the phosphor-based wLED uses herein a blue GaInN LED that pumped a YAG:Ce³⁺ yellow phosphor. The phosphor density and thickness are selected to transmit only a fraction of the blue light. The mixing of yellow phosphorescence with the blue electroluminescence produces white light. The amount, density and distribution of phosphor inside LED packages are varied to optimize the color-rendering characteristics and the device efficiency [39].

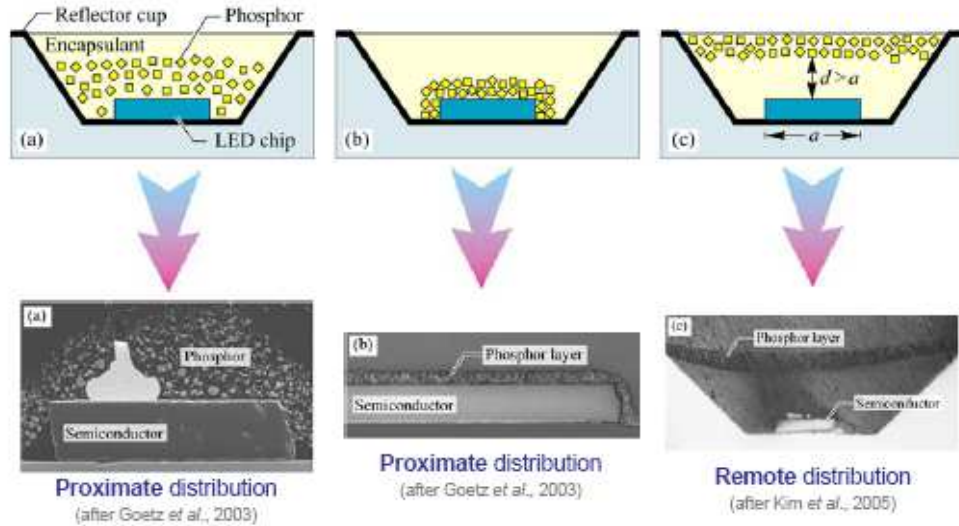


Fig. 1-5 Phosphor placements in LED. (a) Proximate phosphor distribution by conventional dispensing. (b) Proximate conformal phosphor distribution. (c) Remote phosphor distribution [39].

Since the phosphor is close to the LED die in the wLEDs package, a significant fraction of the blue light is backscattered by the phosphor and then absorbed by the LED chips. Additionally, the high temperature of an operating wLEDs causes thermal quenching, which reduces the light radiation efficiency of the YAG phosphor and the InGaN blue LEDs. Hence, this investigation studies distribution of phosphor in the LED package. When phosphor is separated from the LED chip surface, it is said to be remotely distribution [Fig. 1-5 (c)], but when the phosphor is close to the LED chip surface, it said to be proximately distribution [Fig. 1-5 (a) & (b)].

1.2.1 Conformal Phosphor Coating

The placement and arrangement of phosphors are critical for both the luminous source efficiency and color rendering index of the wLEDs. Typical arrangements of phosphor in wLEDs are shown in Fig. 1-5. The conventional wLEDs are fabricated by dispensing the phosphor into epoxy within a reflector cup [Fig. 1-5(a)]. For this process, it is difficult to control the uniformity of the phosphor distribution and result in color variation for different

view angles. Figure 1-5(b) shows another phosphor distribution, in which the phosphor layer conformally coats the LED chip [40- 48]. In this case, the color variation at different viewing angles is reduced dramatically due to the thickness uniformity of the phosphor layer, which provides the blue emission with an equal optical path length in the phosphor material, independent of the emission direction.

In order to coat the yellow phosphor on a GaInN chip conformally, several methods such as slurry, settling and electrophoretic deposition can be available, and the slurry coating scheme is most often employed for reasons of coating efficiency and uniformity [Fig. 1-6]. The slurry method is widely used for manufacturing luminescent phosphor screens of color cathode ray tubes (CRTs). It is based on a phosphor suspension in a water-soluble photoresist, dichromated polyvinyl alcohol (PVA), or other photosensitive emulsions. When phosphor slurry was under exposure, photochemical reactions occur and result in cross-linking in the photoresist. Then the slurry was developed with water to obtain the patterns required [44].

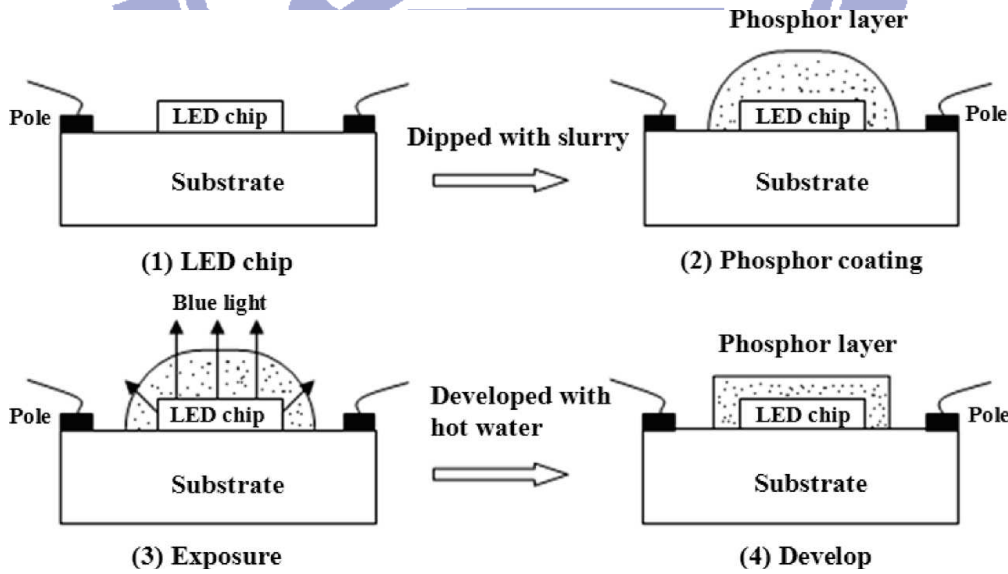


Fig. 1-6 Schematic diagram of the slurry coating process [44].

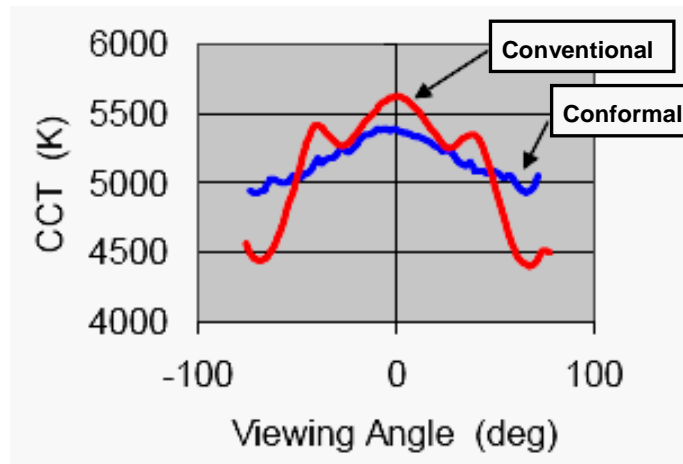


Fig. 1-7 CCT vs. viewing angle for LEDs with conformal phosphor layer showing improvement in uniformity compared to traditional white LED [41].

The uniformity of conformal phosphor layer results in higher color uniformity of the LEDs when compared with the conventional dispensing method. A comparison of CCT as a function of viewing angle is shown in [Fig. 1-7].

For both dispensing and conformal phosphor distributions, phosphors are closely distributed around the LED chip. Because the phosphorescence emission is isotropic, a large portion of the light emitted from phosphor directly impinges on the LED chip. The contacts and bonding metals of the LED chip are absorptive at the phosphorescence wavelength.

1.2.2 Remote Phosphor Coating

Placing the phosphor layer at a sufficiently large distance from the LED chip, as shown in [Fig. 1-5(c)], reduces the probability of the phosphorescence directly hitting the chip. The phosphor forms a uniform layer on the top of the reflector cup, which we refer to as remote phosphor. The thickness of the remote phosphor can be well controlled, which results in varying color temperature [49- 62]. In addition, the separation of phosphor from the LED chip reduces the effect of thermal quenching, which in turn is expected to improve the LED efficiency, reliability and lifetime.

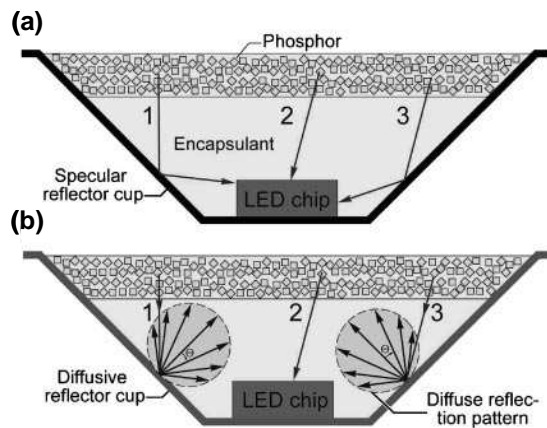


Fig. 1-8 (a) Uniform distribution of thin layer above LED chips (remote phosphor). (b) Remote phosphor distribution in diffuse reflector [49].

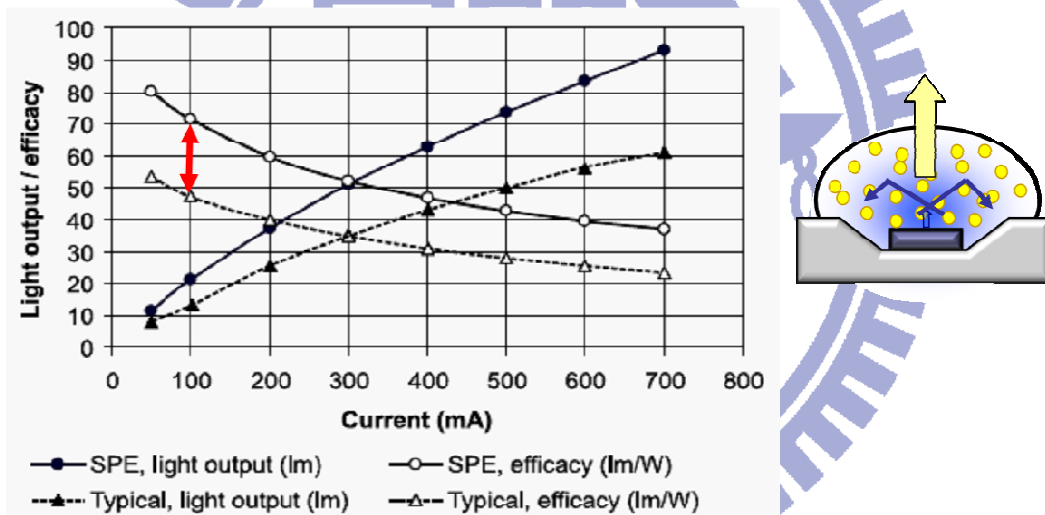


Fig. 1-9 Compared with typical wLEDs lighting, remote phosphor reveals higher light output and efficacy [53].

Figure 1-8 shows a remote phosphor configuration, in which phosphor layer of uniform thickness is distributed over the reflector cup. However, there is still a large probability of lights being reflected by the reflector cup and being re-absorbed by the LED chip, as shown by Ray 1 and Ray 3. This is due to the specular surface of the reflector cup and its particular geometry which can result in trapped optical modes. J. K. Kim *et al.* [49] announced strongly enhanced phosphor efficiency in GaInN wLEDs using remote phosphor configuration and

diffused reflector cup. The improvement of light extraction efficiency by using the remote phosphor arrangement and a diffused reflector cup is 15.4% improvement in experiments.

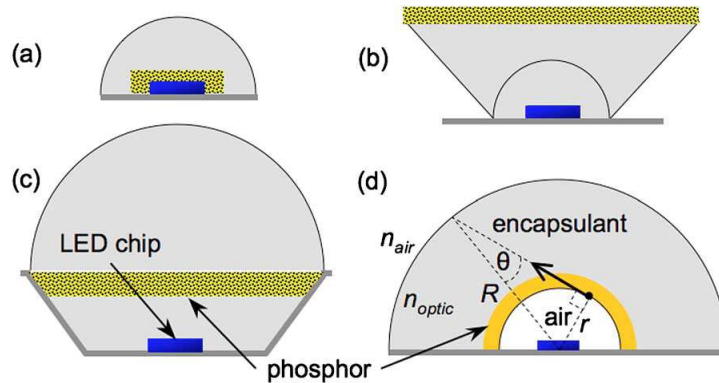


Fig. 1-10 Cross-sectional views of several pcLED packages. (a) conformal phosphor coating; (b) remote phosphor with scattered photon extraction; (c) remote phosphor with hemispherical dome; and (d) ELiXIR [50].

In addition, N. Narendran stated extracting phosphor-scattered photons to improve white LED efficiency [53]. The result illustrates the 61% more light output and efficacy of remote phosphor [Fig. 1-9]. S. C. Allen and A. J. Steckl indicated the configuration [Fig. 1-10(a)] is least efficient because the phosphor directs 60% of total white light emission (consisting of reflected blue and emitted yellow) back toward the chip, where high loss occurs [50]. A remote phosphor LED [Fig. 1-10(b)] was shown more efficient than the LED [Fig. 1-10(a)] because of the separation of the die and extraction of backward-emitted rays from the sides of the optic. Significant losses still occur inside the phosphor layer due to ray trapping by total internal reflection (TIR). The LED configuration of [Fig. 1-10(c)] introduced by Luo *et al.* uses a remote phosphor, diffused reflector cup, and hemispherical optic to minimize trapped light. The enhanced light extraction by internal reflection (ELiXIR) LED [Fig. 1-10(d)] utilizes a remote phosphor with a hemispherical dome that is separated from the chip by an air gap. Internal reflection at the phosphor/air interface redirects much of the backward phosphor emission away from the die and reflective surfaces without loss.

Furthermore, Y. Ito *et al.* announced that all phosphors have thermal quenching characteristic [52]. Figure 1-11 shows the temperature dependence of the relative radiant efficiency of YAG phosphor as an example. An increase in temperature from 25 °C to 100 °C results in a 20% decrease in radiant efficiency. The phosphor remotely is almost at ambient temperature because it does not contact with the LED chips.

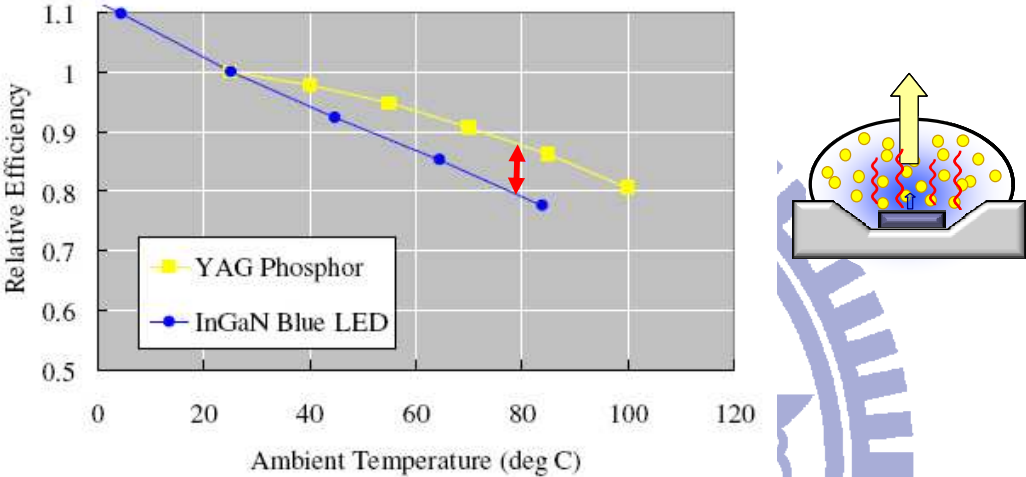


Fig. 1-11 Ambient temperature dependence of relative radiant efficiency of YAG phosphor and InGaN blue LED [52].

Table 1-1 Comparison of different BL systems.

BL Type	Direct-view BL	Edge-view BL	SONY BL
Light Source	CCFL	White LED	Blue LED
Large Configuration	◇	▽	○
Slim Configuration	▽	○	--
Color Saturation	○	▽	◇
Luminous Efficiency	○	▽	--
Thermal Releasing	○	▽	○

○ Superior ◇ Middle ▽ Inferior -- Unknown

1.3 Motivation and Objectives

Conventional planar lighting herein has been developed by exploiting direct-emission using a diffuser plate [Fig. 1-3(a)] or edge-emission using a light guide plate (LGP) [Fig. 1-3(b)] [63- 66]. Direct-emission yields high luminous efficiency in lighting systems, while edge-emission is more suitable for the application of thin module configurations. These approaches cannot easily support high luminous efficiency and a thin lighting module simultaneously.

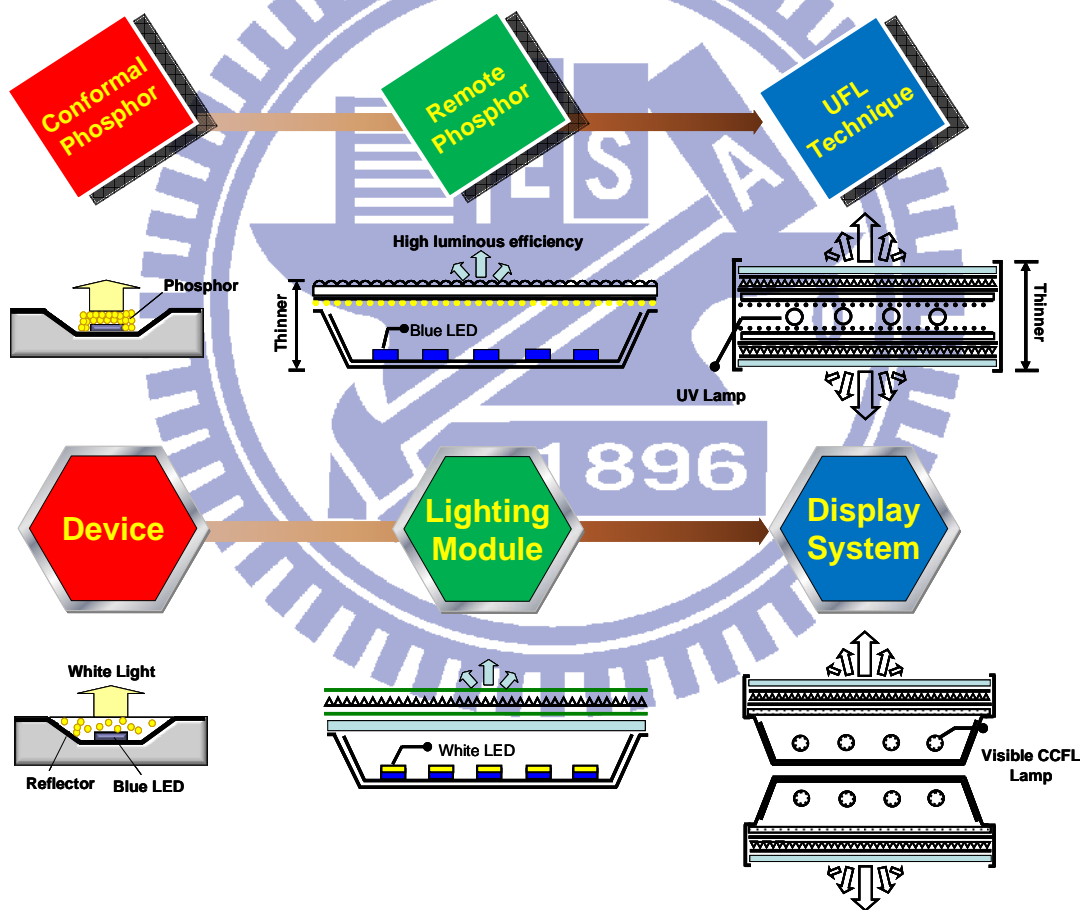


Fig. 1-12 Three parts in this thesis.

A direct-emission BL system, *i.e.* capable of satisfying a high power efficiency and high color saturation requirement by mixing the emitted R, G and B lights, and an edge-emission BL system, capable of generating a uniform, planar and slim BL configuration. Table 1-1

compares the optomechanical features of the above-mentioned BL systems in large sized backlight applications.

A direct-emission BL in contrast with edge-emission BL is especially favorable for large TFT-LCD applications because of its high power efficiency and high luminance. The conventional configuration of a direct-emission BL set generally consists of a metal holder with plural light sources, *e.g.*, CCFL and LED, inside and a diffuser plate above the light source to effectively suppress the non-uniform luminance distribution. The direct-emission BL design [Fig. 1-3(a)] with either a CCFL or an LED light source, does not have a slim configuration. In contrast, edge-emission BL [Fig. 1-3(b)] has thin BL outline, but the issues of inadequate color saturation of the LED light source, LED color binning and the thermal effect must be solved before commercialization is possible [94-102].

In 2008, SONY Corporation announced a novel remote phosphor converter (RPC) method, which has been used in wLEDs packages, and related studies have focused on increasing luminous efficiency [53-57]. Using an array of blue LED light sources, Y. Ito *et al.* generated a planar white light for BL applications by exciting a yellow remote phosphor film. Because of the difference between luminance-angular distribution of blue light and excited yellow light, color deviations are easily observed as the viewing angle varies from a normal to a large viewing angle [52].

In this investigation, a novel planar lighting system that is utilized in display applications is selected. It has a planar and uniform luminous distribution, slim configuration, high luminance, high color saturation, long lifetime and fast manufacturing process, making it effective for future use in a wide range of display applications, including digital signage and public information displays, which cannot all be based on current backlighting schemes. As shown in Fig. 1-12, this thesis has three parts and evaluates small devices, middle-scale lighting module, and finally large-scale backlighting platforms. A study of devices will focus

on color distribution in high-quality lighting applications. A study of lighting modules is conducted with a view to achieving high luminous efficiency, uniform luminous distribution and low color deviation. Accordingly, a novel display system is constructed for a wide range of display applications.

1.4 Organization of This Thesis

Figure 1-13 presents the organization of this investigation; it comprises three parts covering devices, lighting modules and display systems. First, the chapter 1 includes a preface and considers current issues, as well as the motivation for, and the goals of this work. Chapter 2 elucidates the theoretical background, including the use of photometry and colorimetry to evaluate a lighting system. Ray tracing and bidirectional scattering distribution functions (BSDFs) are utilized to develop a model for optical simulation. The proposed planar lighting system is compared with conventional lighting system. Glare, haze, Moiré and full width at half maximum (FWHM) are introduced and used in the optical evaluation.

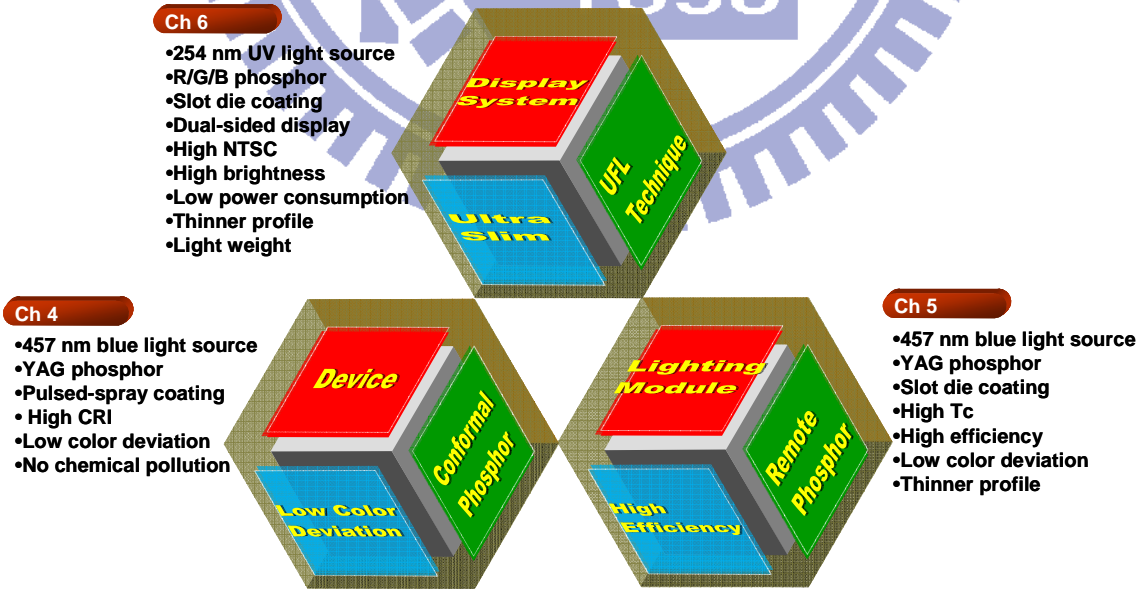


Fig. 1-13 The organization of this investigation.

Afterwards, the Chapter 3 presents the experimental method and materials in this

research. It describes the phosphor, the preparation of the remote phosphor film and related processes. Chapters 4 to 6 present the main developments of this research.

Chapter 4: low color deviation LED device, the distribution of phosphor by the pulse spraying of a conformal coating is discussed in this paragraph. This method differs from conventional dispensing method, settling method, spin coating, self-exposure or electrophoretic deposition (EPD). The proposed pulsed spray process in this investigation involves the application of phosphor by exploiting mechanical principles without risk of chemical pollution. Furthermore, it can be applied to wire-bonded LEDs and an array of LED chips on a substrate to fabricate a large-area, planar illumination system of high optical quality, which is easy to manufacture.

Chapter 5: high luminous efficiency LEDs lighting, the research regarding planar lighting in which an array of blue LEDs is utilized to excite a yellow remote phosphor film is presented. The proposed optics configuration can provide little angular color deviation and uniform luminous distribution using an ultra-slim structure for TFT-LCD backlighting applications. Most importantly, the configuration does not exploit a conventional diffuser plate or a light guide plate. Accordingly, an RP lighting system with strong optical performance in a compact module can be realized.

Chapter 6: ultra slim display system, a particular optical characteristic of UFL lighting is elucidated. Its symmetrical illumination satisfies the requirements of dual-sided LCD application. Additionally, UFL lighting exploits a thermal radiation mechanism to release the large amount of heat that is produced upon illumination, preventing thermal accumulation over the long term, when used in displays. These characteristics of UFL have motivated a wide range of lighting applications of digital signage and public informational displays.

Chapter 7 concludes this investigation. A planar lighting system that utilizes remote phosphor was realized for use in TFT-LCD backlighting and illumination applications.

Remote phosphor provides high optical performance and has a compact mechanical configuration. Future work will study the combined realization of low color deviation and high power efficiency. Therefore, the asymmetric illumination of two sides of dual-sided display will be studied. Furthermore, reduction of the dependency of color filters on the remote phosphor scheme will be increasingly important in combining high luminance with low power consumption. In conclusion, any innovative lighting system that is developed in the future should provide high color saturation (100% NTSC) for backlighting and high color rendering (100% CRI) for general lighting applications.



Chapter 2

Theoretical Backgrounds

The theoretical background regarding this research will be reviewed in this chapter. First of all, the use of photometry and colorimetry to evaluate a lighting system will be introduced. Then, ray tracing and bidirectional scattering distribution functions (BSDFs) are used to develop a model for optical simulation. Moreover, comparing the conventional lighting systems with the proposed planar lighting system is investigated. The measurement of glare, haze, moiré and full width at half maximum (FWHM) are introduced to support in optical evaluation. In addition, color rendering (NTSC), color saturation (CRI), color index, color temperature (Tc) and color deviation ($\Delta u'v'$) are introduced to support in color analysis too.

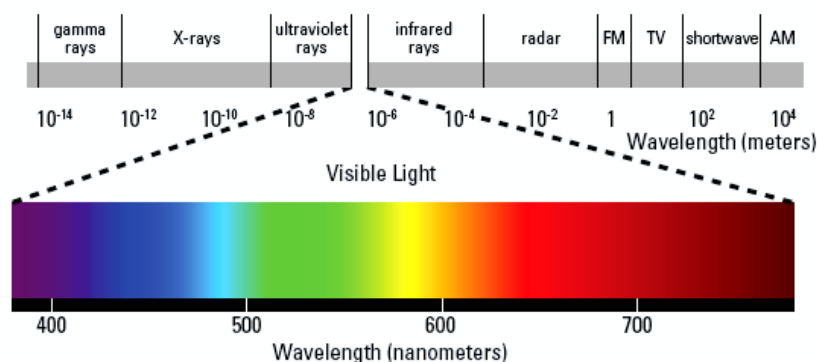


Fig. 2-1 Wavelengths of electromagnetic radiation and light [2].

2.1 Radiometry and Photometry

Radiometry deals with radiant energy (i.e., electromagnetic radiation) of any wavelength. The wavelength field includes the Ultra-Violet (UV), Visible Light and Infra-Red (IR). Generally, radiometry explore the characteristics of electromagnetic wavelength in the range from 10 nm to 10^6 nm [Fig. 2-1] Two out of many typical units encountered are radiant energy by quantity of Joule (J) and radiant power (or radiant flux) by Watt (W). Due to the

scale of measured energy is not too large, the units are expressed by mJ and mW (m represent the value of 1×10^{-3}) customarily.

Photometry is the measurement of visible light based on the response of the average human observer. The visible spectrum covers the wavelengths from approximately 390 to 800 nm. Photometry is like radiometry except that everything is weighted by the spectral response of the eye. Visual photometry uses the eye as a comparison detector, while physical photometry uses either optical radiation detectors constructed to mimic the spectral response of the eye, or spectroradiometry coupled with appropriate calculations to do the eye response weighting. **Figure 2-2** shows the definition of typical photometric units and **Table 2-1** expresses the quantities in lumen (*lm*), lux (*lx*), and candela (*cd*).

The only real difference between radiometry and photometry is that radiometry includes the entire optical radiation spectrum, while photometry is limited to the visible spectrum as defined by the response of the eye [2-5].

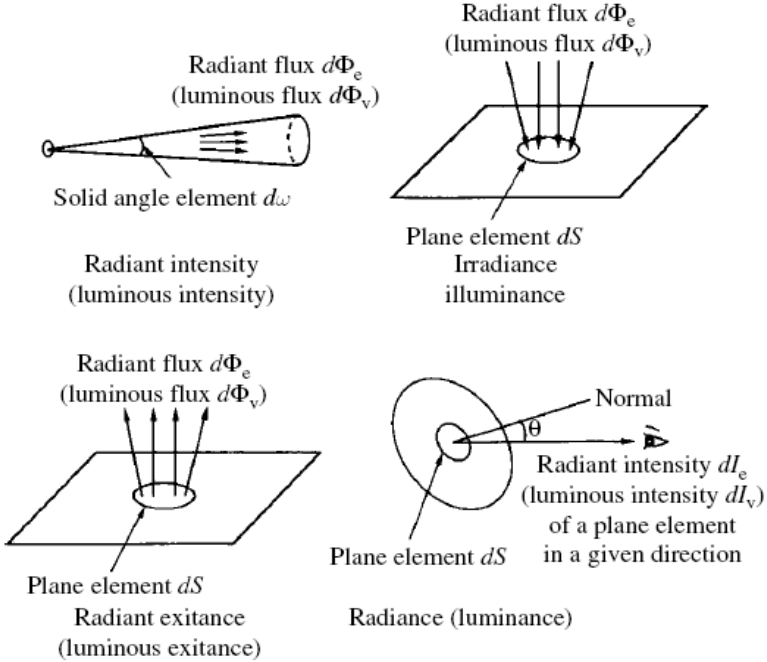
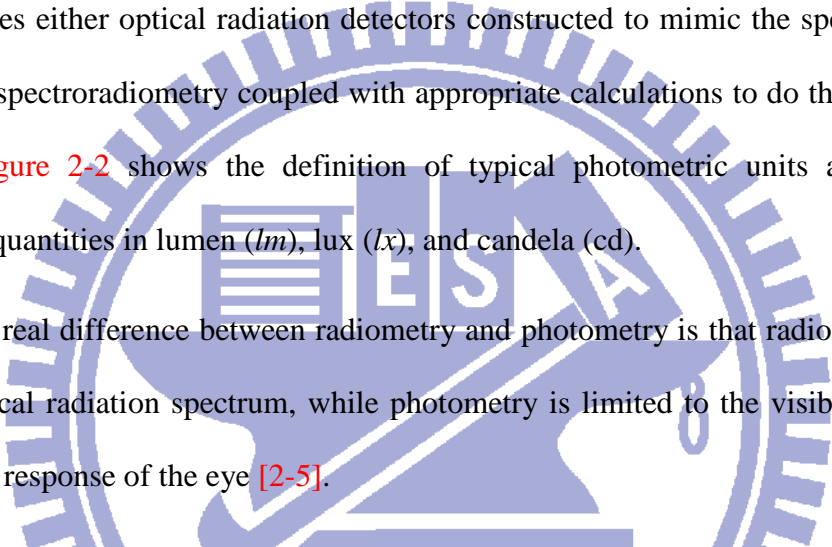


Fig. 2-2 Definition of radiometric and photometric quantities [3].

Table 2-1 SI photometry units.

Quantity	Symbol	SI unit	Abbr.
Luminous flux	Φ_v	lumen	<i>lm</i>
Luminous intensity	I_v	Candela (<i>lm/sr</i>)	cd
Luminance	L_v	candela per square meter (<i>lm/sr · m²</i> or <i>cd/m²</i>)	nits
Illuminance	E_v	Lux (<i>lm/m²</i>)	<i>lx</i>
Luminous exitance	M_v	<i>lm/m²</i>	
Luminous efficacy		lumen per watt (<i>lm/W</i>)	

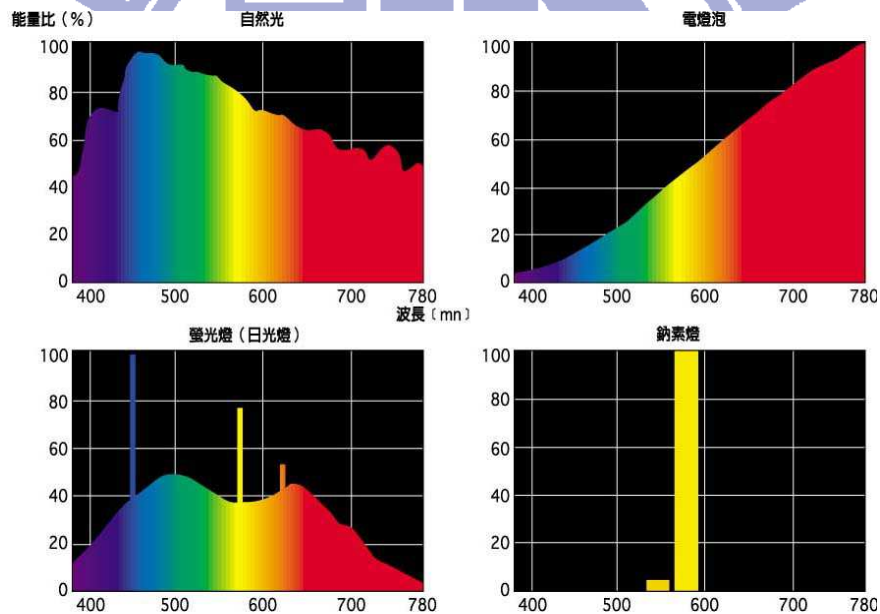


Fig. 2-3 Example of a typical spectral power distribution (SPD) [6].

2.1.1 Spectral Power Distribution

Incandescent, fluorescent, and high-intensity discharge (HID) lamps radiate across the visible spectrum, but with varying intensity in the different wavelengths. The spectral power distribution (SPD) for a given light source shows the relative radiant power emitted by the light source at each wavelength. Incandescent sources have a continuous SPD, but relative

power is low in the blue and green regions. The typically "warm" color appearance of incandescent lamps is due to the relatively high emissions in the orange and red regions of the spectrum as Fig. 2-3 shown.

2.1.2 Eye Sensitivity Functions

The eye sensitivity functions or the luminosity functions or the luminous efficiency functions describe the different visual spectral efficiency of human eye to different wavelength of visible light. There are two kinds of eye sensitivity functions in common usage [Fig. 2-4]. For bright day-light level, the photopic luminosity function approximates the response of the human eye. For dark night-light level, the response of the human eye changes and the scotopic curve applies. Radiometric quantities can be converted into photometric quantities and vice versa by the equation (photometric quantity, $F_l(\lambda)$) = $K(\lambda) \times$ (radiometric quantity, $F_r(\lambda)$). The equations can be written explicitly as

$$F_l(\lambda) = K_m \cdot F_r = 683 \cdot \int SPD(\lambda) \cdot V(\lambda) d\lambda \quad (2.1.1)$$

$$F_l'(\lambda) = K_m' \cdot F_r = 1700 \cdot \int SPD(\lambda) \cdot V'(\lambda) d\lambda \quad (2.1.2)$$

where $F_l(\lambda)$, $F_l'(\lambda)$ represents the quantity of day-light and night-light luminous efficacies, K_m , K_m' represents the maximum luminous efficacies and $V(\lambda)$, $V'(\lambda)$ represents the standard luminosity function, $SPD(\lambda)$ is the spectral power distribution of the radiation and λ is wavelength in metric unit.

The standard day-light luminosity function is normalized to a peak value of unity at 555 nm and the maximum luminous efficacy of radiation for photopic vision is 683 lm/W . Comparatively, the standard night-light luminosity function is normalized to a peak value of unity at 507 nm and the maximum luminous efficacy of radiation for photopic vision is 1700 lm/W . It is a standard function established by the *Commission Internationale de l'Éclairage*

(CIE) and may be used to convert radiant energy into luminous (*i.e.*, visible) energy in 1983. For all of the optics measurement equipments, the characteristics of optical detector should make calibration follow the curve of luminous efficiency functions rules by CIE standard to meet the actual eye sensitivity of human eye.

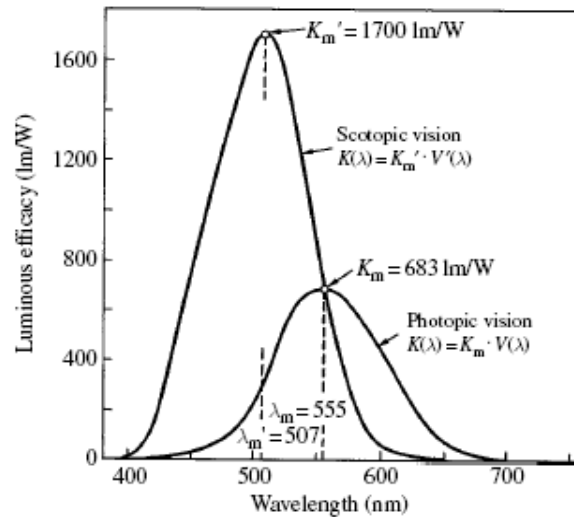


Fig. 2-4 Eye sensitivity function of two types of vision can be described by photopic and scotopic response curves [3].

2.1.3 Solid Angle

A solid angle is used in photometry to measure the portion of a sphere bounded by some irregular surface [Fig. 2-5]. The sphere is defined by the vertex (the center of a luminous body) and the center of the surface (an aperture). An entire sphere has a solid angle of 4π steradians (*sr*).

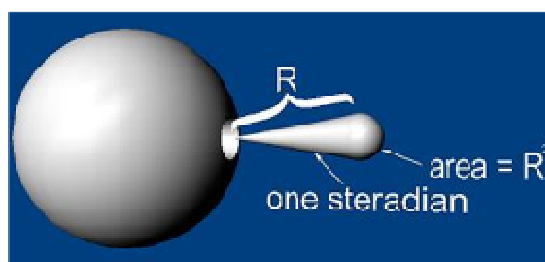


Fig. 2-5 The definition of solid angle [7].

2.1.4 Luminous Intensity

Luminous intensity is the perceived power per unit solid angle. Luminous intensity is a measure of the wavelength weighted power emitted by a light source in a particular direction per unit solid angle, based on the spectral luminous efficiency curve of the human eye sensitivity. The SI unit of luminous intensity is the candela (cd). The concept of luminous intensity requires the assumption of a point source, or at least a source small enough for its dimensions to be negligible compared to the distance between light source and detector and, in principle at least, there is also a requirement that the measurement should be made over a very small element of solid angle.

2.1.5 Luminous Flux

In photometry, luminous flux or luminous power is the measure of the perceived power of light. It differs from radiant flux, the measure of the total power of light emitted, in that luminous flux is adjusted to reflect the varying sensitivity of the human eye to different wavelengths of light.

The SI unit of luminous flux is the lumen (*lm*). One lumen is defined as the luminous flux of light produced by a light source that emits one candela of luminous intensity over a solid angle of one steradian (*sr*).

2.1.6 Luminance

Luminance is used for measuring the brightness of a light source on a surface. It's defined by the luminous flux emitted from a surface per unit solid angle per unit area of the source where the area is calculated by projecting it onto a plane normal to the direction of propagation. Luminance is invariant under transformation by a lens and also gives the same results when measured at any distance from the source.

2.1.7 Illuminance

Illuminance is the luminance flux incident on a surface from all directions. The luminous flux comes from one or several sources. What happens to the light at the surface (where if it is reflected or absorbed) does not matter. Illuminance is measured with a detector placed on the surface pointing toward the light source.

2.1.8 Lambert's Cosine Law and Lambertian Surface

A surface that diffuses light perfectly produces luminous intensity (I_v) in all directions that obeys Lambert's Cosine Law [Fig. 2-6 & Eq. 2.1.3], where the intensity (I_v) varies as the cosine of the angle between normal and the direction of the intensity measurement. The direction of the light incident on the surface has no effect on the luminous intensity (I_v) pattern.

$$I_{\theta} = I_{\text{normal}} \cos \theta \tag{2.1.3}$$

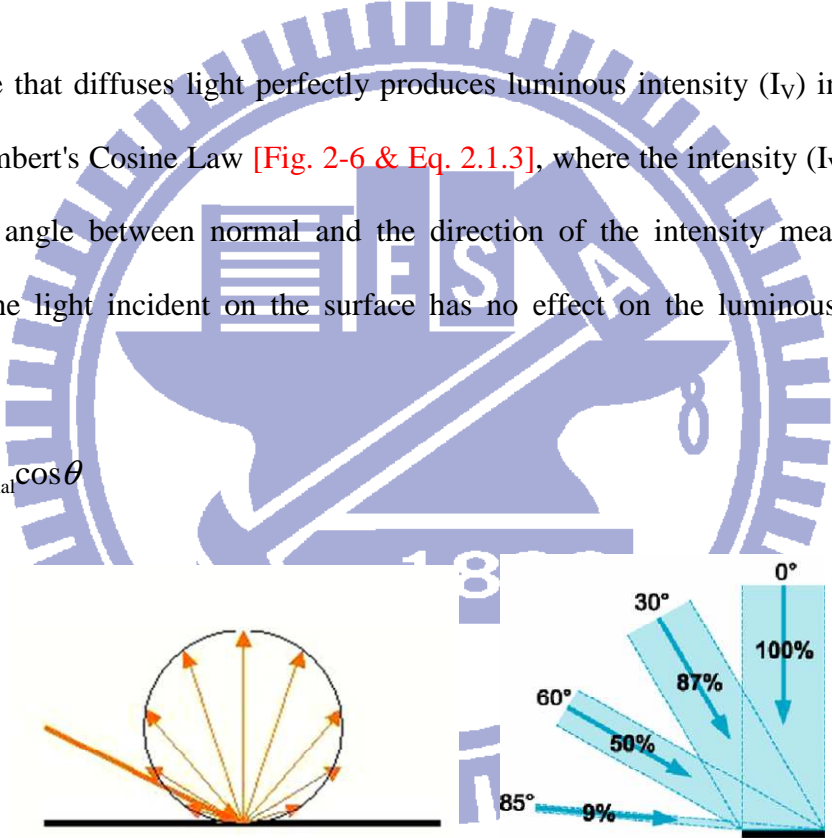


Fig. 2-6 Lambert's Cosine Law [7-8].

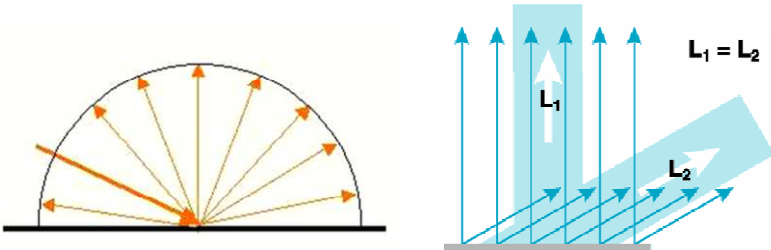


Fig. 2-7 Lambertian surface [7-8].

However, the luminance (L_v) of the surface does not obey Lambert's Cosine Law and it is constant when viewed from any angle. Lambertian surface is a perfectly diffuse surface [Fig. 2-7 & Eq. 2.1.4]. This is because projected area viewed through the luminance aperture varies as the cosine of the angle between the normal and the luminance measurement angle, thus offsetting the cosine effect of the luminous intensity.

$$L_{\text{normal}} = \frac{I_{\text{normal}}}{A_{\text{normal}}}, \quad L_{\theta} = \frac{I_{\theta}}{A_{\text{normal}} \cos \theta} = \frac{I_{\text{normal}} \cos \theta}{A_{\text{normal}} \cos \theta} = \frac{I_{\text{normal}}}{A_{\text{normal}}}$$

$$L_{\theta} = L_{\text{normal}} \quad (2.1.4)$$

2.2 Ray Tracing

Ray-tracing is a method based on Snell's law, Fresnel's equation, and other optical principles. Through electromagnetic theory, light is a wave varies electric and magnetic fields to comply with time. The light takes a spherical form when radiated from a point, and then behaves like plane waves when propagating. The path of a hypothetical point on the wave front of light is called a ray. Such a ray is an extremely convenient fiction for the ray-tracing. It provides a way to discuss the behavior of light and analyze the optics of lighting systems. Several optical software, such as LightToolsTM, OSLOTM, *et al.*, can support the ray-tracing function to build optical module for a simulated environment.

2.2.1 Law of Refraction (Snell's Law)

Snell's law, a law of refraction, defines the refraction of light in the plane of incidence. Snell's law describes the ratio of the incidence angle (θ_i) by the refraction angle (θ_t) equals to a constant which depends on the opposite ratio of the refractive indices of two optical media as:

$$\frac{\sin \theta_i}{\sin \theta_t} = \frac{n_t}{n_i} \quad (2.2.1)$$

where n_i and n_t denote the refractive indices of the incident and transmitted medium, respectively [9].

2.2.2 Law of Reflection

In the incident plane, the behavior of rays prompted by reflection is defined as the law of reflection:

$$\theta_i = \theta_r \quad (2.2.2)$$

where θ_i and θ_r denote the incident angle and reflected angle, respectively. For specular reflection, the angle at which the wave is incident on the surface equals to the angle at which it is reflected [10-11].

2.2.3 Fresnel's Equations

Fresnel's equations describe the energy of transmitted and reflected light at an interface between two different optical media. For defining the polarization waves of P (parallel to the plane of incidence) and S (perpendicular to the plane of incidence), the amplitude of reflection and transmission coefficients, r and t , are respectively given by:

$$r_s = \frac{n_i \cos \theta_i - n_t \cos \theta_t}{n_i \cos \theta_i + n_t \cos \theta_t}, \quad t_s = \frac{2n_i \cos \theta_i}{n_i \cos \theta_i + n_t \cos \theta_t} \quad (2.2.3)$$

$$r_p = \frac{n_t \cos \theta_i - n_i \cos \theta_t}{n_i \cos \theta_t + n_t \cos \theta_i}, \quad t_p = \frac{2n_i \cos \theta_i}{n_i \cos \theta_t + n_t \cos \theta_i} \quad (2.2.4)$$

where n_i and n_t denote the refractive indices of the incident and transmitted medium; θ_i and θ_t denote the angle of incidence and propagation, respectively.

According to the irradiance, the reflectance and the transmittance for polarized light are defined as:

$$R_s = r_s^2, \quad T_s = 1 - R_s \quad (2.2.5)$$

$$R_p = r_p^2, \quad T_p = 1 - R_p \quad (2.2.6)$$

where R_s and R_p denote the reflectance, and T_s and T_p denote the transmittance of S -polarized and P -polarized light, respectively. When a nature light strikes onto a medium, the reflectance (R) and transmittance (T) are defined as the average of the polarized lights as following equations:

$$R = \frac{R_s + R_p}{2} , \quad T = \frac{T_s + T_p}{2} \quad (2.2.7)$$

Base on laws of reflection and refraction, the ray-tracing method could analyze the optical behavior of propagated, reflected, and refracted lights. Furthermore, using Fresnel's equations, the energy of reflected and transmitted light at an interface separating two media could be calculated. Accordingly, the energy of a particular light on the defined receiver could be obtained. Commercial software, LightTools™, is adequate for development of simulated model to optimize the optical performances of the backlight systems [12].

2.3 Bidirectional scattering distribution functions (BSDFs)

Basing on radiometry and photometry, the bidirectional transmittance and reflectance distribution functions (BTDFs and BRDFs) are developed to describe light distributions [Fig. 2-8]. BSDFs is a superset and the generalization of the BRDFs and BTDFs. The BTDFs describes the transmitted characteristic of a sample, while the BRDFs indicate the reflective characteristic of a sample. The schematic setup of BSDFs measurement is shown in Fig. 2-9. In this thesis, the corresponded BTDFs and BRDFs were adopted to describe the phosphor film's light distribution characteristics which combine diffusing with wavelength conversion mechanism.

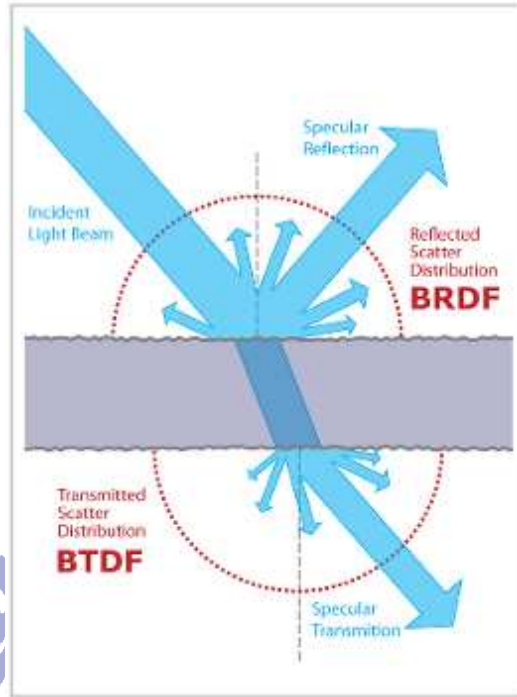


Fig. 2-8 BSDFs is a superset and the generalization of the BTDFs and BRDFs [15].

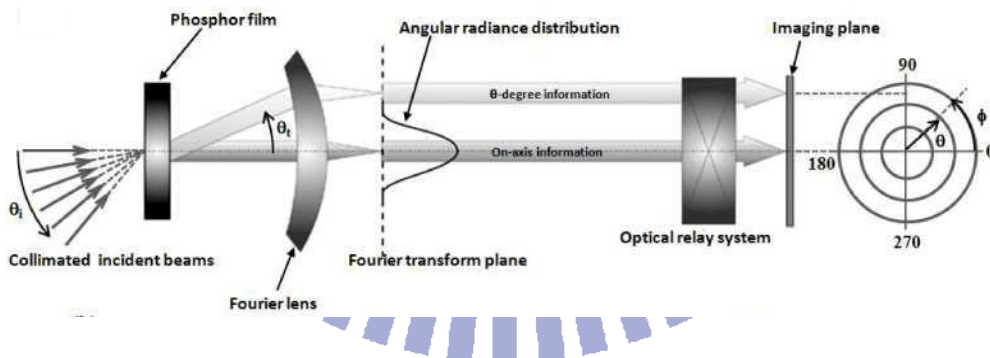


Fig. 2-9 Schematic measurement setup of BSDFs [13].

The defining geometry of BTDFs and BRDFs is shown in Fig. 2-10, where the subscripts i , t , and r denote the quantities of incident, reflective and transmitted rays; θ and ϕ denote the zenith and azimuthal angles in spherical coordinate; and (Ω, ω) denote the solid angle, respectively. If an incident ray with luminous flux $(\Phi_{v,i})$ and solid angle (ω_i) illuminating on the point P located on the sample plane, the transmitted and reflected rays scattered from the sample could be described by BTDFs and BRDFs as following equations:

$$\text{BTDF}(\theta_i, \phi_i, \theta_t, \phi_t, \omega_i, \omega_t) = \frac{L_{v,t}(\theta_t, \phi_t, \omega_t)}{E_{v,i}(\theta_i, \phi_i, \omega_i)} = \frac{d\Phi_{v,t}(\omega_t)/d\Omega_t}{\Phi_{v,i}(\omega_i) \cdot \cos\theta_t} \quad (2.3.1)$$

$$\text{BRDF}(\theta_i, \phi_i, \theta_r, \phi_r, \omega_i, \omega_r) = \frac{L_{v,r}(\theta_r, \phi_r, \omega_r)}{E_{v,i}(\theta_i, \phi_i, \omega_i)} = \frac{d\Phi_{v,r}(\omega_r)/d\Omega_r}{\Phi_{v,i}(\omega_i) \cdot \cos\theta_r} \quad (2.3.2)$$

where $E_{v,i}$ is the illuminance on the sample plane due to incident light, and $L_{v,r}$ and $L_{v,t}$ are the luminance of transmitted and reflective ray at the specific angles, respectively.

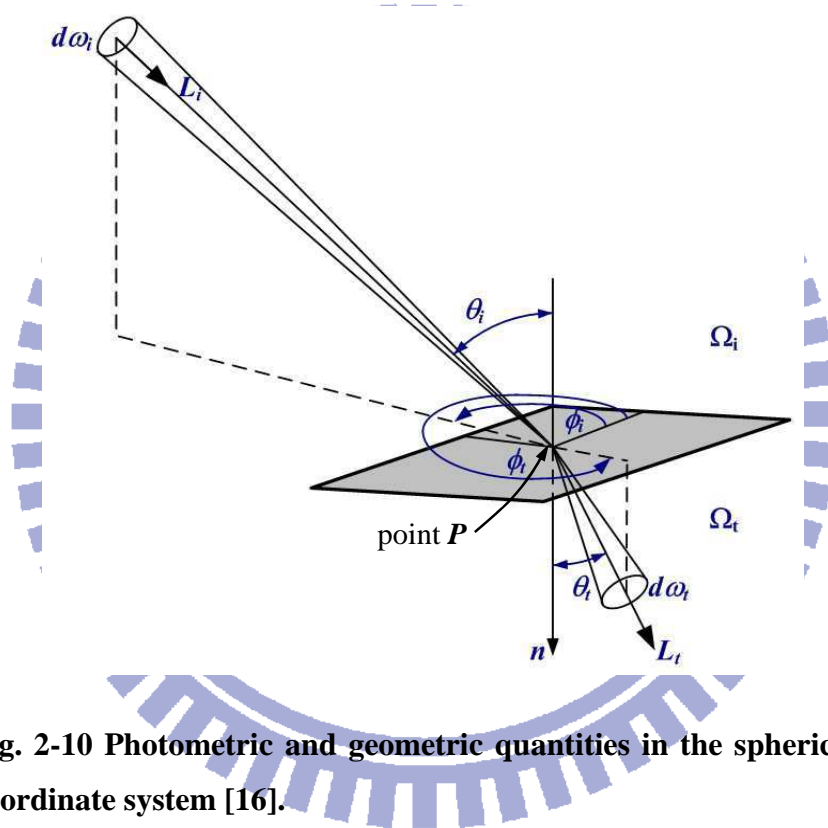


Fig. 2-10 Photometric and geometric quantities in the spherical coordinate system [16].

Besides, the terms of $d\Phi_{v,t}(\omega_t)/\Phi_{v,i}(\omega_i)$ and $d\Phi_{v,r}(\omega_r)/\Phi_{v,i}(\omega_i)$ in BTDFs and BRDFs, which could be obtained by measuring illuminance of incident ray, and luminance of the transmitted and reflective ray. Moreover, the light distribution of conventional diffuser films and phosphor films could be generated, and then be utilized by optical designers, manufacturers, and users to communicate and check requirements.

In this thesis, the BTDFs and BRDFs of phosphor films are measured by a conoscopic system operating under transmissive and reflective mode. The measured BTDFs and BRDFs

were then imported into commercial optical software, LightTools™, to develop the simulation models that could describe the light distribution characteristics of phosphor films. Thus, the optimization of lighting systems could be researched [14- 16].

2.4 Light and Vision

Light is radiation in the form of electromagnetic waves that make vision possible to the human eye. In this section, the full-width at half-maximum (FWHM) is defined to describe the light distribution. A high luminance associated with a broader angle of FWHM, yields benefits for large scale display applications. In addition, the vision of light reflecting (Glare), light scattering (Haze) and Mura, are introduced hereby for the evaluation of light distribution and definition of lighting performance.

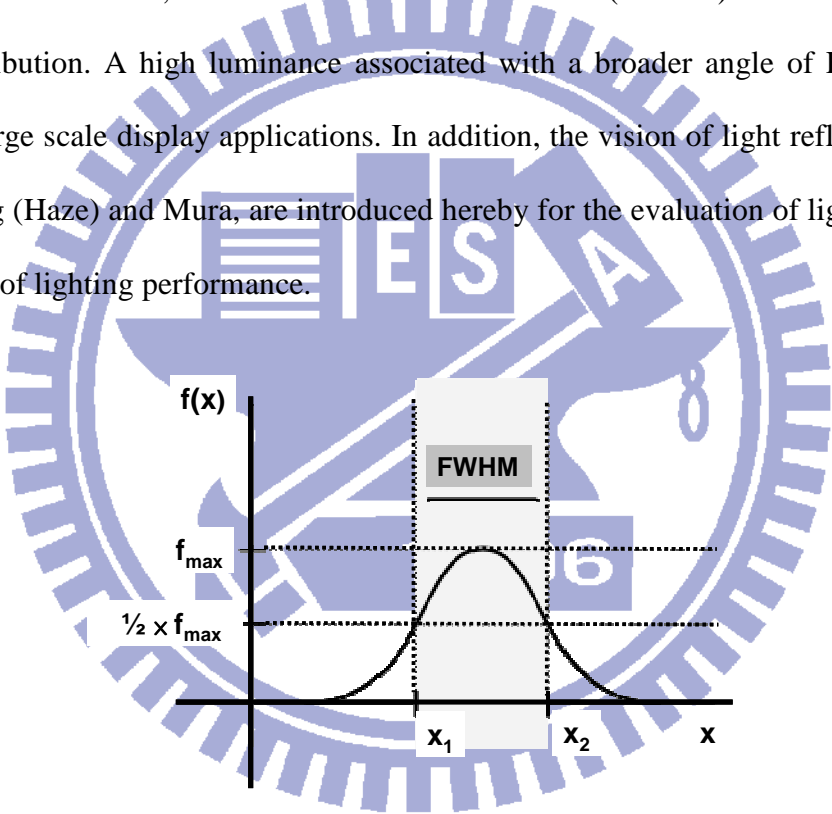


Fig. 2-11 Full width at half maximum (FWHM) [17].

2.4.1 Full-width at half-maximum (FWHM)

A full width at half maximum (FWHM) is an expression of the extent of a function, given by the difference between two extreme values of the independent variable at which the dependent variable is equal to half of its maximum value [Fig. 2-11].

FWHM is applied to such phenomena as the duration of pulse waveforms and the spectral width of sources used for optical communications and the resolution of spectrometers

[17].

2.4.2 Glare

Glare is produced by brightness (luminance) in the visual field that is sufficiently greater than the luminance to which the eyes are adapted to cause annoyance, discomfort or impair visual performance. This term is adapted to evaluate the visual performance of display. The measurement of glare is completed by BRDFs to represent reflection and to the measurement of BRDFs by the use of a spectrogoniophotometer. If the screen surface with the treatment of anti-glare, the phenomenon of light scattering will cause the level of glare to decrease. Low glare refers to the reduced visibility of a target due to the presence of a light source elsewhere in the field. It occurs when light from glare source is scattered by the ocular media. This scattered light forms a veil of luminance which reduces the contrast and thus the visibility of the target. High glare caused by the light irradiation from the light source or luminarie to harsh the eye directly and influence the visual function. A bright light source in the field of view, at a level sufficiently greater than retinal adaptation, can cause direct glare. Direct glare can result from many bright light sources like sunlight or ceiling light. Glare can also occur with indirect lighting. When glare refers to the presence of bright, reflected light sources, typically reflections from luminaires, is defined as reflected glare [18].

2.4.3 Haze

The term "Haze" in optical literature is defined as the forward scattering of light from the surface of a specimen viewed in transmission. Haze is an important appearance attribute which can be quantified and then used to assess the quality of objects such as liquids, glass, plastics and even metals. When measuring haze, the percentage of light diffusely scattered to the total light transmitted is reported as following

$$HZ = (DF/TT) \times 100\% \quad (2.4.1)$$

$$DF = (I_d/I_0) \times 100\% \quad (2.4.2)$$

$$TT = (I_t/I_0) \times 100\% \quad (2.4.3)$$

$$I_t = I_p + I_d \quad (2.4.4)$$

where HZ, DF, TT denote the ratio of total transmitted light, total diffused transmitted light and total parallel transmitted light, respectively [Fig. 2-12]. I_0 , I_t , I_d , and I_p denote the intensity of original input light, total transmitted light, total diffused transmitted light ($\theta > 2.5^\circ$, light scattered from the incident light) and total parallel transmitted light, respectively [19].

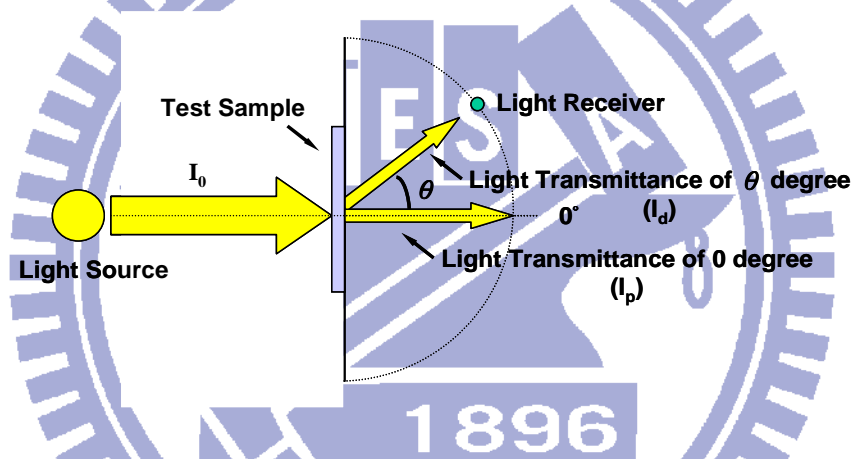


Fig. 2-12 The configuration of Haze measurement.

2.4.4 Mura

Mura is traditional general Japanese term for unevenness, inconsistency in physical matter or human spiritual condition. It is also a key concept in the description of light distribution uniformity in TFT-LCD display or lighting systems.

As Fig. 2-13 shown, the luminous uniformity was evaluated by defining the 9-points planar luminous uniformity (U_{PL}) as following

$$U_{PL} = \frac{\text{Min.}(L_1, L_2 \cdots L_9)}{\text{Max.}(L_1, L_2 \cdots L_9)} \times 100\% \quad (2.4.5)$$

where L_x takes values of nine measured luminance data in the entire illumination area L_1 ,

L_2, \dots, L_9 .

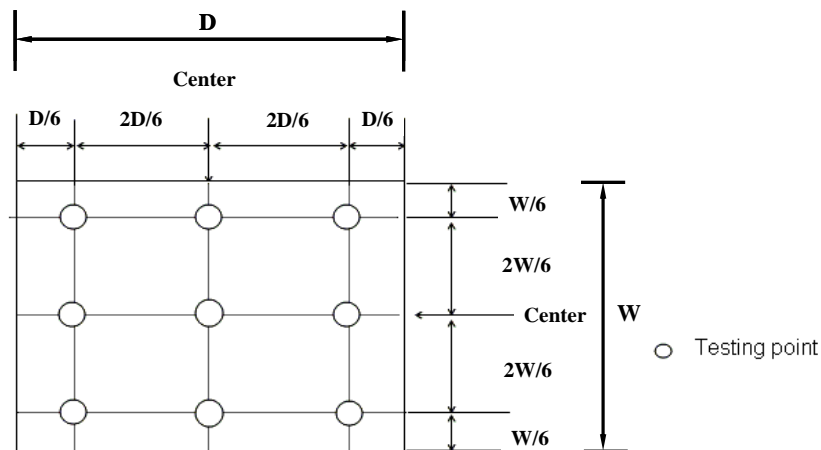


Fig. 2-13 The measured point of light distribution uniformity.

2.5 Colorimetry and CIE Chromaticity Diagram

Colorimetry, the science of color measurement and technology used to quantify and describe physically the human color perception, is widely employed in commerce, industry and the laboratory to express color in numerical terms and to measure color differences between specimens. Applications include paints, inks, plastics, textiles and apparel, food and beverages, pharmaceuticals and cosmetics, displays, general lighting and other parts and products that reflect or transmit color. The basis for colorimetry was established by *International Commission on Illumination* (usually abbreviated CIE for its French name, *Commission internationale de l'éclairage*) in 1931 based on visual experiments. Even though limitations are well recognized, the CIE system of colorimetry remains the only internationally agreed metric for color measurement. The CIE system characterizes colors by a luminance parameter Y and two color coordinates x and y which specify the point on the chromaticity diagram. This system offers more precision in color measurement than do the Munsell systems because the parameters are based on the spectral power distribution (SPD) of the light emitted from a colored object and are factored by sensitivity curves which have been

measured for the human eye.

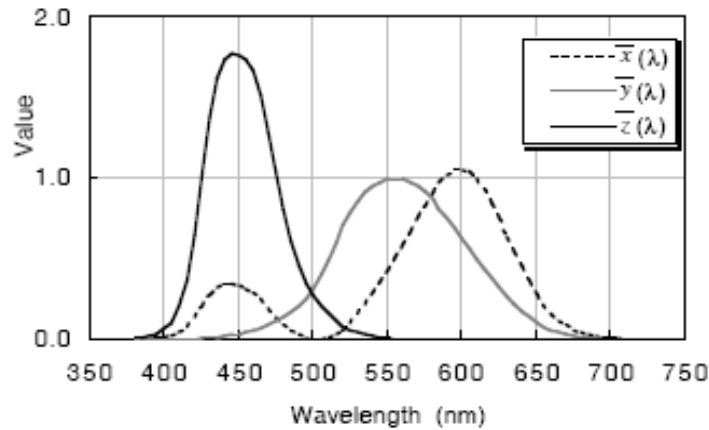


Fig. 2-14 CIE 1931 Color Matching Functions [20].

2.5.1 Tristimulus Values

Color could be matched by combination of three primaries, and result in the basis of the CIE colorimetry system. Figure 2-14 shows the linear transformation of CIE 1931 XYZ color matching function denoted as $\bar{x}(\lambda)$, $\bar{y}(\lambda)$, $\bar{z}(\lambda)$. By using the color matching functions, light stimuli having any spectral power distribution (SPD) can be specified for color by three values:

$$\begin{aligned} X &= \kappa \int_{\lambda} \phi(\lambda) \bar{x}(\lambda) d\lambda \\ Y &= \kappa \int_{\lambda} \phi(\lambda) \bar{y}(\lambda) d\lambda \\ Z &= \kappa \int_{\lambda} \phi(\lambda) \bar{z}(\lambda) d\lambda \end{aligned} \tag{2.5.1}$$

where $\phi(\lambda)$ is the spectral distribution of light stimulus and k is a normalizing constant. These integrated values are called Tristimulus values. For light sources and displays, $\phi(\lambda)$ is given in quantities such as spectral irradiance and spectral radiance. If $\phi(\lambda)$ is given in an absolute unit and $k= 683 \text{ lm/W}$ is chosen, Y yields an absolute photometric quantity such as illuminance or luminance. For object colors, $\phi(\lambda)$ is given by

$$\phi(\lambda) = P(\lambda) \cdot R(\lambda) \quad (2.5.2)$$

where $R(\lambda)$ is the spectral reflectance of object, $P(\lambda)$ is the spectral distribution of irradiating illumination, and

$$\kappa = 100 \int_{\lambda} P(\lambda) \bar{y}(\lambda) d\lambda \quad (2.5.3)$$

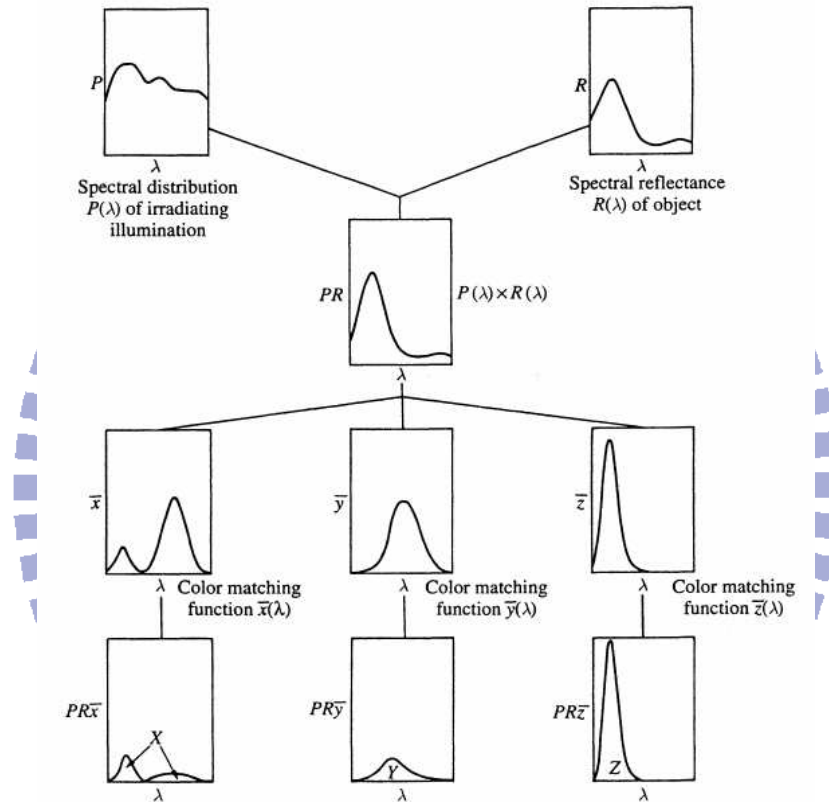


Fig. 2-15 Computation Procedure of Tristimulus XYZ [3].

As Fig. 2-15 shows, actual integration can be carried out by numerical summation of spectral data [3, 20].

2.5.2 CIE Chromaticity Coordinates

By projecting the tristimulus values on to the unit plane ($X+Y+Z=1$), color can be expressed in a two dimensional plane. Such a unit plane is known as the chromaticity diagram.

The color can be specified by the chromaticity coordinates (x,y) defined by

$$x = \frac{X}{X+Y+Z}; y = \frac{Y}{X+Y+Z} \quad (2.5.4)$$

The diagram using the chromaticity coordinates (x,y) is referred to the CIE 1931 chromaticity diagram [Fig. 2-16].

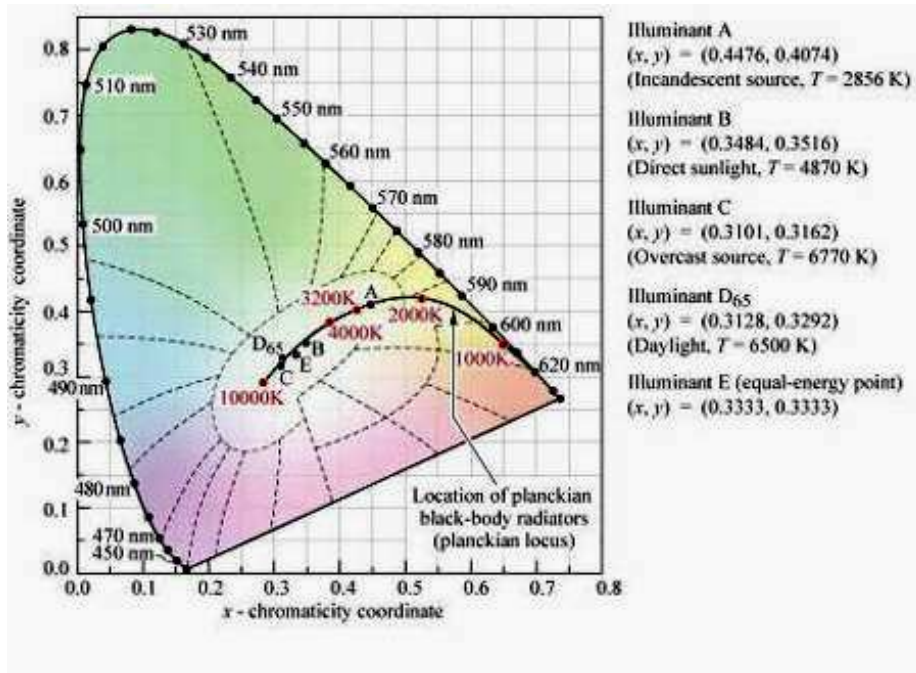


Fig. 2-16 CIE 1931 (x,y) chromaticity diagram. Monochromatic colors are located on the perimeter and white light is located in the center of the diagram [22].

The (x,y) chromaticity diagram is very non-uniform in terms of color difference. The minimum perceivable color differences in the CIE (x,y) diagram, known as MacAdam ellipses. To improve this, in 1960, CIE defined an improved diagram of CIE 1960 (u,v) chromaticity diagram (now deprecated), and in 1976, a further improved diagram of CIE 1976 uniform chromaticity scale (UCS) diagram, with its chromaticity coordinate (u',v') given by

$$u' = \frac{4X}{X+15Y+3Z}; v' = \frac{9Y}{X+15Y+3Z} \quad (2.5.5)$$

The 1976 (u',v') chromaticity diagram [Fig. 2-17] is significantly more uniform than the (x,y) diagram [21].

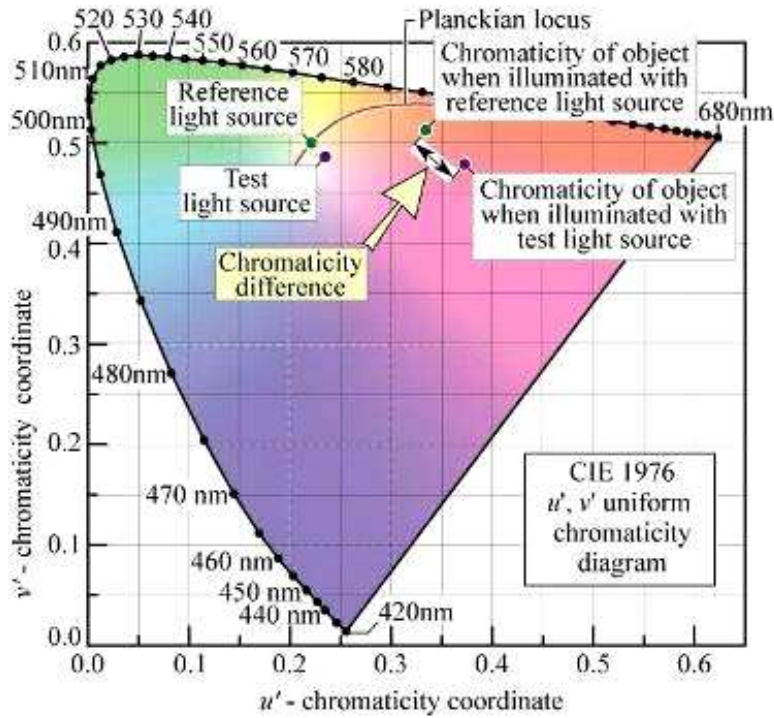


Fig. 2-17 CIE 1976 (u',v') uniform chromaticity diagram calculated using the CIE 1931 (2° standard observer). The chromaticity difference is directly proportional to the geometric distance [22].

2.5.3 Color Difference

To allow accurate specification of object colors and color differences, CIE recommended three dimensional uniform color spaces CIELUV in 1976. These are called the CIE 1976 ($L^* u^* v^*$) color space or CIELUV color space. In this thesis, the color difference, $\Delta u'v'$, of a lighting system is evaluated and described as:

$$\Delta u'v' = ((\Delta u')^2 + (\Delta v')^2)^{1/2} \quad (2.5.6)$$

Color difference ($\Delta u'v'$) is resulted from the illumination of an object with a reference and a test light source. In the CIE 1976 uniform chromaticity diagram, the color difference is directly proportional to the geometric distance. The reference light source is located on the Planckian locus at the correlated color temperature (CCT) of the test light source. In display

system, the color predetermination is precisely calculated by considering the spectra of all the optical components including backlighting unit, polarizer films, liquid crystal and color filters. In the (u',v') color space, it is now required to control the color difference to be smaller than 0.015 for commercial display applications, which must have no perceptible color difference.

2.5.4 Color Temperature

The color of light sources are measured and expressed by the resultant chromaticity coordinates (x,y) or (u',v') . However, it is difficult to relate these values immediately to particular colors. For such practical purposes, the color of "white light" can be expressed by color temperature (T_c) in the unit Kelvin (K). Because it is the standard against which other light sources are compared, the T_c of the thermal radiation from an ideal black body radiator is defined as equal to its surface temperature in Kelvin (K).

The term "black body" was introduced by Gustav Kirchhoff in 1860. The Planckian locus is the path or locus that the color of a black body would take in a particular chromaticity space as the blackbody temperature changes. It goes from deep red at low temperatures through orange, yellowish white, white, and finally bluish white at very high temperatures [Fig. 2-18]. For example, 2800 K is immediately associated with the warm color of incandescent lamps, and 9000 K is the bluish white from a CRT. In Planckian locus, 6500 K almost located in the center of CIE1931 diagram and the color is named "neutral light". Illumination D65 is the standard light source has T_c equal to 6500 K.

The NTSC and PAL TV norms call for a compliant TV screen to display an electrically signal. Current versions of NTSC standards specify a color temperature of 9300 K, but PAL standards allowed this data to be 6500 K. As Fig. 2-18 shown, 2700 K is the warmest option that most closely approximates a standard incandescent bulb. It is most often used in areas like living rooms. 3500- 4100 K is a whiter light and is most often selected for work spaces.

Daylight (6000- 6500 K) is recommended for reading areas and is a more bluish white that most closely approximates an outdoor overcast sky.

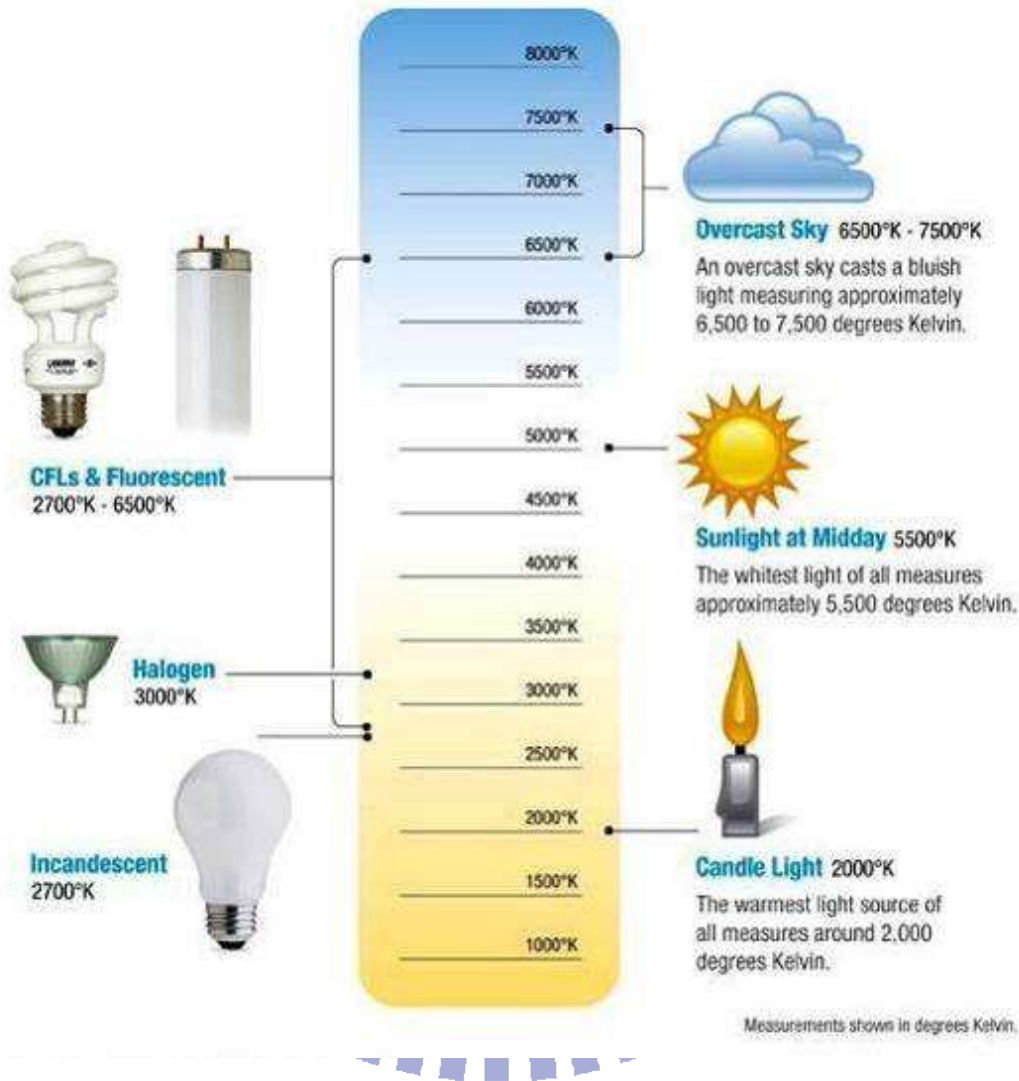


Fig. 2-18 Color temperature chart of general light sources [23].

2.5.5 Correlated Color Temperature

The correlated color temperature (CCT) is the temperature of the Planckian radiator whose perceived color most closely resembles that of a given stimulus at the same brightness and under specified viewing conditions. The mathematical procedure for determining the CCT involves finding the closest point to the light source's white point on the Planckian locus. The isotherms are perpendicular to the Planckian locus, and are drawn to indicate the

maximum distance from the locus that the CIE considers the CCT to be meaningful is $\Delta u'v' = \pm 0.05$.

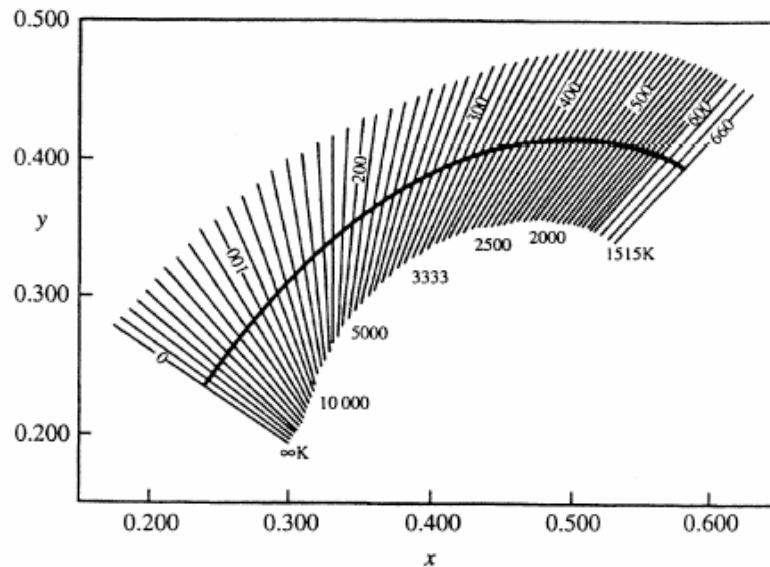


Fig. 2-19 Planckian locus (thick line) and iso-temperature lines (fine lines) [3].

Although the CCT can be calculated for any chromaticity coordinate, the result is meaningful only if the light sources are nearly white. The CIE recommends that the concept of CCT should not be used if the chromaticity of the test source differs more than $\Delta u'v' = \pm 0.05$ from the Planckian radiator. To determine the CCT from the chromaticity coordinates, McCamy's formula can be used. McCamy claims that the formula can provide a maximum absolute error of less than 2 degrees Kelvin for color temperatures ranging from 2,856 to 6,500 K (corresponding to CIE illuminants A through D65) given a particular (x,y) chromaticity coordinate.

$$\text{CCT} = 437N^3 + 3601N^2 + 6831N + 5517 \quad (2.5.7)$$

$$N = (x - 0.3320)/(0.1858 - y) \quad (2.5.8)$$

The calculated CCT becomes less meaningful as the source moves further away from the

Planckian locus. For instance, it would be possible to generate a CCT for a green LED, but the value would be meaningless as the point on the chromaticity diagram would be too far from the Planckian locus. In other words, the CCT is only meant to characterize near white lights [3, 24].

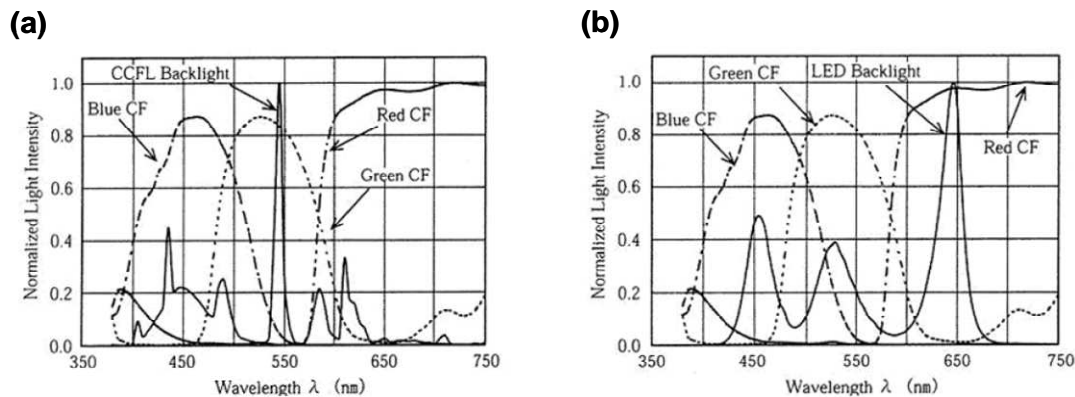


Fig. 2-20 Spectral properties of the CCFL lighting versus RGB-LED lighting when matching with the spectral transmittance factor of color filter [25].

2.5.6 Color Saturation

Color saturation or color gamut is the range of color that a display can reproduce and is commonly expressed as a percentage of NTSC standards. NTSC stands for *National Television System Committee*, which developed television standards for North America, in this instance, 100% of NTSC refers to the full range of color that can theoretically be displayed. Color saturation is commonly represented as areas in the CIE 1931 chromaticity diagram. The color saturation of conventional display is about 72% of NTSC standard due to the irradiation of light source at wavelengths of 590 and 490 nm. These two peaks of wavelength will cause the degradation of the color saturation. As [Fig. 2-20] shown, the narrow spectral distribution of RGB-LED can match with color filters perfectly and perform color saturation over 100% NTSC standard. Therefore, a display that can combine both high luminance and a high percentage color gamut should provide the best image of reproduction

display with the color domain of 72% when compared with the area of three primary color (RGB) defined by NTSC standard [26- 30].

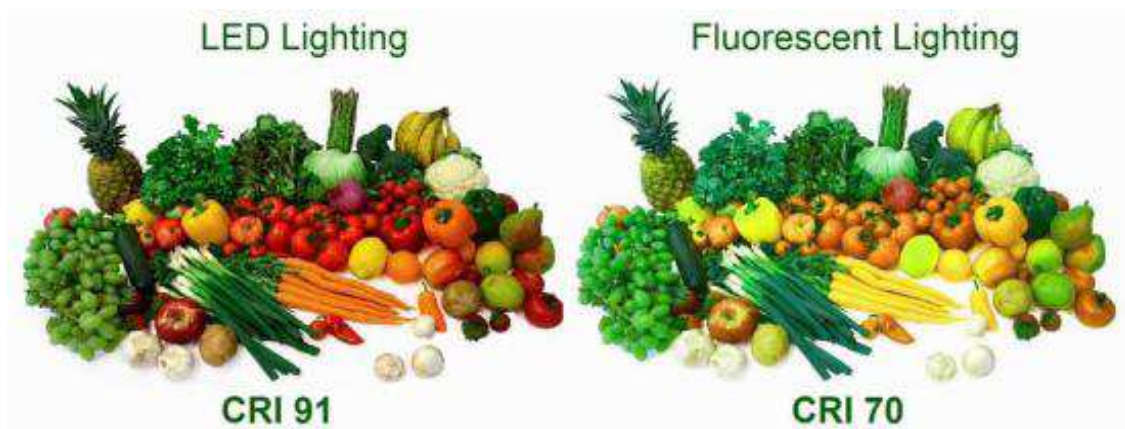


Fig. 2-22 The higher CRI provides richer and fuller looking surfaces, merchandise and food [38].

2.5.7 Color Rendering Index

An object looks whitish under the fluorescent lamp and meanwhile, the same object looks yellowish under the incandescent lamp. The same object looks different under different light sources. The light source will change the color of objects by comparing under fluorescent lamp, incandescent lamp, daylight and etc [31- 37]. Color rendering index (CRI) is a numerical representation to evaluate the color rendering properties of the light source. CRI shows how accurately a sample light source reproduces an object color compare to the reference light source. The CRI value of 100 means the sample light source reproduces the same color as the reference light source does. Therefore, the higher the value of CRI, the more it resembles to the reference light source [Fig. 2-22]. When evaluating CRI, the reference light source is chosen to have the same CCT as the sample light source. CRI evaluates how accurately the sample light source renders the 14 colors in comparison to the reference light source [Fig. 2-23 & 2-24].

There are two types of CRI. One is general CRI, which is also named as R_a and the other

is special CRI, which is named as R_i . The definition is as:

$$R_a = \sum_{i=1}^8 R_i \times \frac{1}{8} \quad (2.5.11)$$

$$CRI(R_i) = 100 - 4.6 \times \Delta E_i \quad (i = 1 \text{ to } 14) \quad (2.5.12)$$

ΔE_i refers to the color difference between reference light source and test light on CIE 1964 ($U^*V^*W^*$).

$$\Delta E_i = ((\Delta U^*)^2 + (\Delta V^*)^2 + (\Delta W^*)^2)^{1/2} \quad (2.5.13)$$

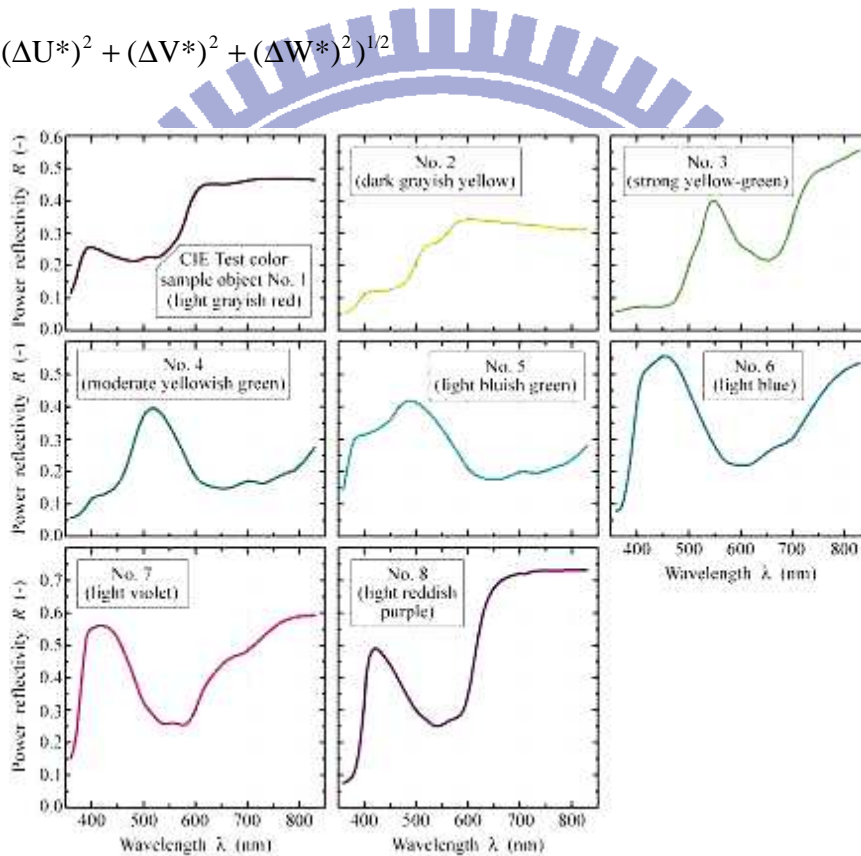


Fig. 2-23 CIE test color samples used to calculate the general color rendering index (Ra) (CIE 13.3 -1995) [22].

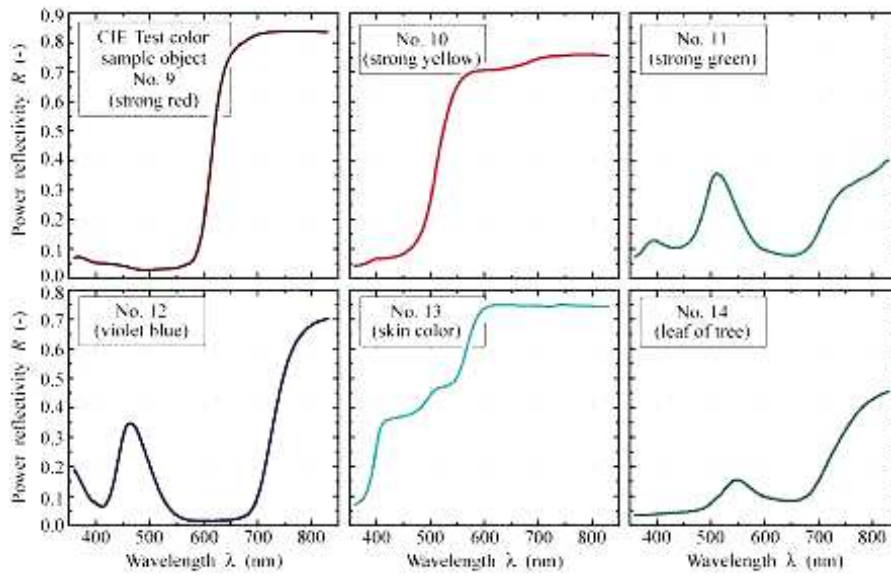
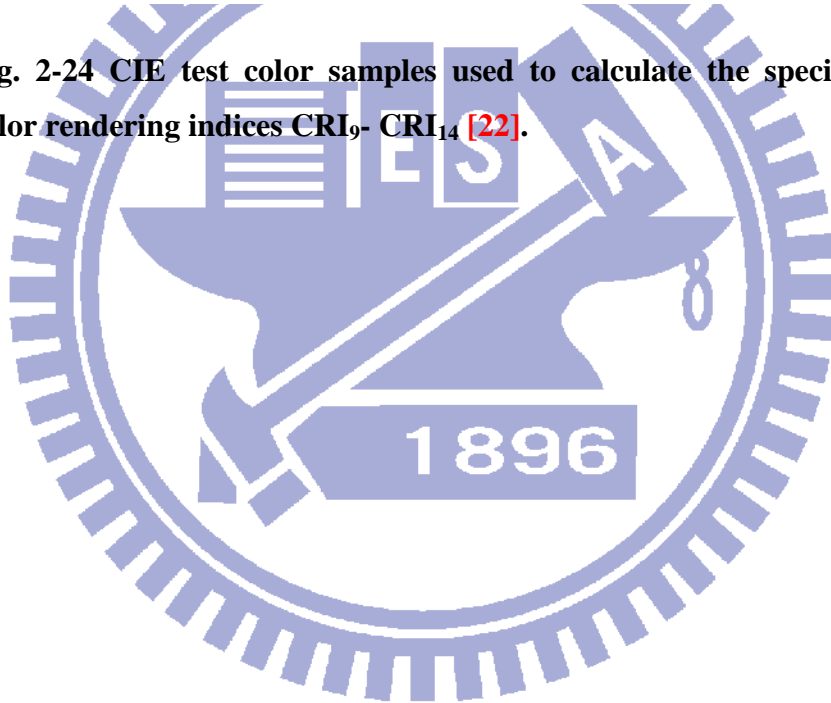


Fig. 2-24 CIE test color samples used to calculate the special color rendering indices CRI_9 - CRI_{14} [22].



Chapter 3

Experimental Details

This chapter describes the experimental materials and processes including phosphor materials, the preparation of a remote phosphor converter (RPC), light-diffusing/collimating optical materials and related processes. In the study of LED devices herein [Fig. 1-12], YAG phosphor, excited by 457 nm blue light, and the pulsed-spray process are introduced. Then, an LED light module was developed using the same materials, but pulsed-spray process was changed to slot-die coating, to enable coating over a larger area. In addition, R/G/B phosphor, excited by 254 nm UV light, and the slot-die coating method were used in a dual-sided display.

3.1 Phosphor

A phosphor, is mostly solid inorganic materials consisting of a host lattice, usually intentionally doped with impurities, is a substance that exhibits the phenomenon of luminescence. The impurity concentrations generally are low in view of the fact that at higher concentrations, the efficiency of the luminescence process usually decreases (concentration quenching). The required characteristics of phosphor based on the applications. For example, the application in general lighting, light emission with broadband and continued spectrum will be easy to reach the requirement of higher color rendering. Besides, the applications in TFT-LCD backlighting, light emission with narrow band and matching with the spectrum of color filters transmittance factors can reach higher color saturation [70-73].

In this research, the phosphor powder that was excited by blue light, was a cerium-doped yttrium aluminum garnet (YAG:Ce³⁺) with a wavelength distribution (irradiating wavelengths of 490~ 680 nm) [Fig. 3-1]. As show in Fig. 3-1(b), phosphor powder has an irregular morphology [74,75]. The mean size of phosphor particles (D50) is 7.44 μm [Fig. 3-1(c)]. An

indium gallium nitride (InGaN)-based blue LED, which emits a wavelength of 457 nm, is applied to excite YAG:Ce³⁺ phosphor and white light is generated by mixing these complementary colors.

Despite YAG phosphor already developed by Blasse and Bril in 1967 [76], the early purpose was applied on cathode ray tube. Nichia Corporation started developing Blue LEDs in 1989, and built up the technology for industrialization of GaN-based Blue LEDs in 1991. Nichia Corporation succeeded in the commercial production of high-brightness Blue LEDs in November 1993. Further, by applying its expertise as a phosphor manufacturer, and by combining YAG phosphor with Blue LEDs, Nichia Corporation developed and started commercial production of wLEDs in 1996 for the first time in the world.

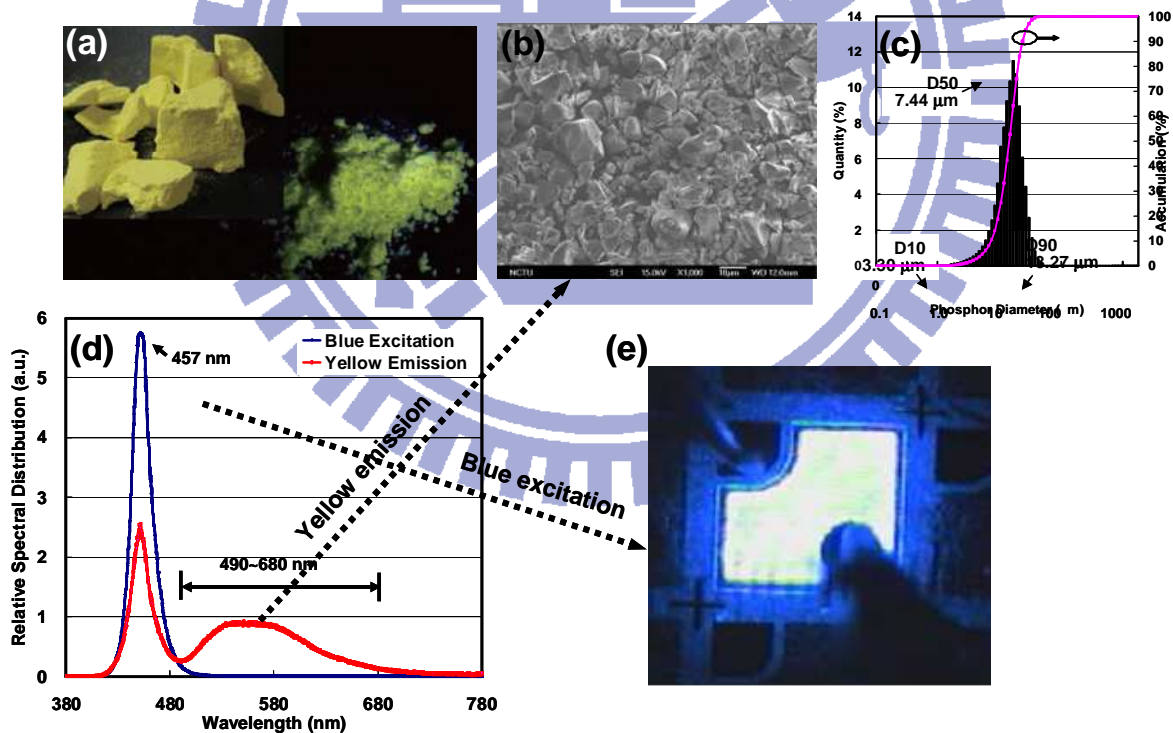


Fig. 3-1 (a) YAG phosphor powder [124]. (b) SEM morphology of YAG:Ce³⁺ phosphor. (c) The size distribution of phosphor particles. (d) The spectral properties of the blue excitation and yellow emission. (e) Blue light excitation.

In this work, another novel lighting system, UFL, that depends on a UV light to excite a

trichromatic RGB phosphor, instead of a blue light to excite a YAG phosphor. The UFL lighting system can combine the advantages of a direct-emission BL system, *i.e.* capable of satisfying a high power efficiency, and an edge-emission BL system, capable of generating a uniform, planar and slim BL configuration.

For TFT-LCD display, color saturation is determined by integrating the spectral properties of the light source and the spectral transmission factor of color filter (CF). Hence, the phosphor adopted in UFL lighting system is blended mainly by trichromatic phosphor with red phosphor of $Y(P,V)O_4:Eu^{2+}$ phase (620 nm emission), green phosphor of $BaMg_2Al_{10}O_{17}:Eu^{2+},Mn^{2+}$ phase (515, 545 nm) and blue phosphor of $Sr_5(PO_4)_3Cl:Eu^{2+}$ phase (450 nm) [Fig. 3-2]. The derived phosphor prescription shows less phosphor irradiation at wavelengths of 590 nm and 490 nm than the conventionally adopted phosphor does, where the two wavelength peak decreases the color saturation [20-21].

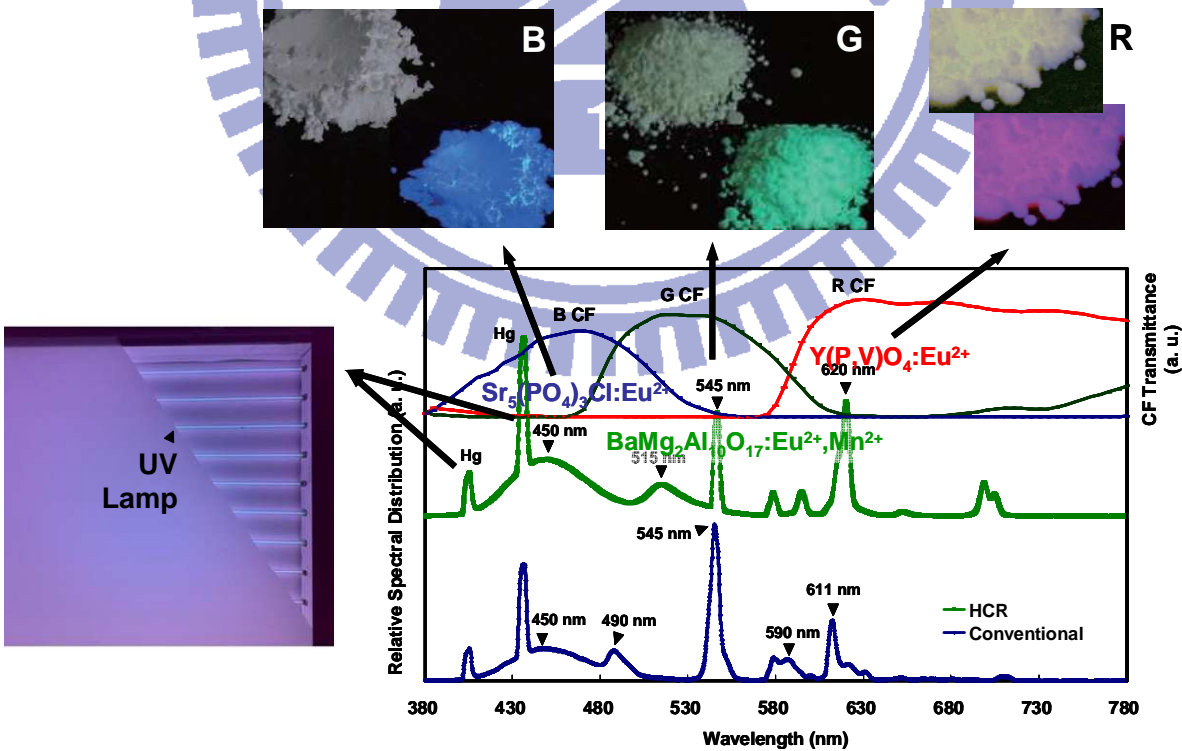


Fig. 3-2 The spectral properties of the phosphor versus the spectral transmittance factor of CF (phosphor photo cited from [124]).

3.2 Remote Phosphor Converter

In this research, phosphors were mixed together with binders, *i.e.* fluoride content, in a tank and applied on the polyethylene terephthalate (PET) film by coating approaches. **Figure 3-3** schematically depicts the simplified coating process by pulsed spray method. Notably, controlling the applied phosphor layer thickness to within 15-20 μm could yield the optimum luminance conversion efficiency.

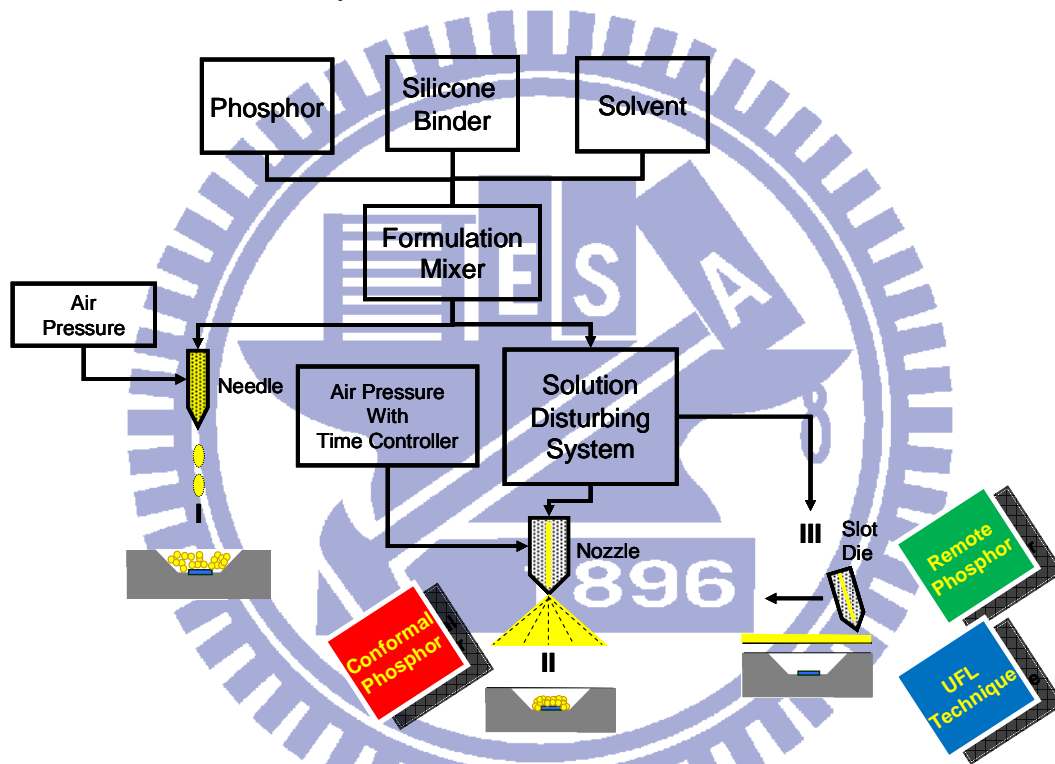


Fig. 3-3 The scheme of coating process in this research.

The phosphor film was then adhered to a plastic substrate to achieve a remote phosphor converter (RPC) [Fig. 3-4]. This composite plate was used in proposed lighting systems and placed remotely from the light sources. **Table 3-1** presents the optical characteristics of this RPC plate with a high haze ratio. It is especially effective at scattering incident light. Hence, RPC can be used for simultaneous wavelength conversion and light diffusion. **Figure 3-5(a)** shows the YAG phosphor film. **Figure 3-5(b)** reveals the morphology of phosphor film is irregular and full of voids. It contributes to light scattering and yields a high haze ratio.

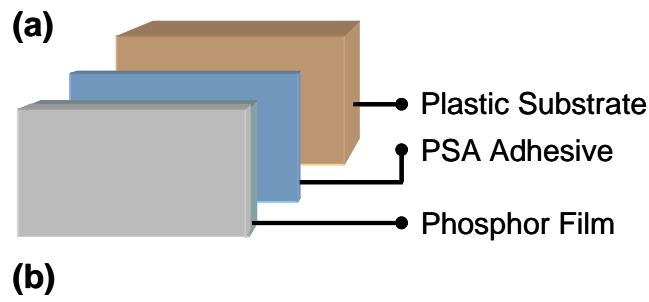


Fig. 3-4 (a) The remote phosphor converter (RPC); (b) the coated PET films with trichromatic phosphor.

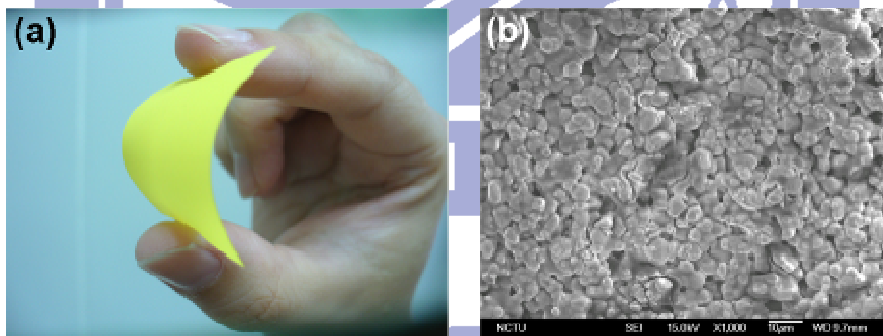


Fig. 3-5 Views of YAG phosphor film. (a) Appearance. (b) SEM micrograph.

Table 3-1 Optical Characteristics of RPC.

HZ ¹	TT ²	DF ³	PT ⁴
99.29	68.5	68.02	0.49

unit: (%)

¹HZ: haze ratio, $HZ=(DF/TT)\times 100\%$

²TT: transmittance of total output light;

³DF: transmittance of diffused light;

⁴PT: transmittance of parallel light.

3.3 Optical Materials

In this research, LED lighting module and display system are constructed with RPC on a substrate with diffusion for light scattering, collimation for light distribution controlling or polarization conversion for light recycling. The Brightness Enhancement Film (BEF) uses a translucent micro structured surface to employ both refraction and reflection, for the improvement of backlight efficiency and increased on-axis brightness [68]. Utilizing a micro replicated prismatic structure; unusable light outside of the normal viewing cone is reflected back and recycled, for re-emission at an optimum viewing angle. The BEF film substantially boosts display brightness, and can also be used in conjunction with other optical film for even greater illumination increases [Fig. 3-6].

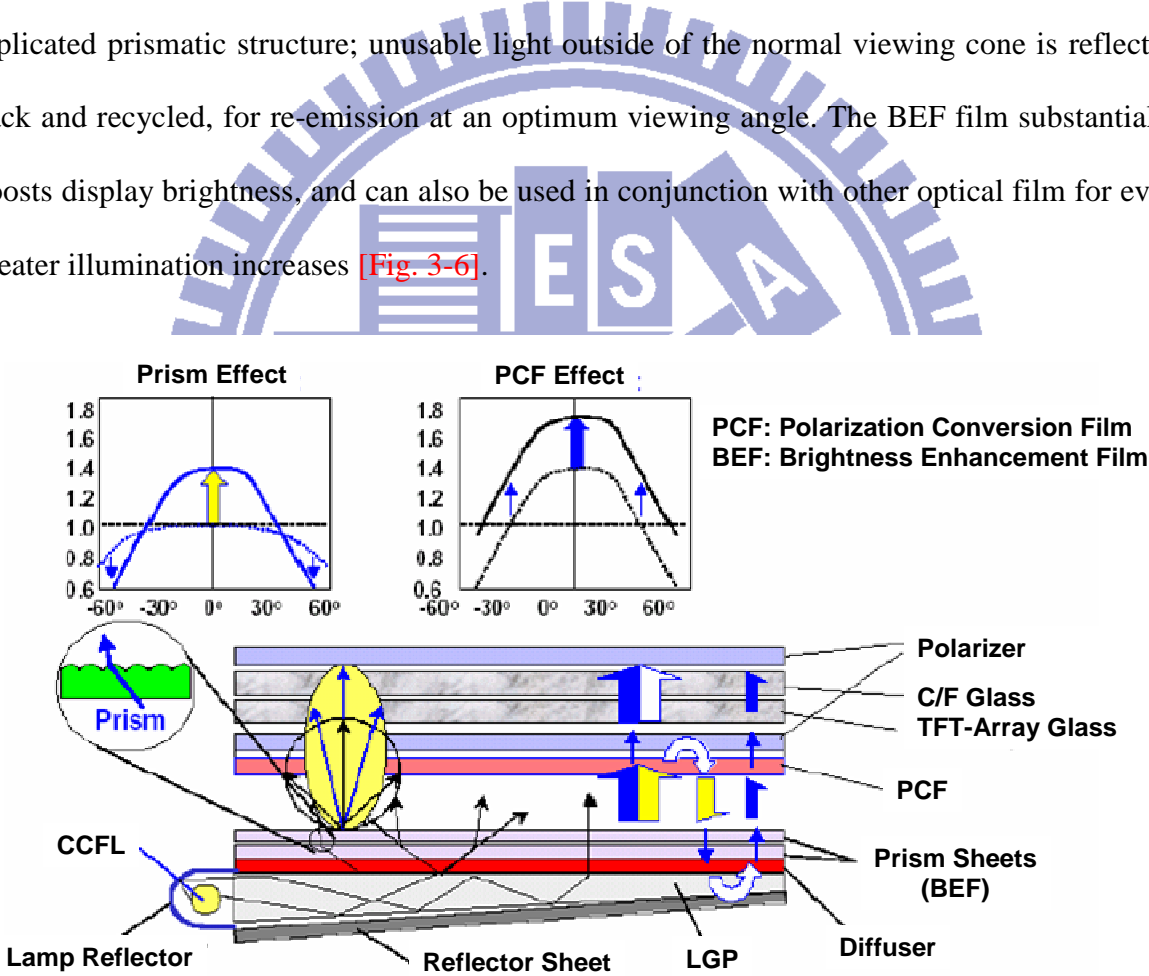


Fig. 3-6 The scheme reveals the effective function of BEF and PCF materials [67].

Polarization Conversion Film (PCF) works through polarization recycling. A conventional lighting system emits *P* and *S* polarized light. A typical polarizer absorbs *S*, but

PCF reflects S into the lighting system, where it is recycled into P and S light. With PCF, more P -polarized light is available to be transmitted through the LCD, increasing on-axis luminance by up to 60% ~ 97% for TFT-LCD backlighting applications [69].

The BEF and PCF are commonly used optical materials in backlighting applications. In this research, these two materials are also introduced to modify the output light distribution and increase on-axis luminance to meet backlighting optical requirement.

3.4 Experiment Process

The pulsed spray method is adopted to prepare the phosphor coating in this investigation. Figure 3-7 shows the mechanical structure of pulsed spray coater. The velocity of the spray, the amount of phosphor in the slurry, the ejected air pressure and the spraying interval (pulsing frequency) were controlled. The suspended slurry was prepared and disturbed mechanically to prevent the phosphor from settling before it was sprayed out. Then, the slurry was poured into the coating system to be atomized, and sprayed at a pulsing frequency of 5-10 Hz, phosphor loading of 1.2 mg/cm^2 , and color temperature of 9500 K onto the surfaces of bare LED chips. Eventually, the LED with CPC was annealed at 170°C for three hours.



Fig. 3-7 Mechanical structure of pulsed-spray coater.

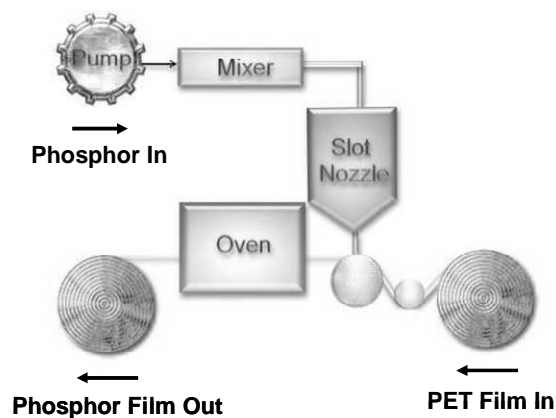


Fig. 3-8 Schematically depicts the simplified process of slot-die coating.

In the preparation of RPC in this investigation, the slot-die coating was used. **Figure 3-8** schematically depicts the process of slot-die coating and **Fig. 3-9** presents a photograph of the coater that was used in the experimental. Slot-die coating process is especially effective for coating large areas as required to make TFT-LCD displays. KISmart Corporation, Hsinchu, Taiwan, helped in the preparation of the LED devices that were used in this work by pulsed-spray coating. The LED lighting module and dual-sided display samples were made by slot-die coating.

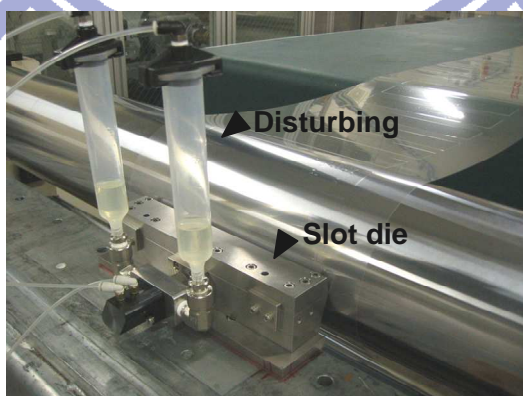


Fig. 3-9 Mechanical structure of slot-die coater.

Chapter 4

Low Color Deviation LED Devices using Conformal Phosphor Coating

4.1 Why Conformal Phosphor

White LEDs are becoming increasingly important light sources for illumination applications, because they are compact, mercury-free, and energy-efficient. However, conventional wLEDs that are fabricated by dispensing [Fig. 3-3], settling method, spin coating, self-exposure or electrophoretic deposition (EPD) have problems [40-42]. The dispensing method is the most popular approach in industry, but the settling of the phosphor powder before curing causes disharmony between blue light and yellow light. Additionally, the settling approach is a chemical reaction and requires a flip-chip LED with a flat surface for phosphor coating. Spin coating centrifugally separates phosphor from slurry. Self-exposure or EPD can produce an uniform phosphor coating, but these chemical processes causes Cr ion pollution. Therefore, an environmentally friendly phosphor coating on InGaN chips with uniform thickness was formed to optimize the performance of wLEDs. This investigation uses a novel approach that applies the pulsed spray (PS) process to ensure that the phosphor coating conforms to the LED chip outline.

This coating is called the conformal phosphor coating (CPC). The PS approach with an interval control is used to feed phosphor slurry through an air atomizing nozzle to spray and pile up the phosphor layer by layer. It yields a thin, uniform phosphor along the perimeter of the chip [Fig. 4-1]. Experimental results show that the PS approach can be used to form LEDs with an accurate color distribution achieving a wide range of color temperatures (T_c from 2500 to 9500 K), for use in a great diversity of applications, including TFT-LCD backlights and general lighting. Additionally, PS can be applied to LED chips of the wire-bonded type.

Therefore, this investigation uses a lighting system with an array of blue LED chips on a board (COB), which are coated with yellow phosphor by the aforementioned PS scheme for evaluation [Fig. 4-1(a)]. Additionally, as one of the means of phosphor coating, PS is fast and inexpensive, and yields a uniform phosphor layer and reproducible results.

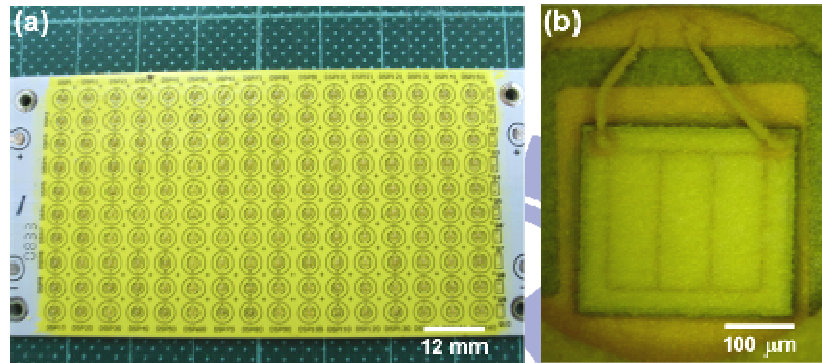


Fig. 4-1 Phosphor coating using PS scheme. (a) An array of blue LED chips on board (COB); (b) the magnification of individual LED.

4.2 Color Distribution Analysis

The phosphor coating using dispensing method and PS method are both uncomplicated and involves no chemical reaction. In the following, the color distribution, the color temperature and the other optical performance parameters will be evaluated for these two methods and compared [77,78].

The color deviation of a lighting system, $\Delta u'v'$ [Eqs. (2.5.5) & (2.5.6)], is evaluated. For dispensing method, the suspended phosphor is easily delaminated by gravity before the silicone binder is cured, causing color deviation at various viewing angles [Fig. 4-2(a)]. LED packages must therefore be sorted and when necessary binned before use, resulting in high production costs. The experimental $\Delta u'v'$ value reveals that the PS scheme yields a much greater spatial color uniformity [Fig. 4-2(b), $\Delta u'v'$ of 0.07] than does the dispensing method

($\Delta u'v'$ of 0.23) when the light is emitted at angles from -60° to $+60^\circ$. Therefore, PS scheme allows the accurate control of color distribution for high-quality lighting applications. Table 4-1 summarizes the comparison of optical data regarding conventional dispensing method and CPC by PS scheme. When controlling T_c of experiment around 9500 K, CPC by PS reveals accurate color distribution and higher luminous efficacy (8% improvement).

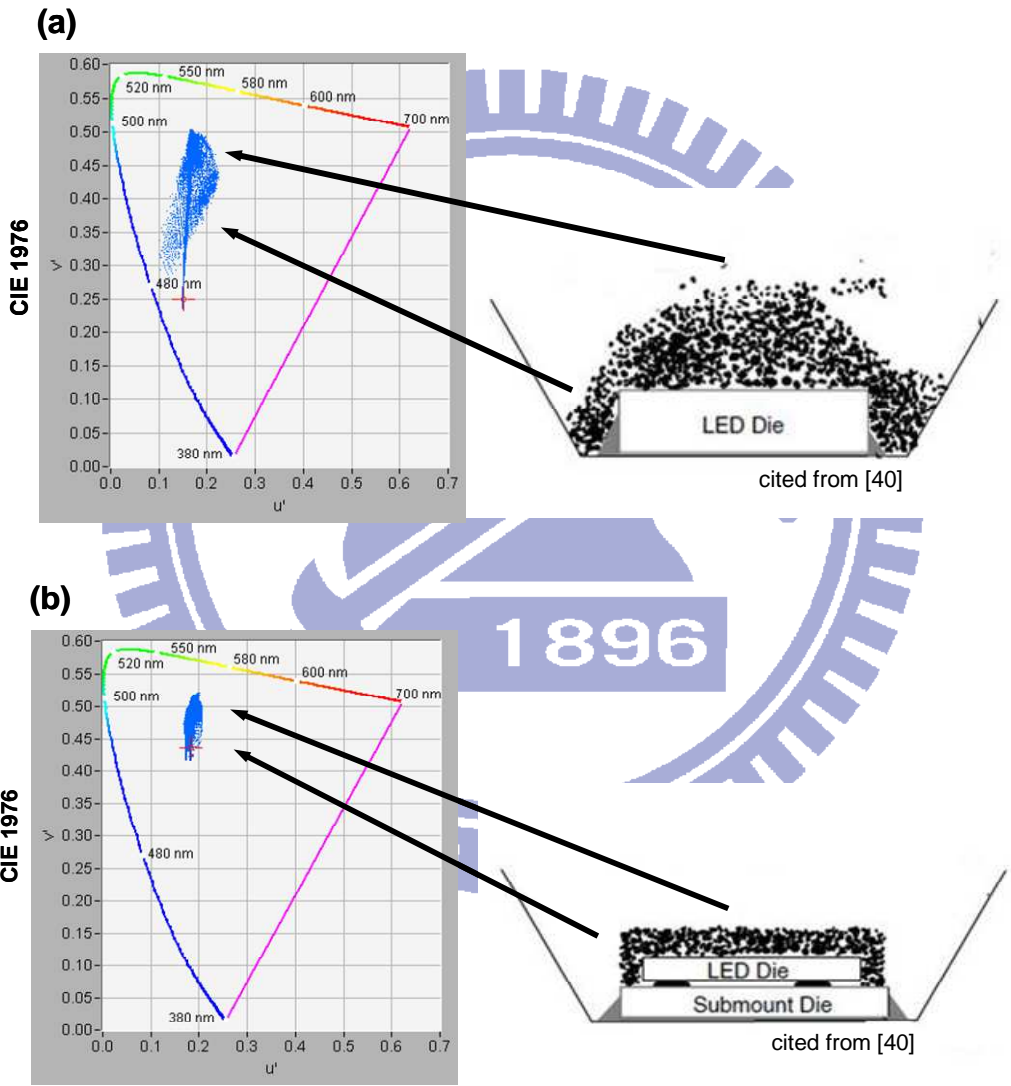


Fig. 4-2 CIE 1976 chromaticity indices versus angular distribution of LED when the light is emitted at angles from -60° to $+60^\circ$. (a) Conventional dispensing; (b) conformal coating using PS.

Table 4-1. Optical comparison between conventional dispensing and CPC by PS^a.

	C_x	C_y	Y (lm)	$u'v'$	T_c (K)
Conventional dispensing	0.290	0.276	48.80	0.23	9533
CPC by PS	0.284	0.290	52.70	0.07	9519

^aPower consumption: 0.5 W (forward voltage (V_F): 3.5 V, forward current (I_F): 150 mA).

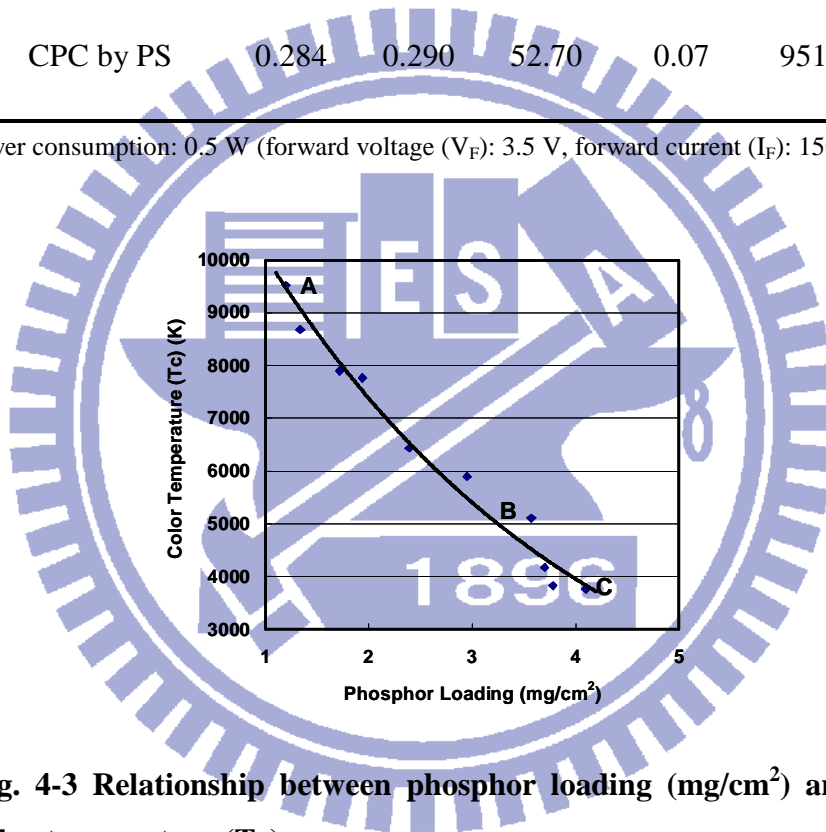


Fig. 4-3 Relationship between phosphor loading (mg/cm²) and color temperature (T_c).

4.3 Color Temperature Range

Different applications have different T_c requirements. TFT-LCD TV applications require illumination at a high color temperature ($T_c > 9000$ K). However, general lighting has a T_c range of 3000 K (warm white) to 5000 K (cool white). This work studies the dependence of T_c for white light on phosphor loading (mg/cm²) [Fig. 4-3]. The experimental results reveal that wLEDs based on the PS scheme have a T_c value that is inversely proportional to the

phosphor loading. Whereas a low Tc is achieved at high phosphor loading (point C), a high Tc is achieved at low phosphor loading (point A), and is associated with strongly non-uniform color distribution [48]. Therefore, the color distribution of wLEDs at high Tc was explored. As shown in Fig. 4-4(a), the conventional dispensing approach cannot easily ensure color uniformity with a Tc at 9533 K.

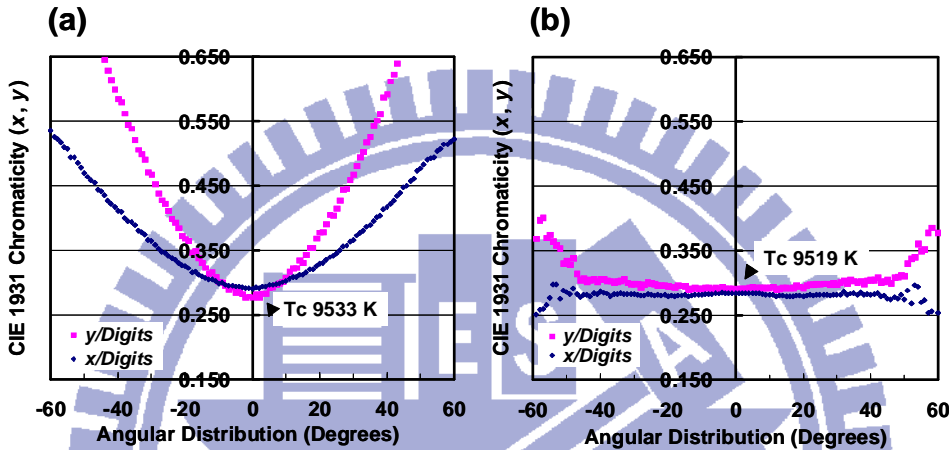


Fig. 4-4 CIE 1931 chromaticity indices versus angular distribution of LED at Tc centre around 9500 K. (a) Conventional dispensing; (b) conformal coating using PS.

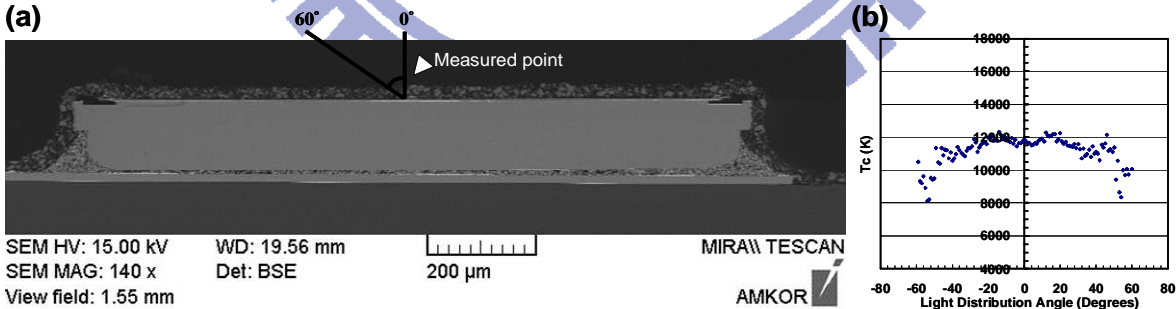


Fig. 4-5 (a) Conoscopic measured point and range from +60° ~ 0° ~ -60°. (b) Color temperature (Tc)-angular distribution.

The chromaticity indices display a severe variation with the viewing angle from -60° to +60°. When the PS approach is used at a phosphor loading of 1.20 mg/cm², the resulted Tc is 9519 K [Fig. 4-4(b) & Fig. 4-5] with a harmonic chromaticity distribution. When the spraying

interval in PS is varied to control the amount of deposited phosphor, a thin and uniform phosphor layer can be coated on the surface of the LED chips. In this case, when a higher percentage of yellow light (complementary wavelength) is mixed in, the Tc is shifted toward the yellow side (low Tc). Figures 4-3 and 4-6 reveal that a Tc of 5100 K (cool white, point B), a Tc of 4174 K (warm white, point C) and a Tc of 9519 K (high color temperature, point A) can be achieved using the PS approach.

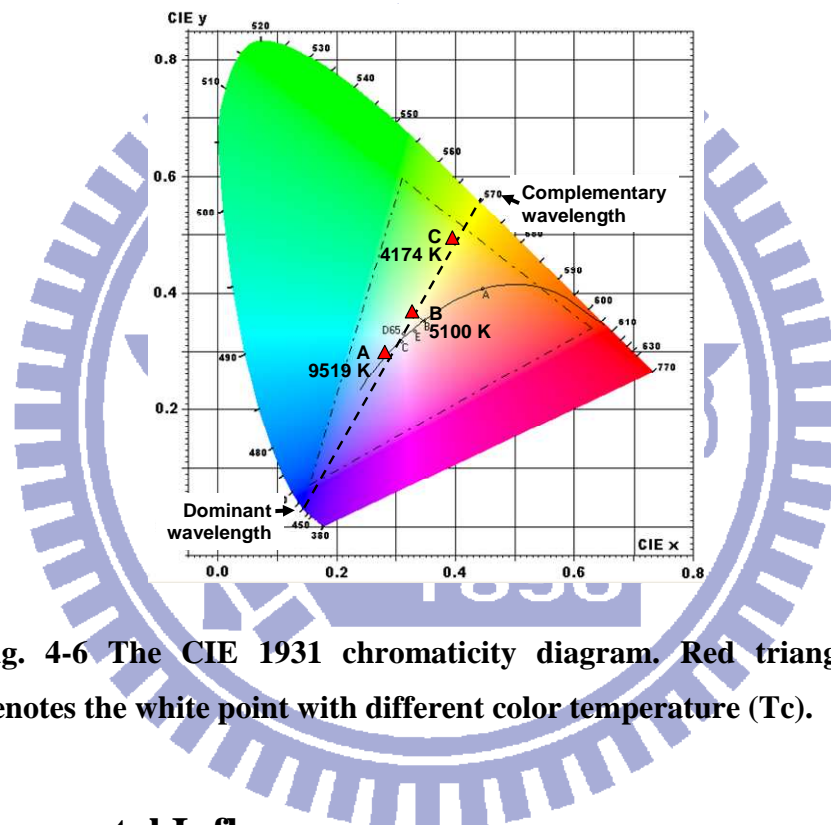


Fig. 4-6 The CIE 1931 chromaticity diagram. Red triangle denotes the white point with different color temperature (Tc).

4.4 Environmental Influence

In contrast with conventional approaches, PS yields an environmentally friendly and uniform phosphor coating. After PS process, the binder (silicone based) in slurry will be cured (100 °C heating for 4 hours) and the solvent (alkyl based) will be evaporated. However, the aforementioned EPD or self-exposure process uses ammonium dichromate ((NH₄)₂Cr₂O₇) ADC solution as a photosensitizer, producing Cr ions that can reduce the intensity of emitted light [43,44]. Additionally, ionic Cr is a hazardous substance in electrical and electronic equipments, which is restricted by the Restriction of Hazardous Substances (RoHS) directive.

Since EPD is performed using a water soluble photoresist in exposure reactions, polyvinyl alcohol ($[-CH_2-CH(OH)-]_n$) PVA and ADC in slurry can be introduced into the phosphor coating. When the photochemical oxidation of the PVA and the reduction of the ADC occur, cross-links are formed between the PVA chains, and the Cr^{3+} ions are generated by the reduction of the Cr^{6+} ion. Cr ions that are in the phosphor layer not only contaminate the irradiative recombination sites of phosphor, but also cause the light intensity to be low, since Cr^{6+} ions absorb light. However, the PS approach applies phosphor by exploiting mechanical principles without pollution risk of chemical reaction.

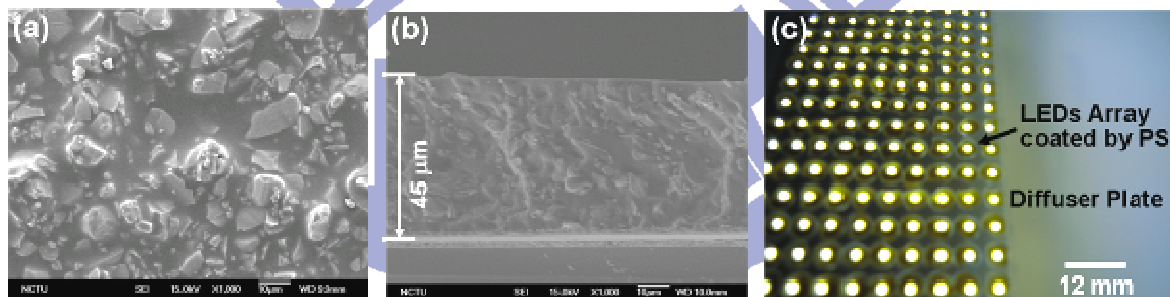


Fig. 4-7 SEM micrographs of phosphor coating using PS. (a) Top view; (b) cross-sectional view; (c) illuminated lighting module with phosphor coated by PS.

By EPD or self-exposure approaches, LED chips must be flip-chip mounted with a flat emitting surface [44]; the top of the LED chips must be free of wire bond pads. In contrast, LED chips that are coated by PS need not have a flat emitting surface, as shown in [Fig. 4-1(b)]. Although the surface of the diode is still connected using gold wires to an electrode pad, PS can be applied uniformly to the surface of LEDs. Figure 4-7(a) presents a top view of a PS coated LED with phosphor particles in the silicone binder. Figure 4-7(b) presents a cross-sectional view with an uniform mean coating thickness of 45 μm and the left side of [Fig. 4-7(c)] is an illuminated demonstration of LEDs array on board coated by PS scheme. The right side of [Fig.4-7(c)] is CPC covered with another diffuser plate to get a planar

illumination.

4.5 Summary

This investigation proposes a novel pulsed spray (PS) method of conformal phosphor coating (CPC) for LED illumination applications. The phosphor is applied directly to LED chips of the wire-bonded type. This approach is also applied to an array of blue LED chips as an inexpensive method with a high manufacturing throughput. The PS yields LEDs with superior optical characteristics including low color deviation ($\Delta u'v'$ of 0.07) when observed from various illumination angles (-60° to $+60^\circ$). Additionally, PS can yield a wide range of color temperatures (T_c) from 2500 K to 9500 K with high color accuracy, supporting a diversity of TFT-LCD backlights and general lighting applications. Meanwhile, unlike other coating schemes, such as dispensing, the settling method, spin coating, self-exposure and electrophoretic deposition (EPD), PS is a mechanical spray-based, environmentally friendly method that does not cause harmful ion pollution by chemical reactions. This investigation successfully demonstrates CPC by PS for future wLEDs lighting systems.

Chapter 5

High Efficiency LED Lighting Module using Remote Phosphor Scheme

5.1 Why Remote Phosphor

In recent years, wLEDs have become more important light sources of illumination in TFT-LCD BL and general lighting applications than conventional incandescent, fluorescent or halogen lamps, because wLEDs are compact, mercury-free, and energy-efficient [79,80]. However, in conventional wLEDs, phosphor is dispersed in an epoxy resin that surrounds the LED die [Fig. 5-1(a)]. Since the phosphor is close to the LED die in the wLEDs package, a significant proportion of the blue light is backscattered by the phosphor and lost by absorption by the LED chips [49-51]. Additionally, the high temperature of an operating wLEDs causes thermal quenching, which reduces the light radiation efficiency of the YAG phosphor and the InGaN blue LEDs [52,81]. Hence, the placing phosphor away from the die, as in a remote phosphor converter (RPC), has been developed to increase luminous efficiency [Fig. 5-1(b)]. The RPC method enables the backscattered photons to be extracted and the effect of thermal quenching to be reduced, increasing the ultimate overall light output and luminous efficiency [82,83].

Earlier studies have shown that RPC method can significantly improve the luminous efficiency of a single wLEDs package [53-55]. However, studies of the application of the RPC method to large-area illumination are relatively few. Conventional planar lighting herein has been developed by exploiting direct-emission using a diffuser plate [Fig. 1-3(a)] or edge-emission using a light guide plate (LGP) [Fig. 1-3(b)]. Direct-emission yields high luminance efficiency in lighting systems, while edge-emission is more suitable for the

application of thin module configurations. These approaches cannot easily support high luminous efficiency and a thin lighting module simultaneously. Therefore, the use of an array of blue LEDs to excite a remote yellow RPC film and generate an area of white light distribution is demonstrated herein. In this investigation, the optical characteristics of RPC lighting system are studied. Subsequently, a thin lighting module with high brightness, uniform luminance and low color deviation is proposed, providing as a planar lighting system. It can be used in a wide range of TFT-LCD BL and general lighting applications [84-88].

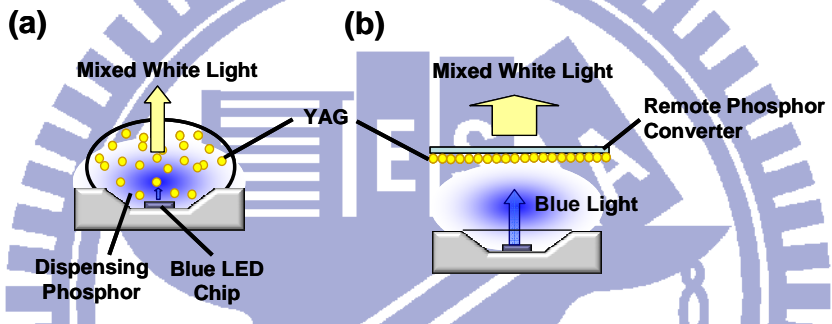


Fig. 5-1 Schematically depicts the packing method of LED. (a) The package of dispensing phosphor; (b) The package of remote phosphor.

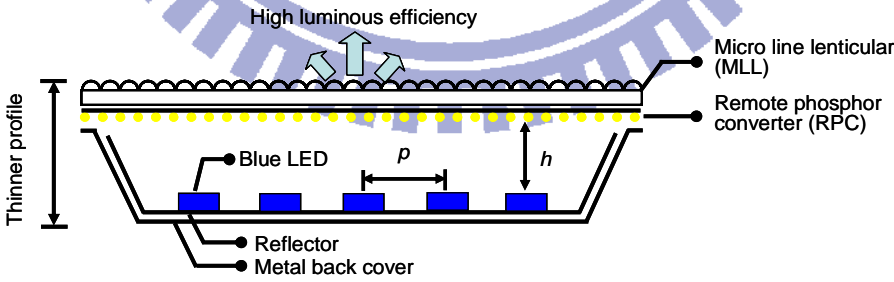


Fig. 5-2 The proposed light-emission system constructed by RPC.

5.2 Sample Preparation

This section elucidates the experimental components of a remote phosphor converter (RPC), the manufacturing method and the configuration of proposed lighting module.

The phosphor powder that was used in this experiment was a cerium-doped yttrium aluminum garnet (YAG:Ce³⁺) with a wavelength distribution (irradiating wavelengths of 490~ 680 nm). As show in [Fig. 3-1(b)], phosphor powder has an irregular morphology. The mean size of phosphor particles (D50) is 7.44 μm [Fig. 34-1(c)]. An indium gallium nitride (InGaN)-based blue LED, which emits a wavelength of 457 nm, is applied to excite YAG:Ce³⁺ phosphor and white light is generated by mixing these complementary colors.

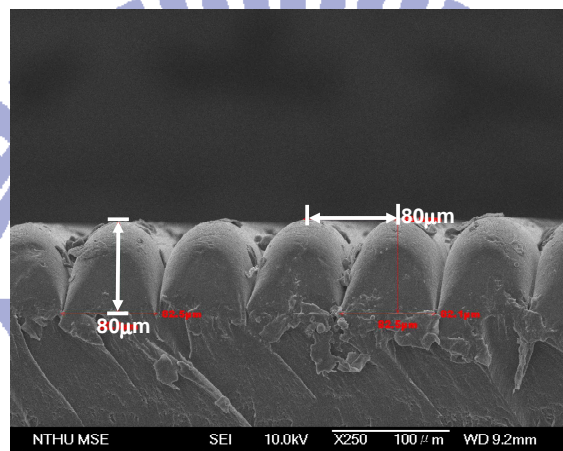


Fig. 5-3 The SEM picture of the plastic substrate with micro line lenticular (MLL) arrays. (pitch: 80 μm , height: 80 μm).

As shown in [Fig. 5-4(a)], the aluminum substrate that is used in the lighting module is 7inch diagonal. Blue LEDs are directly mounted on the substrate. The total input power of this lighting system is 28 V_{DC} at 150 mA and the power consumption is 4.2 W. Next, optical sheets using micro line lenticular (MLL) structure [Fig. 5-3] are exploited to integrate with the RPC film and blue LEDs light source in this experiment. As presented in [Fig. 5-4(b)], MLL structure along the y-axis can convert the light from an array of point LEDs into horizontal light. MLL along the x-axis can yield vertical light; crossed MLL can yield planar blue light to excite the assembled YAG RPC. The arrow-mark indicates the direction of the

MLL structure. MLL arrays are not only functional for the improvement of on-axis luminance, but also contribute to luminous distribution in this lighting module configuration.

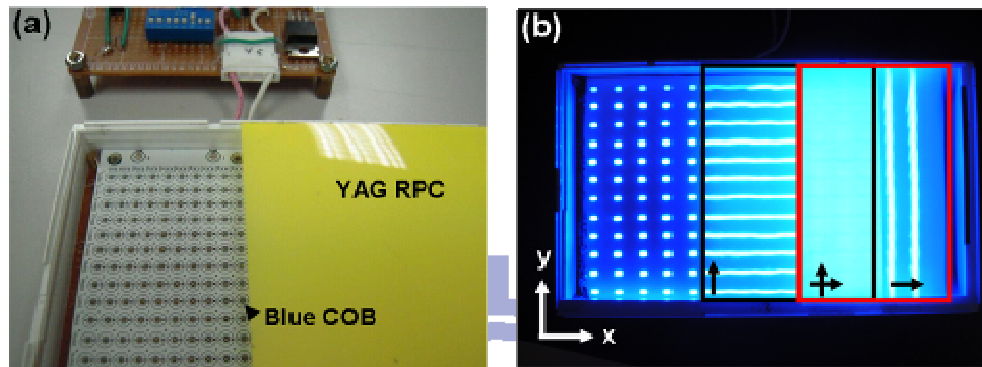


Fig. 5-4 (a) The lighting module integrates an array of blue LEDs with YAG RPC layer; (b) The obverse view of RPC coupled with two sheets of micro line lenticular (MLL) array (arrow marked the structural direction on MLL).

5.3 RPC Light-emission Measurement

The optical mechanism of the RPC method will be modeled as it differs from that of illumination by conventional wLEDs. Because of the complexity of the experiments, theoretical calculations will be made and a simulation model established to determine the values of the parameters LED gap (h) and LED pitch (p) [refer to Fig. 5-2], that optimize an RPC lighting system. Subsequently, a mockup sample that uses the RPC method will be demonstrated to achieve uniform luminous distribution when applied in an ultra-slim lighting module.

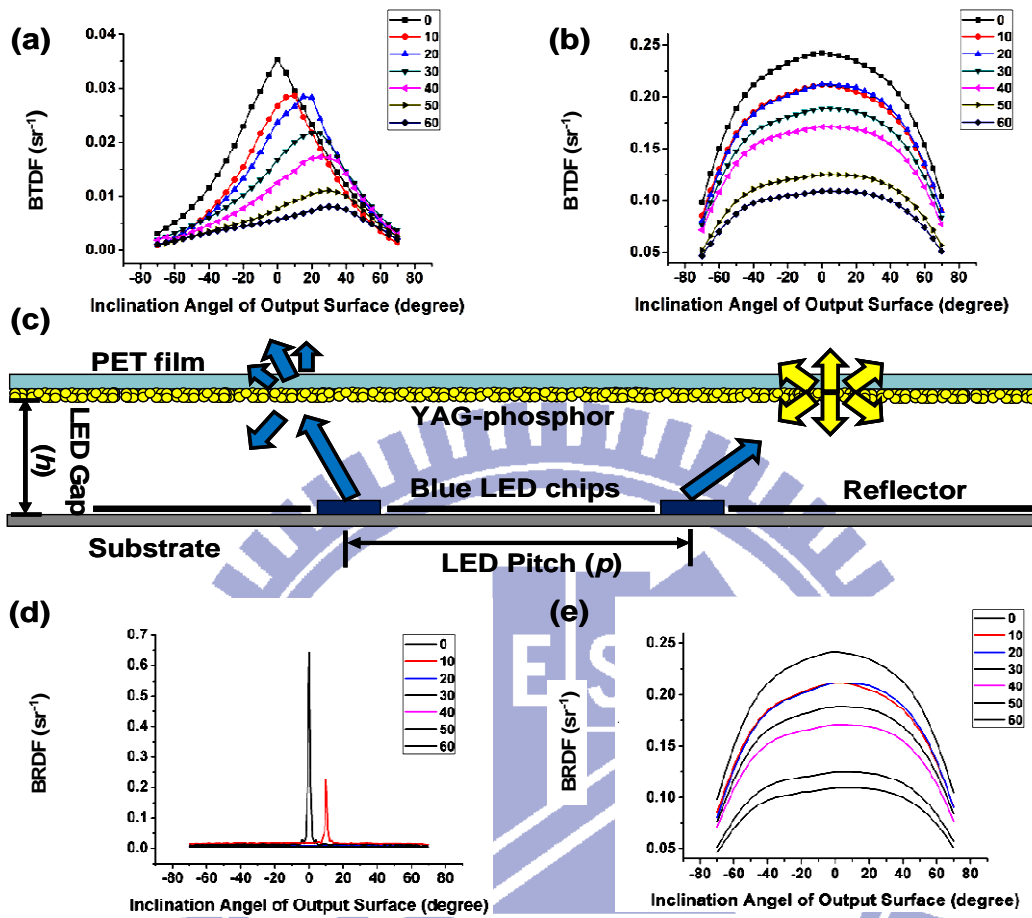


Fig. 5-5 Measured BTDFs result of (a) diffused blue light, (b) up converted yellow light; (c) light-emitting mechanism of RPC lighting system; measured BRDFs result of (d) reflected blue light, (e) down converted yellow light.

In the RPC lighting system, light scattering and light converting occur simultaneously, as presented in [Fig. 5-5]. The diffused blue light and the excited yellow light were measured separately in this experiment to identify the optical mechanism of RPC method, owing to these two kinds of lights with different light distribution. First of all, the optical characteristics of the RPC lighting system are described using bidirectional scatter distribution functions (BSDFs). The BSDFs is typically split into reflected and transmitted components, which are treated separately as the bidirectional transmittance distribution functions (BTDFs) and the

bidirectional reflectance distribution functions (BRDFs) [14,16,89].

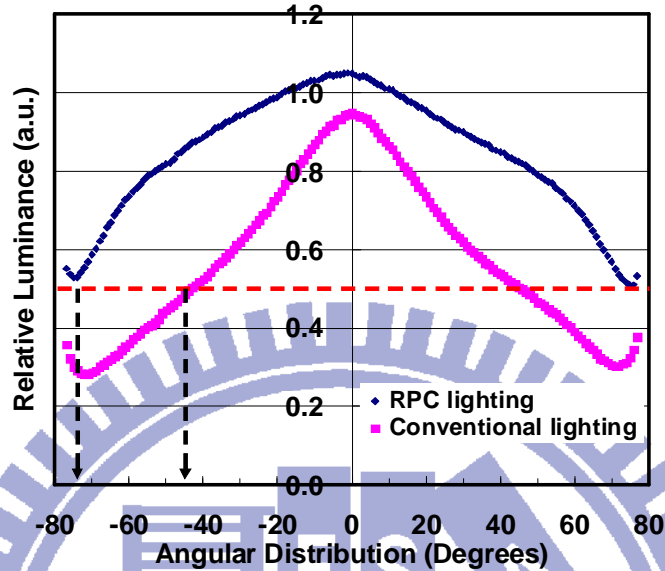


Fig. 5-6 The comparison of luminance in angular distribution, between conventional lighting and RPC lighting.

When the blue light radiated from LEDs to excite the RPC, some of the incident blue light are converted to yellow light with Lambertian distribution [Fig. 5-5(b)]. The rest of the incident blue light is diffused [Fig. 5-5(a)]. Figure 5-5(d) and (e) represent the reflective distribution of blue light and yellow light, respectively. Finally, these rays are mixed to generate a white light distribution with broad angular distribution [Fig. 5-6, blue line]. By these measured BTDFs and BRDFs results, the RPC method could be characterized to develop the light-emitting mechanism.

5.4 Theoretical Modeling

The optimal parameters of RPC configuration like LED gap (h) and LED pitch (p) are difficult to determine the relationship with luminous distribution. Therefore, we setup an

optical simulation model used light-emitting mechanism of RPC method to predict the optimal configuration. Firstly, the light-emitting properties of RPC could be characterized by the measured BTDFs and BRDFs. In order to simplify the analysis, we restrict the discussion to the transmitted type (BTDFs) [90]. Certainly, the investigation can be easily applied to the reflected type (BRDFs) without loss of generality. The BTDFs is defined as

$$\text{BTDFs}(\theta_i, \phi_i, \theta_t, \phi_t) = \frac{L_t(\theta_t, \phi_t)}{E_i(\theta_i, \phi_i)} \quad (5.4.1)$$

where E_i is the illuminance on the sample plane due to the incident blue-light; L_t stands for the luminance of emitted light from the sample surface. The incident and emitted angles are represented by the coordinates of (h, θ_i, ϕ_i) and (h, θ_t, ϕ_t) , where h , θ and ϕ denote the radius, zenith angle and azimuthal angles in spherical coordinate, respectively. Since the scattering characteristics of RPC caused by the randomly distributed phosphor are rotationally symmetric, the data processing of BTDFs can be simplified by merely considering the variance of zenith angle θ along a constant azimuthal angle $\phi = 90^\circ$.

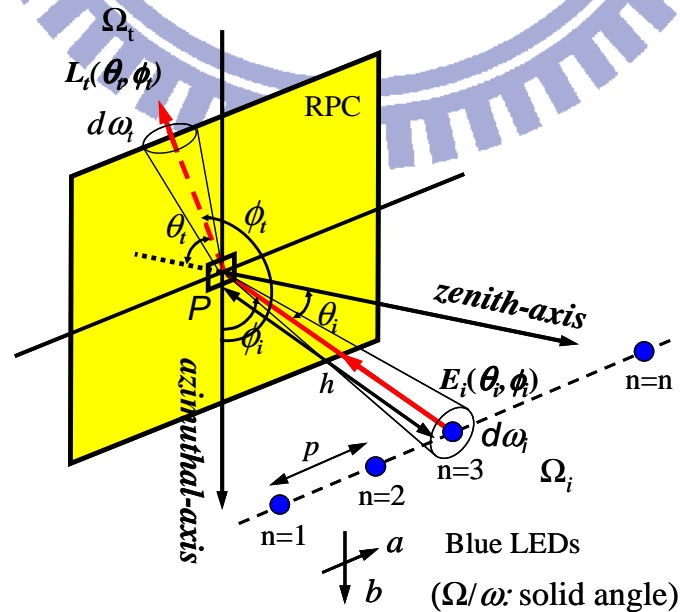


Fig. 5-7 The definition of photometric in this theoretical calculation.

There are four parameters of the RPC lighting configuration regarding the theoretical calculation: (a) the BTDFs of RPC, (b) the intensity distribution (I_s) of LED chips, (c) the LED gap (h), and (d) the LED pitch (p). Through the definition of photometric [Fig. 5-7], the illuminance (E_i) of the RPC at the point P excited by the blue light can be calculated as

$$E_i(\theta_i, \phi_i) = \frac{I_s(\theta_i, \phi_i) \cdot \cos^3 \theta_i}{h} \quad (5.4.2)$$

Then, the emitted luminance (L_t) from the RPC at point P can be transferred from Eq. (1) as

$$\begin{aligned} L_t(\theta_t, \phi_t) &= \int_{\Omega_i} \text{BTDFs}(\theta_i, \phi_i, \theta_t, \phi_t) \cdot E_i(\theta_i, \phi_i) d\omega_i \\ &= \int_{\Omega_i} \text{BTDFs}(\theta_i, \phi_i, \theta_t, \phi_t) \cdot \frac{I_s(\theta_i, \phi_i) \cdot \cos^3 \theta_i}{h} d\omega_i \end{aligned} \quad (5.4.3)$$

Finally, the total radiating luminance (L_{output}) from the RPC lighting system can be calculated by the convolution between the single LED luminance L_t and a two dimensional comb function as

$$L_{\text{output}}(\theta_t, \phi_t) = \sum_n \sum_m \left[\int_{\Omega_i} \text{BTDFs}(\theta_i, \phi_i, \theta_t, \phi_t) \cdot \frac{I_s(\theta_i, \phi_i) \cdot \cos^3 \theta_i}{h} d\omega_i * \delta(a - np, b - mp) \right] \quad (5.4.4)$$

where the counting number n and m indicate the n -th and m -th LED along a and b direction, respectively. In this case, the summation and integration were performed by Monte Carlo simulation [91].

Then, we import the measured BSDFs into the commercial software LightToolsTM to accomplish the optical simulation of RPC lighting system. In order to keep the luminous uniformity of lighting system as the first merit, the ratio (h/p) of LED gap (h) to the LED pitch (p) were modulated as parameter to simulate the relationship with luminous uniformity

(U_{PL}). The definition of U_{PL} refers to [Eq. 2.4.5].

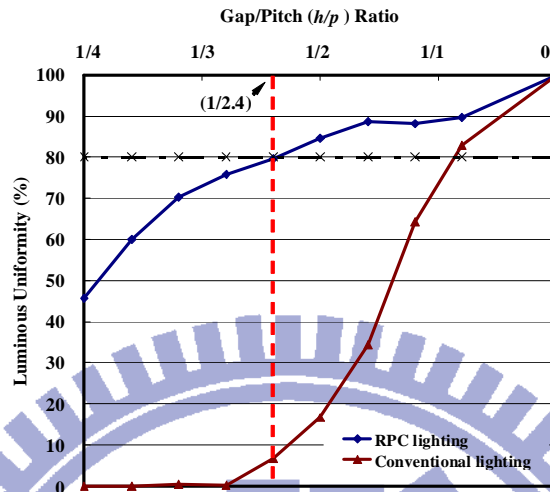


Fig. 5-8 The comparison of luminous uniformity (U_{PL}) with (h/p) ratio.

The simulated results are shown in [Fig. 5-8] to compare the conventional wLEDs lighting with the RPC lighting. The target of luminous uniformity is set at 80% to keep an acceptable vision quality [92,93]. The smaller LED gap (h) and larger LED pitch (p), the luminous uniformity is worse. The acceptable ratio (h/p) of RPC lighting by simulated result is (1/2.4).

5.5 Optimized Configuration and Luminous Uniformity

As a result of the phosphor particles inside the RPC are stacked with voids during coating [Fig. 3-5(b)], the air contained in the voids is easily to cause the light scattering. Therefore, the function of RPC is similar to a diffuser with a high haze value [Table 3-1] and contributes to thin the thickness of lighting system. Figure 5-5(a) shows the light distribution of transmitted blue light with diffusing characteristics. Moreover, the converted yellow light reveals a Lambertian distribution [Fig. 5-5(b)]. Then, these two type of lights are mixed

together and displays a broader angle of full-width at half-maximum, $\theta_{FWHM} = \pm 74^\circ$, subsequently contributing to reduce the lighting module thickness than with conventional lighting system by wLEDs, $\theta_{FWHM} = \pm 48^\circ$ [Fig. 5-6].

Additional, the cross MLL sheets integrates with RPC also contributes to luminous uniformity too [Fig. 5-4(b)]. A cross MLL sheets can achieve a planar and uniform blue light-emitting before exciting the RPC. Eventually, a broader θ_{FWHM} associated with planar blue light-emitting can contribute to the luminous uniformity of RPC lighting module.

Finally, the RPC lighting system is verified by a 7inch demonstrated sample and reveals a uniform luminous quality perfectly under ultra-slim lighting configuration without the use of conventional diffuser plate or light guide plate (LGP). [Fig. 5-9(b)]. The luminous uniformity of conventional lighting at $(h) = 5$ mm, $(p) = 12$ mm conditions (h/p ratio equals to $1/2.4$) demonstrate a luminous uniformity (U_{PL}) = 12% [Fig. 5-9(a)]. At the same situation, the RPC lighting can reach $U_{PL} = 82%$ [Fig. 5-9(b)].

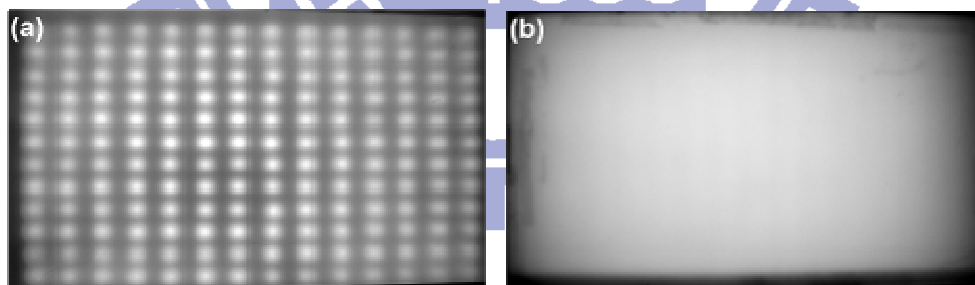


Fig. 5-9 The comparison of luminous uniformity (U_{PL}) at $(h) = 5$ mm and $(p) = 12$ mm. (a) conventional wLEDs lighting, (b) RPC lighting integrated with MLL sheets.

5.6 Color Temperature

The RPC method reportedly has a higher luminous efficiency than conventional

phosphor coating methods when applied to individual LED packages [53-55]. However, the applications at TFT-LCD backlighting and color performance of the RPC method have not been comprehensively explored. Therefore, the factors that affect the color temperature (T_c), angular color deviation ($\Delta u'v'$) of an RPC lighting system are analyzed herein.

This investigation will investigate such parameters as the thickness of the phosphor layer, the LED gap (h) and the LED driving current to elucidate their relationships with color temperature (T_c) of achieved using the RPC method.

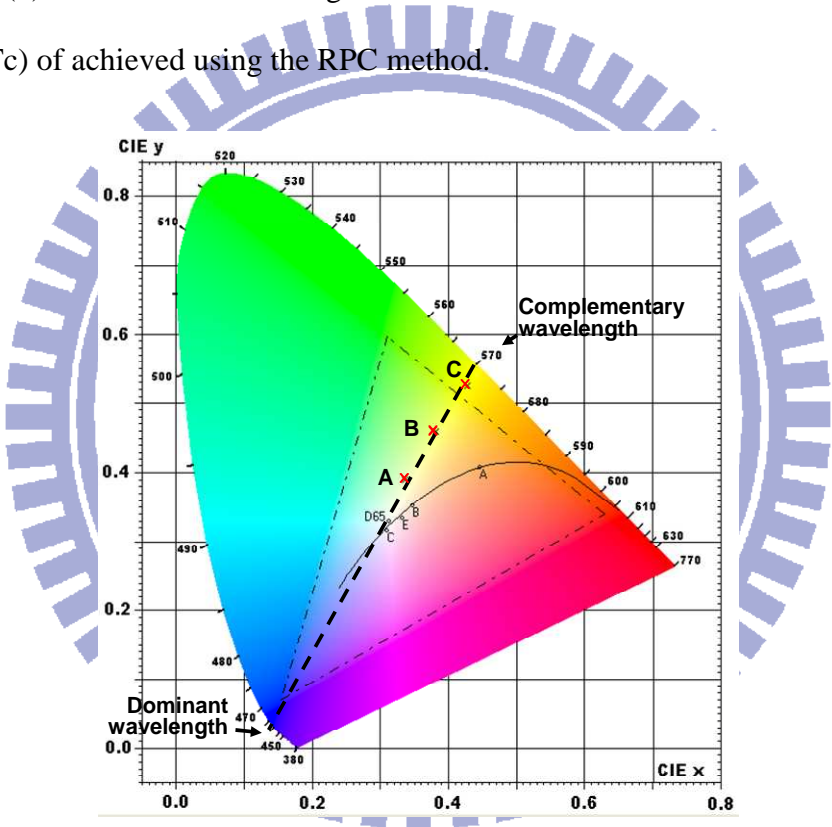


Fig. 5-10 The CIE 1931 chromaticity diagram. Red cross-mark denotes the white point with different color temperature (T_c).

As presented in [Fig. 5-10], white light that is forming by mixing blue lights (λ : 457 nm, dominant wavelength) and yellow lights (λ_p : 570 nm, complementary wavelength, where suffix p denotes peak wavelength) exhibits a linear function of chromaticity x against chromaticity y in CIE 1931 diagram. As the percentage of complementary light in the optical mixture increases, the white point moves along this line and toward the yellow side (low T_c ,

such as at point C). In contrast, as the percentage of the dominant wavelength increases, the white point moves to the blue side (high Tc, such as at point A). Experimental results [Fig. 5-11(a)] reveal that adjusting the thickness of the phosphor coating can change the ratio of yellow to blue light intensities. Point C corresponds to a thick phosphor layer (35 μm) with a high percentage of yellow light, and a Tc of 3854K. Point A corresponds to the low phosphor thickness (15 μm) with a high percentage of blue light, and a Tc of 5290K. The LED driving current is also investigated. Figure 5-11(b) indicates that Tc is unrelated to the LED driving current when the tested current is less than the maximum LED current rating (320 mA).

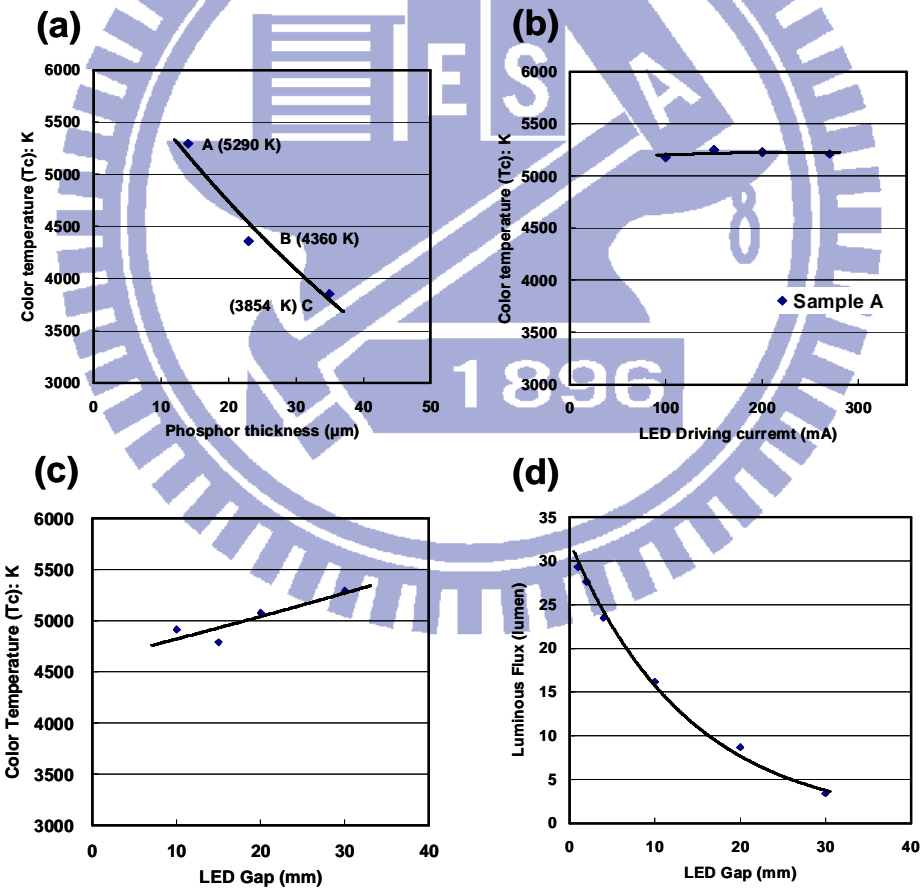


Fig. 5-11 Relationship between Tc and (a) phosphor thickness, (b) LED driving current, (c) LED gap. (d) The relationship of luminous flux with LED gap.

As presented in [Fig. 5-11(c)], the LED gap (h) affects the Tc of an RPC lighting system. As the LED gap (h) increases, Tc gradually increases. As the LED gap (h) increases, the luminous flux declines exponentially [Fig. 5-11(d)]. Therefore, the LED gap (h) in this investigation was kept less than 10 mm to maintain a high luminous flux. A small LED gap (h) also supports the design of ultra-slim modules too.

5.7 Angular Color Deviation

To evaluate the angular color deviation of RPC lighting system, the conoscopic approach is applied to measure the optical characteristics from varied viewing angle [Fig. 5-12(a)]. The zenith-axis is assumed to be the surface normal. The zenith angle (θ) and the azimuthal angle (ϕ) are varied from $\theta = -60^\circ$ to $+60^\circ$ and $\phi = 0^\circ$ to 360° in measurement, respectively. For the compared of conventional wLEDs lighting system with RPC lighting system, Figures. 5-12(b) and (c) plot the color distribution over the angular distribution in diagram of CIE 1976, respectively. The color deviation of a lighting system, $\Delta u'v'$ [Eqs. 2.5.5 & 2.5.6], is limited to 0.015 for commercial display applications, which must have no perceptible color deviation.

For conventional wLEDs lighting, the color deviation at various viewing angles is serious [Fig. 5-12(b)]. It comes from the dispensing of phosphor slurry onto the LED surface is easily delaminated by gravity before cured. The experimental $\Delta u'v'$ value reveals that the conventional wLEDs lighting yields a worse color spatial uniformity [Fig. 5-12(b), $\Delta u'v' = 0.098$] than does the RPC lighting system [Fig. 5-12(c), $\Delta u'v' = 0.025$]. Meanwhile, Figures. 5-12(d), (e) and (f) compared the spectral properties between point X ($\phi = 0^\circ$, $\theta = 0^\circ$) and point Y, Y' ($\phi = 0^\circ$, $\theta = 60^\circ$) of tested lighting systems.

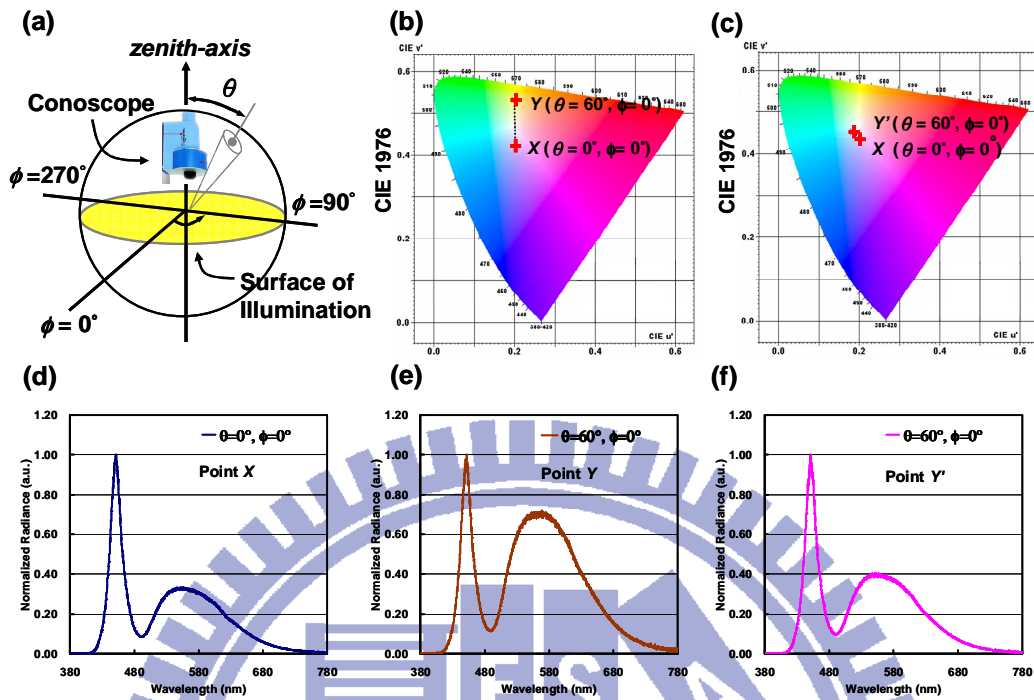


Fig. 5-12 (a) The measurement of optical characteristics by conoscopic approach. The color distribution of (b) conventional wLEDs lighting system, (c) RPC lighting system when view angle varies from $\theta=0^\circ$ to $\theta=60^\circ$ at fixed $\phi=0^\circ$. (d) The spectral properties of both conventional and RPC lighting at view point of $\theta=0^\circ$, $\phi=0^\circ$. The spectral properties of (e) conventional wLEDs lighting system, (f) RPC lighting system at $\theta=60^\circ$, $\phi=0^\circ$.

For conventional lighting, the portion of yellow light increase when the viewing angle (θ) increase from $\theta=0^\circ$ to $\theta=60^\circ$ [compared Fig. 5-5(b) & (d)]. It causes the illuminated white light with a yellow ring at large light-emitting angle. Comparatively, RPC method indicates less increase of yellow portion [compared Fig. 5-5(b) & (f)] and revealed a low color deviation [Fig. 5-12(c)]. Therefore, the RPC lighting system allows the accurate control of color distribution for high-quality illumination applications. Table 5-1 makes an optical comparison of these two types lighting at Tc around 9500K.

Eventually, when the RPC lighting combines with TFT-LCD panel (with 4.5%

transmittance), the high performance display can be achieved. It integrates the slim feature of conventional edge-emission lighting and the high luminance of direct-emission backlighting. The volume of the proposed TFT-LCDs configuration can be reduced to 9.5 mm without deteriorating the optical behavior, the luminance is 504 cd/m^2 at 7inch size, and the luminous efficiency is 12.8% higher (64.71 lm/W to 72.99 lm/W) than those of a conventional wLEDs lighting system. Additionally, the power consumption is 4.2W.

Table 5-1 Optical comparison between conventional lighting and RPC lighting.^{a,b}

	Cx	Cy	Tc (K)	$\Delta u'v'$	Central Luminance (cd/m^2)	Efficiency (lm/W)
RPC lighting system	0.280	0.300	9487	0.025	504	72.99
Conventional wLEDs lighting system	0.287	0.286	9364	0.098	447	64.71

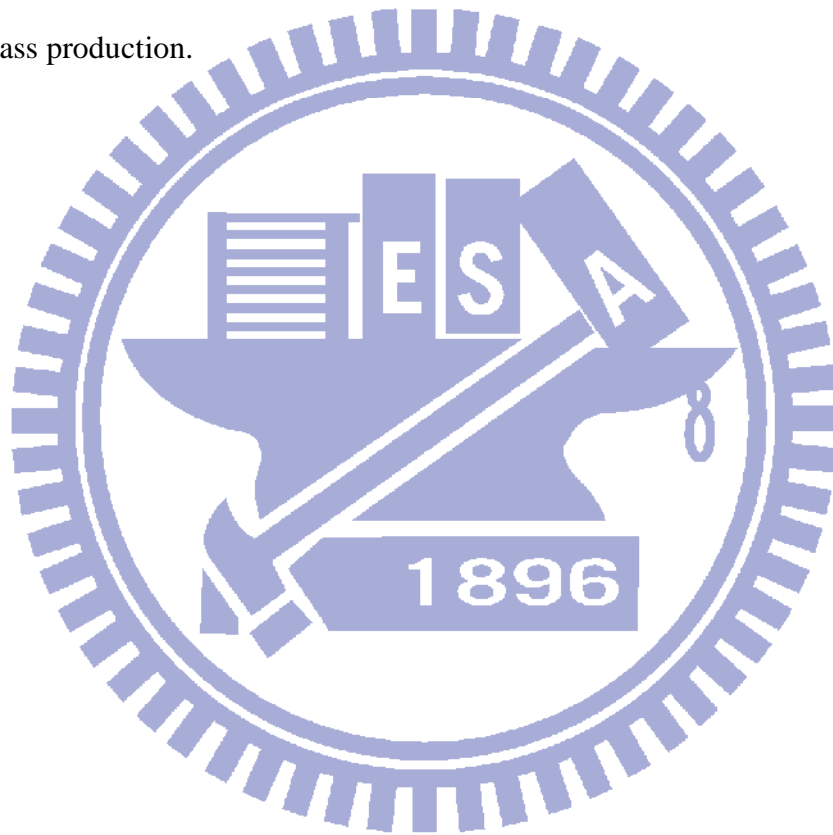
^aPower consumption: 4.2W; TFT-LCD panel with 4.5% transmittance, color gamut: 72% NTSC

^bConventional lighting system and RPC lighting system use the same specifications of blue LEDs & phosphor.

5.8 Summary

This work presents a novel lighting system that is constructed from a yellow YAG:Ce^{3+} phosphor film and placed away from the blue LED light source. Unlike a conventional wLEDs lighting system, the proposed configuration can yield less angular color deviation ($\Delta u'v' = 0.025$), higher luminous efficiency (72.99 lm/W) and uniform luminous distribution ($U_{PL} = 82\%$) at an ultra-slim structure (module thickness 9.5 mm) for TFT-LCD backlighting or general lighting applications. Most importantly, the configuration is without the use of conventional diffuser plate or light guide plate (LGP). Meanwhile, the optical simulation by Monte Carlo is used to predict an optimal LED gap (h) to LED pitch (p) ratio of ($h/p = 1/2.4$)

and successfully been demonstrated by a 7inch backlight at (h)=5 mm and (p)=12 mm conditions. Additional, the RPC lighting assembled with TFT-LCD panel (with 4.5% transmittance) can achieve a display with luminance of 504 cd/m² at power consumption of 4.2 W. Therefore, an RPC lighting system with strong optical performance in a compact module can be obtained. Furthermore, the use of slot-die coating to prepare RPC is also an inexpensive process with high manufacturing throughput, thus can be possible for an economical mass production.



Chapter 6

Ultra Slim Dual-sided Display System using UV-excited Fluorescent Lighting (UFL)

6.1 Why Dual-sided Display

The great diversity of future display applications, such as digital signage and public information displays, among others cannot all be based on single-sided LCDs. Dual-sided display can create added value in public spaces like shopping centers, stations, airports and etc., by way of running two displays synchronously [108]. Conventionally, two sets of single-sided LCDs are installed back-to-back to display in two directions, as presented in [Fig. 6-1(a)]. The occupied volume is very large; the system is heavy, thermal release is poor, and power consumption is high. Therefore, a LCD system with dual-sided screens is studied by several research teams [109,110]. As presented in [Fig. 6-1(b)], this work constructs a novel lighting inside dual-sided LCD system with symmetrical illumination. In order to reach uniform display performance, this illumination should irradiate light in two opposite surface brightly and uniformly.

When conventional light sources (such as fluorescent lamps (FLs) or LEDs) are used in dual-sided illumination system, the elimination of metal back holder and optical reflector [compare Fig. 6-1(a) & (b)] from single-sided BL affect not only the uniformity of light distribution, but also the dissipation of the large amount of heat that is generated by plural light sources. The elimination of the optical reflector causes a lack of reflected light, such that a dark area exists between the light sources. Accordingly, the light is not distributed uniformly. Additionally, the remove of metal back holder will lose the thermal releasing by thermal conduction mechanism. Hence, ultraviolet excited flat lighting (UFL) is employed in

this work as a solution of dual-sided lighting system [111,112].

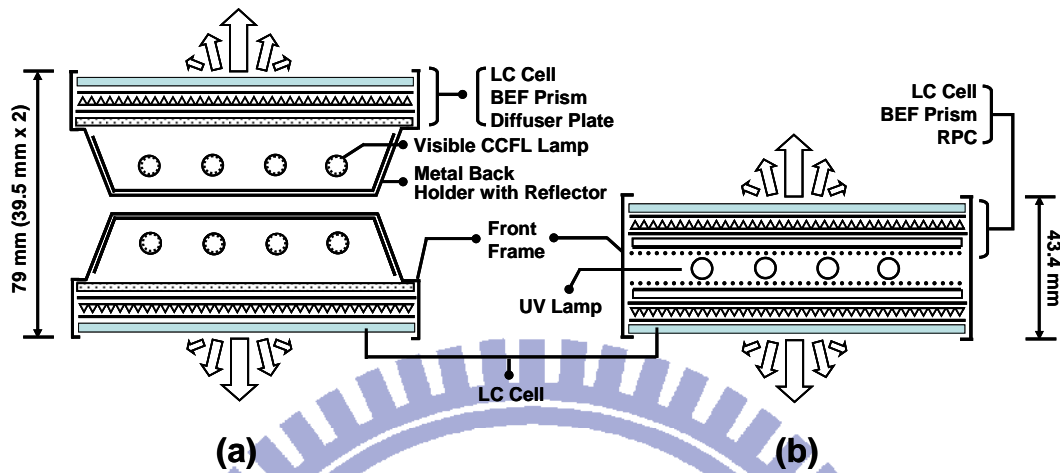


Fig. 6-1 Dual-sided application constructed by (a) A conventional pair of single-sided display applied back-to-back; (b) UFL dual-sided display.

6.2 What UV-excited Flat Lighting (UFL)

UFL scheme is based on a direct-emission BL configuration with a UV light source to excite phosphor film placed remotely. Characteristics of the UFL scheme, *e.g.*, luminous uniformity, luminance, slim configuration, color uniformity and color saturation are discussed. Such features are especially attractive for large scale TFT-LCD applications. With respect to UFL BL, the 254 nm wavelength is irradiated by UV lamps. The UV rays are then converted by RPC to achieve a visible, uniform and planar light distribution. Therefore, the UFL could yield a thinner backlighting system than that of the conventional direct-emission BL with CCFL or a wLEDs light source.

The proposed UFL BL design can also ensure an adequate uniformity and lifetime of phosphor coating. For conventional CCFL lamps, uniformity of phosphor coating inside the lamp tube by siphon theorem worsens with an increasing lamp tube size. Meanwhile, the ion

bombardment and 185 nm UV deteriorate the phosphor coating, subsequently decreasing the lifetime of CCFL lamps [105-107]. However, in this work, phosphor is coated using slot-die coating [Figs. 3-7 & 3-8] and has a longer lifetime than in conventional CCFL lamps owing to its ability to prevent phosphor from contacting with a vapored mercury atom and 185 nm UV wavelength radiations directly. Therefore, UFL scheme allows for phosphor to achieve uniform coating and a long lifetime simultaneously when applied to large scale display applications.

6.3 Experimental Indices Definition

According to [Fig. 6-2], the included angle (δ) denotes that the angle of neighboring adjacent lamps is linked to point “O” located on the bottom surface of the diffuser plate and in the central position of two lamps. Notably, a large (δ) implies a distant pitch (P) or a close gap (d).

The mechanical configuration and luminous uniformity of lighting system were evaluated by defining the included angle (δ) and the 9-points planar luminous uniformity (U_{PL}) as [Eqs. (6.3.1) & (2.4.5)], respectively:

$$\text{Included Angle, } \delta = 2 \tan^{-1} \left(\frac{P}{2d} \right) \quad (6.3.1)$$

By using triangular relations, (δ) is then determined by the function of lamp gap (d) and lamp pitch (P), as shown in [Eq. (6.3.1)]. In our experiment involving 42-inch BL, (δ) represents 135° ($P= 24.6$ mm, $d= 5.1$ mm).

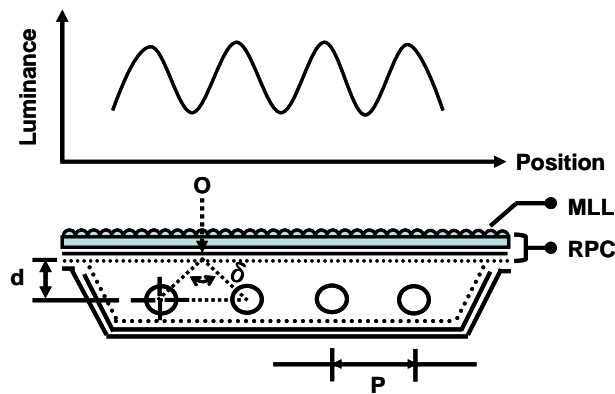


Fig. 6-2 Schematic relations between the included angle (δ) and luminous distribution in the entire illumination area.

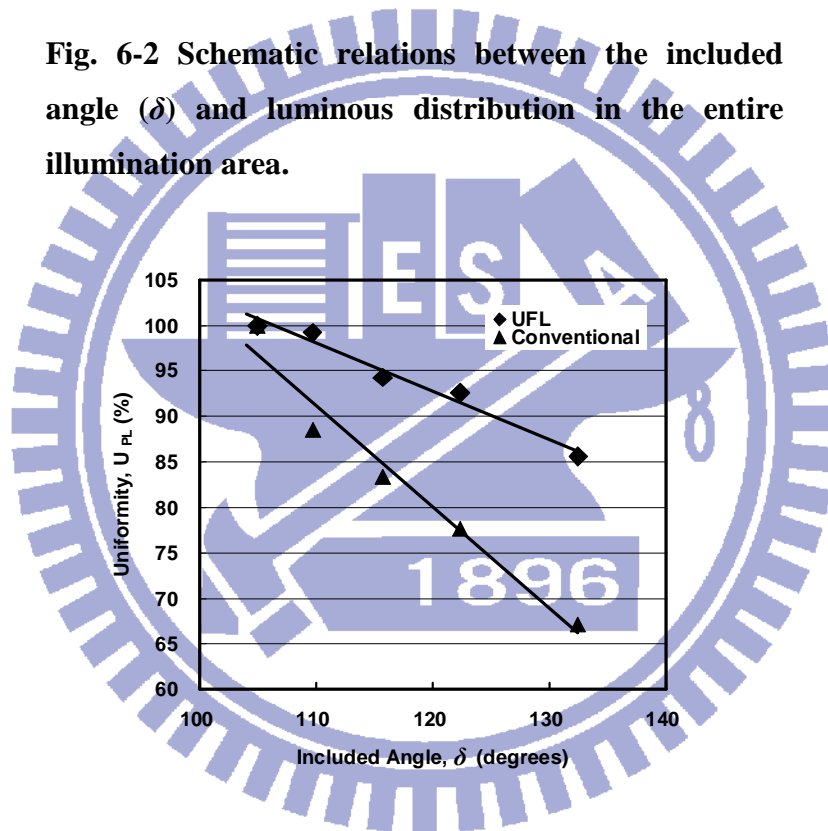


Fig. 6-3 The relationship between (δ) and (U_{PL}) according to UFL and conventional direct-emission BL system.

These equations are also appropriate for a lighting system with a CCFL or LED type light source. In this investigation, however, the light source focuses mainly on the UV lamp since 254 nm UV-LED is insufficient for practical applications.

According to **Fig. 6-3**, (δ) 105° represents a point in which UFL BL must have luminous uniformity superior to that of conventional direct-emission BL system. Varying (δ) from 105°

to 135° ensures that UFL BL always displays a better uniformity (U_{PL} : 86%) than conventional direct-emission BL (U_{PL} : 67%). When (δ) exceeds 120° , the (U_{PL}) of conventional direct-emission BL is 79% and may not satisfy BL application requirement. The variation of illumination is maintained under an average value of $\pm 15\%$ to ensure uniformity (U_{PL}) of at least 85% for large scale TFT-LCD applications [100].

6.4 Sample Preparation

In this experiment, UV was applied to a UFL lighting system to ensure satisfactory dual-sided display. Since the UV LED light sources cannot be produced efficiently, mercury vapor lamps are used to produce UV radiation in this work. The lamp is chosen to ensure the efficient conversion of UV rays with a wavelength of 254 nm. For UFL with a remote phosphor converter (RPC), Huang et al. have revealed the experimental procedure related to the manufacturing of the samples [103,104]. To form RPC plate, trichromatic phosphors were blended and then applied on PMMA substrate by slot-die coating method.

In the proposed dual-sided lighting system [Fig. 6-1(b)], UV irradiates two opposite RPC plates' surfaces and is converted into visible light. Moreover, the phosphor prescription eliminates irradiation at wavelengths of 590 nm and 490 nm, achieving a high color rendering (HCR) at 92% of the NTSC standard [31] for digital signage applications with vivid color distributions. Additionally, UFL lighting reportedly yields high luminance uniformity, high brightness, compact configuration, low power consumption, and a long lifetime [104,104].

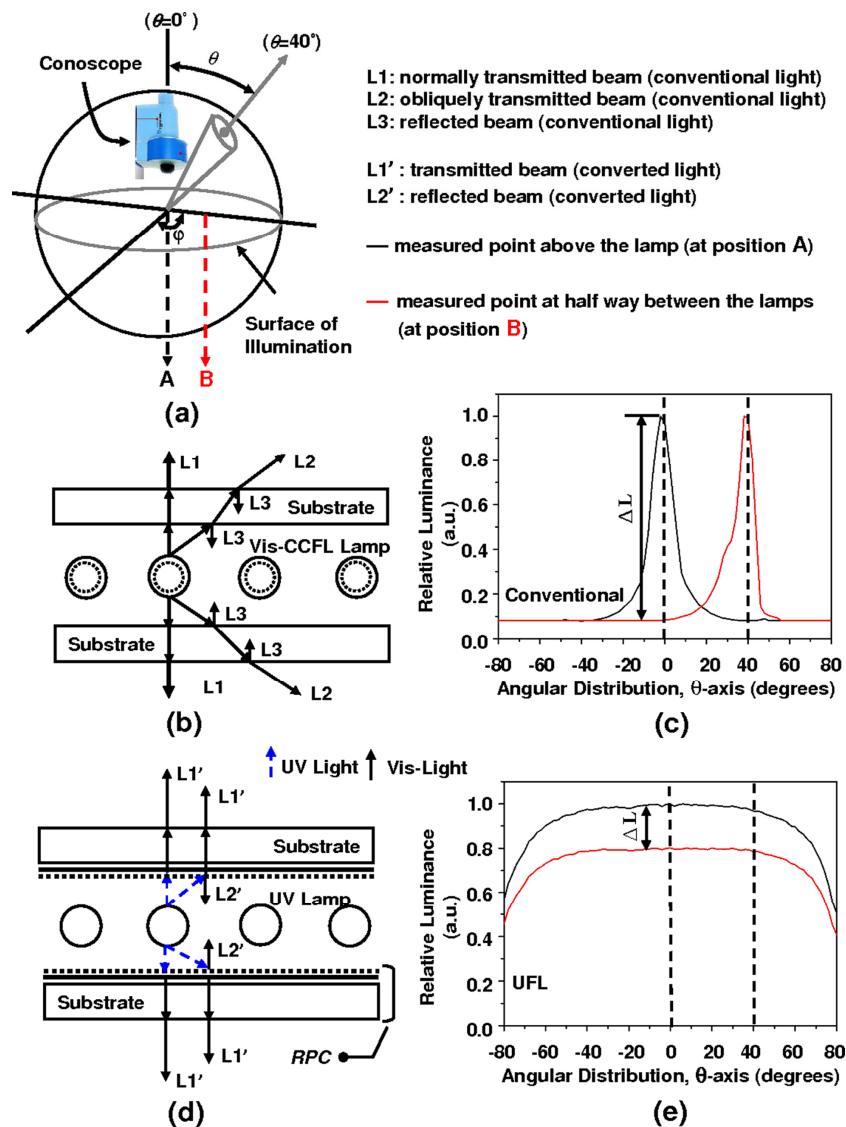


Fig. 6-4 (a) Measurement construction of angular-luminance distribution. (b) & (c): ray tracing and luminous distribution of FLs dual-sided illumination. (d) & (e): ray tracing and luminous distribution of UFL illumination.

6.5 Luminous Uniformity Analysis

Figure 6-5 demonstrates the luminous uniformity simulation result using [Eq. 5.4.4] by LighToolsTM. The predicted uniformity (U_{PL}) by [Eq. 2.4.5] can be over 90%. As a result of the undesirable lamp mura is difficult to eliminate by using conventional direct-emission

structure for slim backlight. **Figure 6-6(f)** displays the quality of UFL BL without undesirable lamp mura-related phenomena issue when compared with conventional direct-emission BL **[Fig. 6-6(c)]** at the same parameters of $(\delta) = 135^\circ$ and $(d) = 5.1 \text{ mm}$. Obviously, UFL BL can alleviate undesirable lamp mura-related issue, and thus, slim thickness with uniform luminance distribution can be achieved. According to **[Fig. 6-6(d)]**, the luminance difference of UFL BL is smaller than that of conventional direct-emission BL at the same (δ) , as shown in **[Fig. 6-6(a)]**. By ray tracing analysis, conventional direct-view BL shows the Lambertian distribution center of visible light located on the lamps **[Fig. 6-6(b)]**.

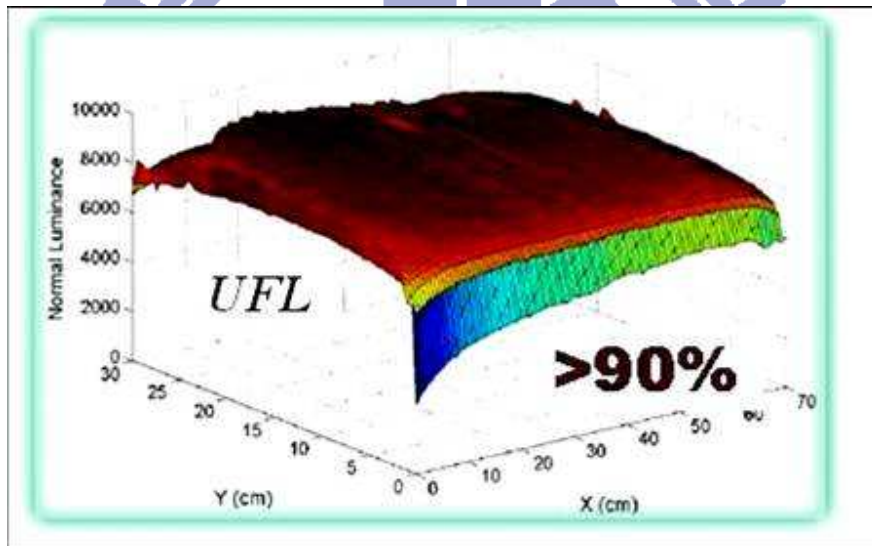


Fig. 6-5 The luminous uniformity simulation result.

UFL BL exhibits a trend in which the visible light Lambertian distribution center moves from lamps to the remote phosphor layer **[Fig 6-6(e)]**. Therefore, for UFL BL system, the entire surface of RPC (includes the area between the lamps) has visible light irradiation with Lambertian distribution and the luminance difference between lamps can be eliminated effectively.

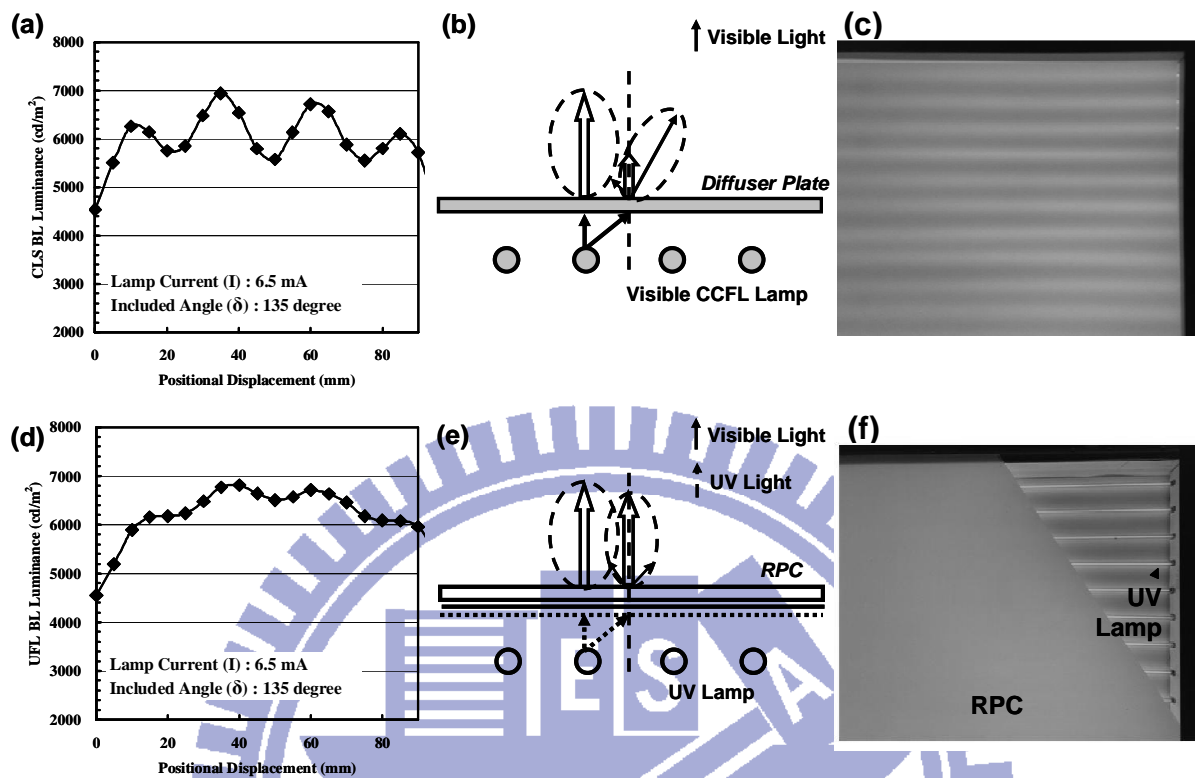


Fig. 6-6 The BL luminance in spatial distribution, ray tracing and luminous uniformity of the experimental samples at $\delta= 135^\circ$, $I= 6.5$ mA. (a), (b) and (c) represent conventional direct-emission BL; (d), (e) and (f) represent UFL BL.

6.6 Dual-sided Displays

The optical characteristics of the dual-sided display are verified using 42-in configurations of UFL lighting and FLs lighting. The angular-luminance distribution was measured using the conoscopic [89] approach [Fig. 6-4(a)]. Firstly, measurements are made at position (A), the area above the lamp, and then the conoscope is moved to position (B), in the area half way between the lamps. Figures 6-4(b) & (c) trace the rays and plot the luminous distribution of FLs lighting in a dual-sided illumination sample. Figures 6-4(d) & (e) present the optical behavior of an UFL-illuminated sample.

Ray tracing for FLs illumination [Fig. 6-4(b)] reveals that the normally transmitted beam

(L1), which is in the direction of the incident beam, is the strongest ray at position (A). In contrast, the reflected beam (L3) is weak at position (B), when observed at $\theta = 0^\circ$ direction. By the same rules as were applied to the case of UFL dual-sided illumination [Fig. 6-4(d)], the transmitted beams (L1') are all normal to the illuminated surface at both positions (A) and (B). The L1' are also associated with reflected beams (L2'), which illuminate the dark area at position (B).

The luminous distribution at positions (A) and (B) when $\theta = 0^\circ$ (normal view) is compared with that at $\theta = 40^\circ$ (oblique view). Under FLs illumination [Fig. 6-4(c)], the relative luminance at position (A) is higher and that at position (B) is lower when observed at $\theta = 0^\circ$. Similarly, the relative luminance is lower at position (A) and higher at position (B) when observed at $\theta = 40^\circ$. Large luminance difference (ΔL) causes the non-uniform luminance distribution (lamp mura). However, in UFL dual-sided illumination [Fig. 6-4(e)], a slight ΔL between positions (A) and (B) exist at both $\theta = 0^\circ$ and 40° . Therefore, dual-sided UFL illumination can eliminate undesired lamp mura by light conversion over a complete RPC surface with Lambertian distribution. Uniform luminance is achieved without the use of optical reflectors. Figure 6-7 demonstrates the luminous distribution of dual-sided illumination by FLs lighting and by UFL lighting.

Table 6-1 The comparison of different dual-sided display.

	Dual-sided display (back-to-back installation)	UFL dual-sided display	Improvement
LCD Weight	30 kg	15 kg	50%
LCD Thickness	79.0 mm	43.4 mm	45%
Power Consumption	350 W	245 W	30%
Lamps number (piece)	40	22	--
Luminance	527 cd/m ²	567 cd/m ²	8%

Figures 6-7(c) & (d) is a construction of 42-in, dual-sided UFL illumination. When this illumination is combined with two TFT-LCD panels with 4.5% transmittance, the dual-sided display can provide an average luminance of 567 cd/m^2 . The total power consumption is 245 W. Table 6-1 summarizes the UFL dual-sided display features and compares them with those of a conventional pair of single-sided displays applied back to back. The UFL dual-sided display has luminous uniformity of 92% at a small module thickness of as low as 43.4 mm (The backlighting module thickness is 28.8 mm, referred to Fig. 6-8). It reduced the volume by 45% and the weight by 50% because of the removal of the metal back holders and simple optomechanical construction. The power consumption is reduced by 30% by less number of lamps adopted (40 to 22 pieces). Additionally, the resulting color gamut reaches 92% of the NTSC standard.

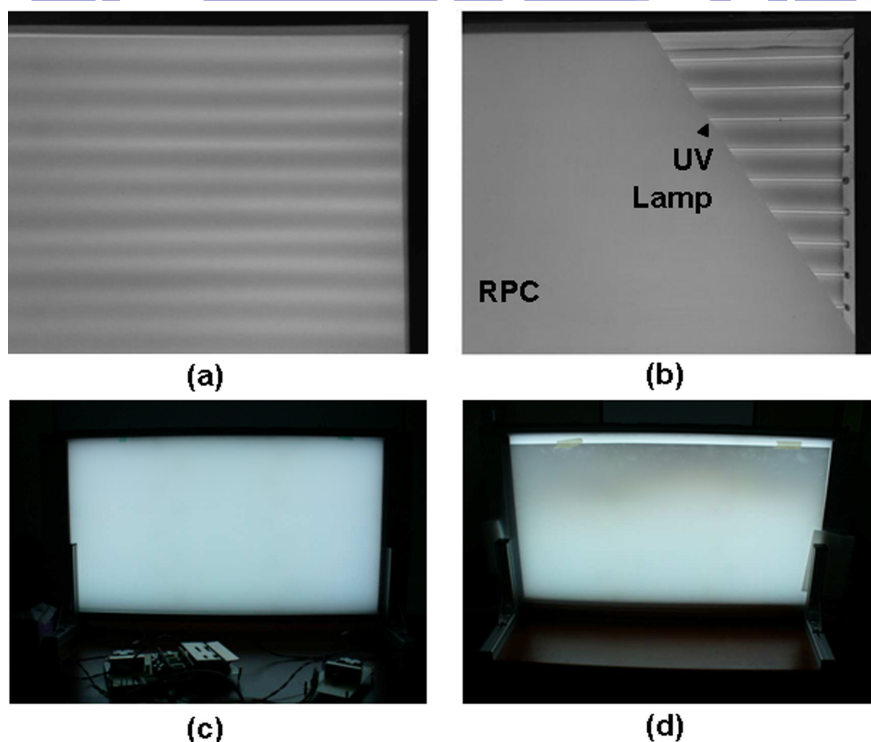


Fig. 6-7 Luminous distribution of dual-sided illumination (a) FLs lighting; (b) UFL lighting, (c) UFL front view, (d) UFL back view.



Fig. 6-8 Ultra-slim dual-sided backlighting module (28.8 mm thickness).

6.7 Thermal Releasing Analysis

In a UFL dual-sided display, the metal back holder that is used in a single display is removed. In conventional single-sided FLs BL, the metal back holder was considered to release the heat from the lamps by thermal conduction mechanism. The most popular metal back holder material is aluminum, which has a thermal conductivity of 237 W/m·K. This material is therefore a good thermal conductor. However, in our proposed structure, there is no metal back holder. There are two RPC plates which are plastic with a low thermal conductivity of 6 W/m·K, were placed on both sides of UV lamps. Therefore, the thermal releasing mechanism from the RPC plates has to be analyzed. According to prior report [113], the thermal emissivity (ϵ) of a plastic plate is 0.94 and that of a metal is 0.22. The equation of thermal radiation power, P_{RAD} , is expressed as follows:

$$P_{\text{RAD}} = \sigma \epsilon (A) T^4 \quad (6-6-1)$$

where σ denote the Stefan-Boltzmann constant, ϵ denote the thermal emissivity, (A) denote the radiation area and T denote the absolute temperature. From [Eq. (6-6-1)], thermal

radiation dominates the thermal release from a UFL dual-sided display because the radiation area (A) is doubles that of a conventional single-sided display.

A computational fluid dynamic tool, FloTHERM[®], and a thermal infrared camera, FLIR[®], are adopted to analyze the thermal distribution of experimental displays. Due to the poor thermal conductivity of the plastic composite plate, dual-sided display lost good thermal conduction mechanism; hence, thermal radiation of plastic composite plate will be evaluated for thermal releasing. Therefore, in a dual-sided UFL display the main thermal releasing mechanism is thermal radiation. From thermal simulation result, dual-sided UFL lighting system with Aluminum extrusion frame can perform better uniform thermal distribution compared with original single sided backlight design, as shown in [Fig. 6-9]. The variation in color represents the thermal distribution of the display. A low and uniform thermal distribution was expected across the display. Afterwards, the temperature variation (ΔT) is defined as

$$\Delta T = T_{\max} - T_{\min} \tag{6-6-2}$$

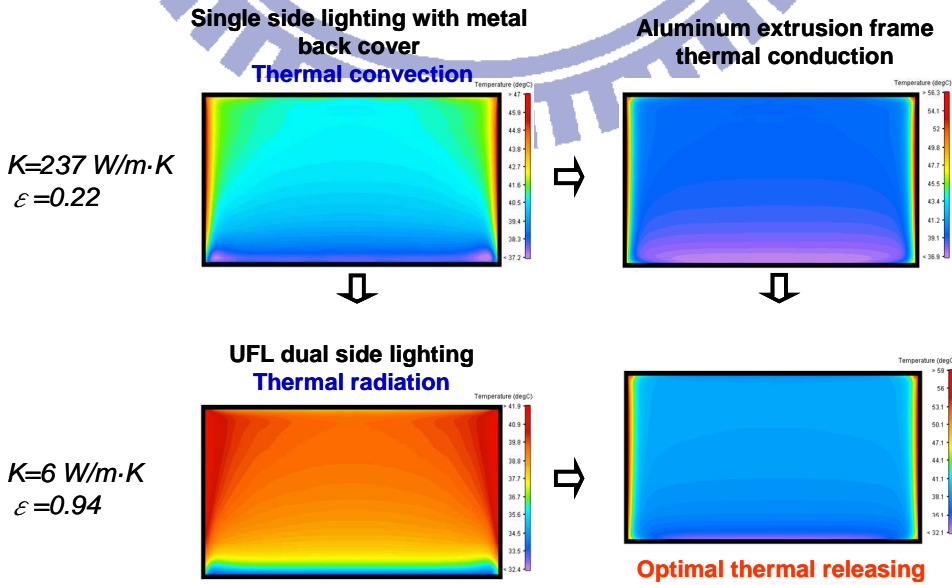


Fig. 6-9 Thermal simulation by FloTHERM[®].

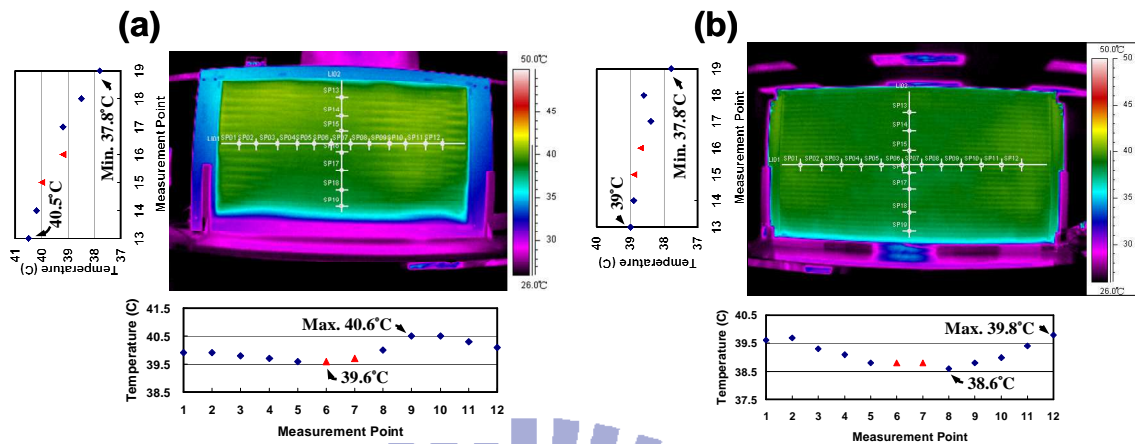


Fig. 6-10 Thermal distribution measurement by FloTHERM[®] regarding (a) FLs dual-sided BL; (b) UFL dual-sided BL.

Table 6-2 Comparison of measured temperature of conventional single-sided display with UFL UFL dual-sided display.^a

	ΔT	Top surface of display	Metal back holder	Inside the illumination
single-sided display	2.8°C	40°C	47°C	53.9°C
UFL dual-sided display	2.0°C	38.9°C	--	52.2°C

FLIR[®] measured result agrees with thermal simulation prediction. The thermal radiation mechanism from UFL dual-sided BL yields a lower temperature variation ($\Delta T = 2.0$ °C) compare with the thermal conduction mechanism in a conventional single-sided BL ($\Delta T = 2.8$ °C). Moreover, the single-sided BL also reveals a higher metal back holder temperature (47.0 °C). **Table 6-2** presents the temperature measured in practice using T-type thermocouples at an ambient temperature of 25 °C. (Power supplies to both BL were 245 W). The data indicate that the UFL dual-sided display has a lower top surface temperature (38.9 °C) than that of conventional single-sided display (40.0 °C), and the temperatures inside of the UFL lighting are also lower (52.2 °C < 53.9 °C). These data indicate that thermal radiation mechanism can

efficiently release heat from the UFL dual-sided display when compared with thermal conduction mechanism of conventional single-sided display.

6.8 Summary

In summary, UFL dual-sided scheme effectively eliminated the dark area between lamps, yielding a symmetrical, dual-sided illumination without the need for conventional optical reflectors. The UFL dual-sided display can yield a brightness of 567 cd/m^2 , with a luminous uniformity of 92% and a color gamut of 92% NTSC. It perfectly satisfies the optical requirement for display applications. The thickness is 45% lower (79.0 mm to 43.4 mm); the weight is 50% lower (30 kg to 15 kg) and the power consumption is 30% lower (350 W to 245 W) than those of a conventional pair of single-sided displays applied back-to-back. The mechanism of thermal radiation from the UFL dual-sided system can replace the conventional thermal conduction mechanism, lowering the temperature both on the surface ($38.9 \text{ }^\circ\text{C}$) and inside ($52.2 \text{ }^\circ\text{C}$) the illumination system without thermal accumulation. Consequently, the proposed UFL dual-sided illumination was successfully demonstrated for dual-sided display applications with high optical, thermal and mechanical performance.

Chapter 7

Conclusion and Future Works

7.1 Conclusion

In summary, the RPC lighting scheme differs from illumination using conventional fluorescent lamps or LEDs. It involves using a wavelength conversion mechanism, providing high brightness, planar and uniform illumination. In particular, RPC lighting that is used in UFL can be realized using a compact size with low power consumption and symmetrical dual-sided illumination. Additionally, RPC lighting can eliminate the thermal quenching effect associated with phosphor which produces a large amount of heat during illumination. These characteristics of the RPC scheme are exploited in wide range of lighting applications and a great diversity of new backlighting applications, including outdoor advertising, electrical signage and displays that can be read in the sunlight.

7.1.1 Part I: LED Devices

Part I of this investigation solves the problem of color deviation in a conventional white light-emitting diodes (wLEDs) device using a conformal phosphor coating. The use of pulsed spray to coat phosphor is a physical, environmentally friendly method that does not generate polluting ions. Furthermore, in other methods, LED chips must be of the flip-chip-mounted type and have a flat emitting surface. Pulsed spraying can be performed to apply phosphor uniformly to wire-bonded type LEDs.

Accordingly, different conformal coating technology was compared in Fig. 7-1. Except NCTU scheme, all others are chemical reaction solutions. It means the chip will be limited to flip chip, the process with chemical pollution and importantly the high process cost. NCTU pulsed-spray scheme is a mechanical process and it also an environmentally friendly process.

KAIST KOREA, 2001	Lumileds Lighting USA, 2003	Unv. E. Sci. & Tech. CHINA, 2009	NCTU TAIWAN, 2009
Chemical	Chemical	Chemical	Mechanical
Electrophoretic deposition (EPD)	sintering	Electrophoretic deposition (EPD)	Pulsed spray
Flip chip requirement	Flip chip requirement	Flip chip requirement	No limitation
Cr ion pollution	Indirect & high cost	Decrease Cr ion pollution	Without Cr ion pollution

Fig. 7-1 Conformal coating technology comparison.

7.1.2 Part II: LED Lighting Module

In the second part of this work (**lighting module**), the remote phosphor conversion (RPC) method is used in a lighting module. The configuration is optimized by developing a mathematical model for use in an optical simulation, and its effectiveness is verified using practical samples. Base on the results of this work, the phosphor film herein serves simultaneously as a wavelength converter and a light diffuser. The proposed configuration with a micro line lenticular (MLL) microstructure can be utilized in a lighting module with high luminous efficiency, high luminous uniformity and high color uniformity. Its optical behavior was elucidated. **Figure 7-2** plots the relationship between lighting module thickness with luminous efficiency for various types of planar lighting modules. RPC lighting has outstanding optical performance with a very compact mechanism. In particular, the RPC lighting method generates 1.5 times as much luminous efficiency in lighting module as side-emission method.

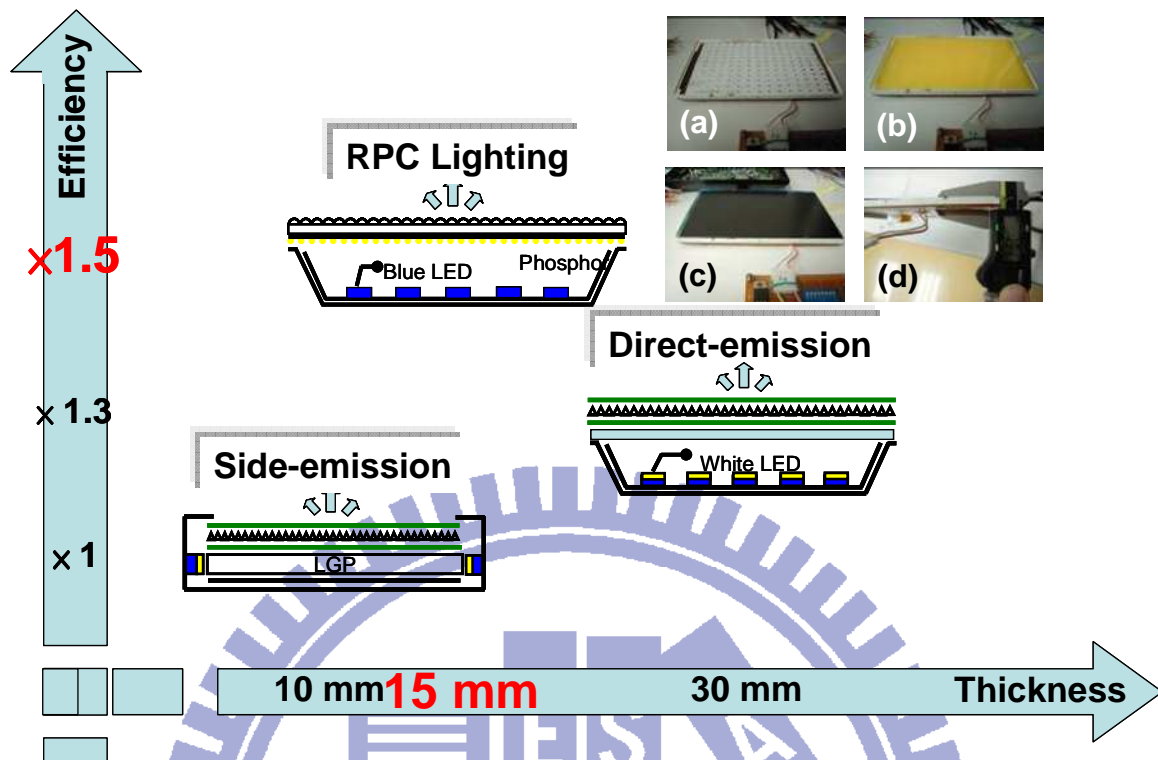


Fig. 7-2 Correlations between lighting module thickness and luminous efficiency in different planar lighting modules.

In 2008, SONY states RPC can apply to large size backlight module with 20% luminous improvement due to release thermal quenching effect. However, there is no certain data to support it and there is also no data regarding slim configuration. Therefore, we repeated SONY conditions and found serious color shifting issue in spite of high luminous efficiency. Figure 7-3 demonstrates the ratio of blue-light to yellow-light is different from angle 0° , 30° to 45° . SONY states the inserted diffuser can alleviate this issue, but our repeated data shows the effect is limited. The mechanism of light diffusion for blue light didn't work effectively [Fig. 7-4(a)]. In contrary, [Fig. 7-4(b)] shows light collimation can modify yellow-light distribution to fit blue-light distribution effectively. Finally, we achieves RPC scheme with high brightness and low color deviation. CIE 1976 shows the same result that light collimation is good than light diffusion [Fig. 7-5].

Compared with conventional direct-emission and edge-emission backlighting, PRC

reveals a 1.5 times improvement of efficiency under similar mechanical thickness. Figure 7-6 compares NCTU RPC backlighting with other RPC scheme, it exhibits UV light combines with color-filter-less has the chance to improve luminous efficiency [120-122], but high energy of UV light will cause liquid crystal to be damaged. Therefore, Univ. of Cincinnati change UV light to lower energy of violet light [123], but it should combine with special wavelength conversion materials. In 2008, SONY announced the RPC scheme using blue light excitation [52]. In 2009, NCTU published RPC using light collimation can solve color deviation effectively and also contribute to shrinkage the lighting module configuration [85-86].

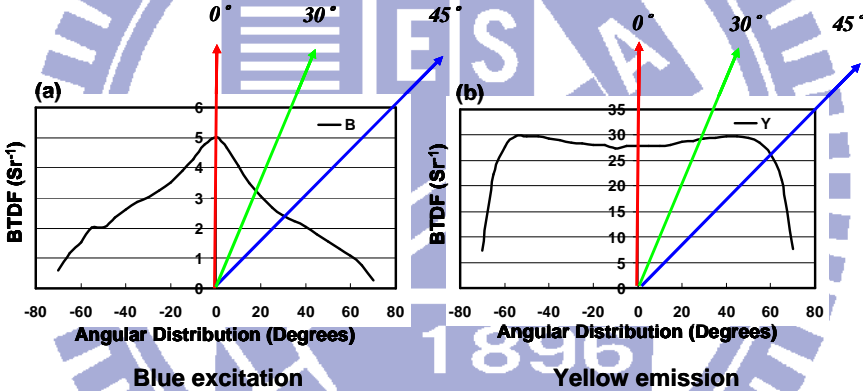


Fig. 7-3 BTDF-angular distribution of (a) blue excitation; (b) yellow emission.

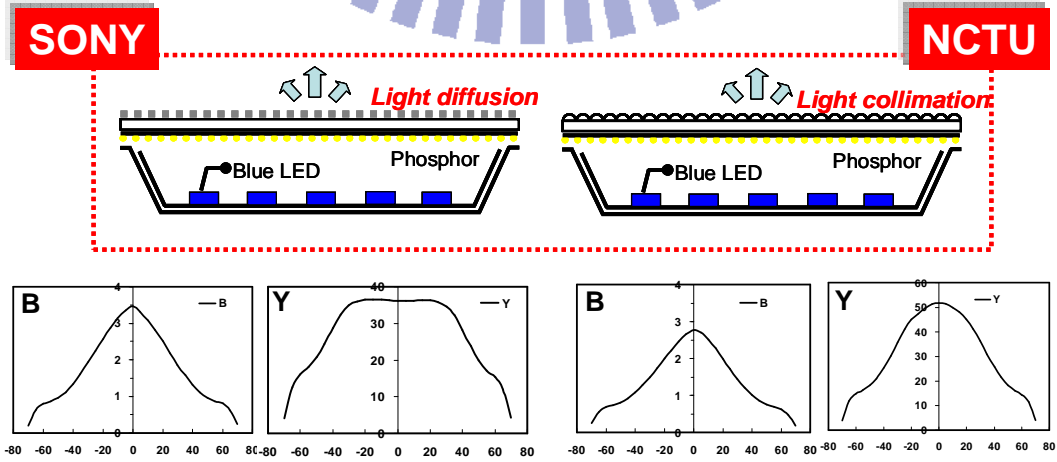


Fig. 7-4 Color shifting of remote phosphor scheme by light diffusion and by light collimation.

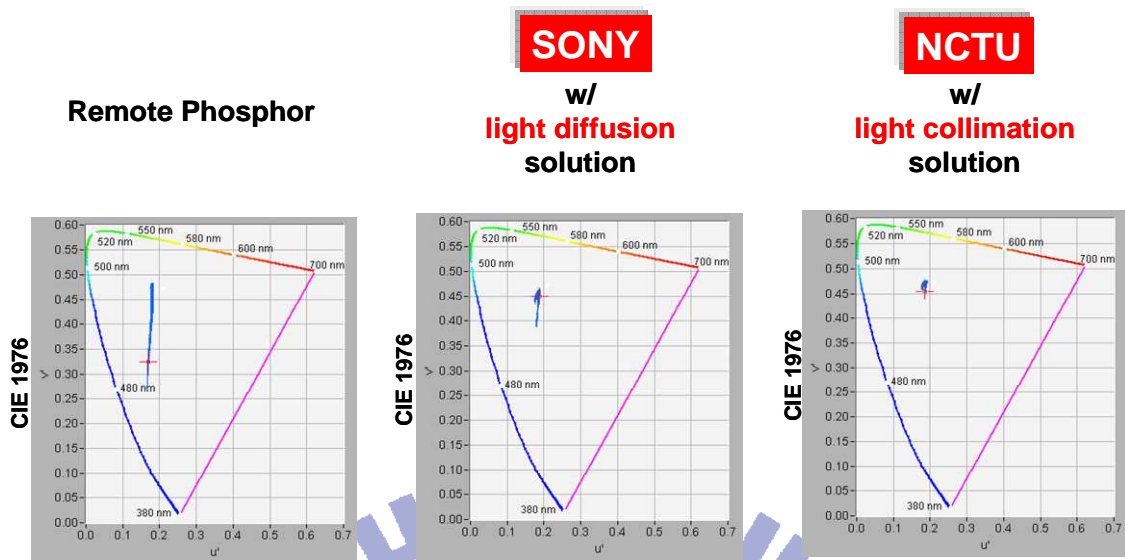


Fig. 7-5 Comparison of color deviation mapped in CIE 1976.

Univ. of Cambridge UK, 1998	Philips Netherlands, 2000	Univ. of Cincinnati USA, 2003	SONY JAPAN, 2008	NCTU TAIWAN, 2009
UV light	UV light	Violet light	Blue light	Blue light
High efficiency	High efficiency	High efficiency	High efficiency	High efficiency
Color-filter-less	Color-filter-less	Color-filter-less	Low light scattering & thermal quench	Low light scattering & thermal quench
Compact module ??	Compact module ??	Compact module	Compact module ??	Compact module
Difficult process	Difficult process	Special material	Simple process	Simple process

Fig. 7-6 Planar lighting module technology comparison.

7.1.3 Part III: Dual-sided Display System



Fig. 7-7 Ultra-slim dual-sided display system using UFL lighting by RPC scheme.



Fig. 7-8 Ineffective applications of two conventional sets of single-sided LCDs installed back-to-back.

In the third part of this work (**display system**), the RPC method in which UV light is used to excite trichromatic phosphor (UFL lighting) was studied. Novel planar lighting provides high luminance, low power consumption and dual-sided illumination in an ultra-slim display system [Fig. 7-7]. In contrast, Fig. 7-8 presents an ineffective application of two conventional sets of single-sided LCDs installed back-to-back. UV light (wavelength 254 nm) is invisible and does not participate in color mixing after wavelength conversion. Accordingly, it can be utilized in flat lighting to prevent angular-color deviation. In this investigation, phosphor with a particular spectrum that does not include emission at a wavelength of 590 nm and 490 nm generate planar lighting with high color saturation. Dual-sided illumination can be used in a symmetrical dual-sided display without the need for conventional optical reflectors. It is useful for large TFT-LCD display applications.

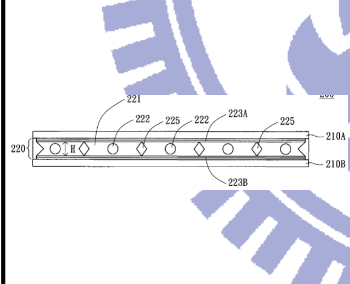
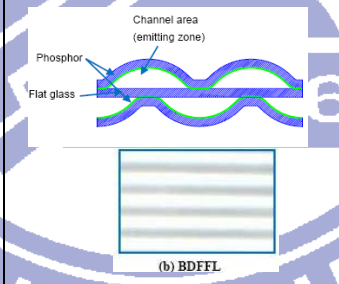
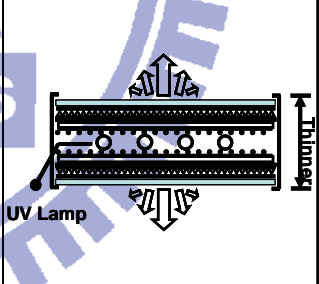
AUO TAIWAN, 2006	Dankook Univ. KOREA, 2009	NCTU TAIWAN, 2009
		
CCFL	External electrode fluorescent lamp (EEFL)	UV lamp
Lamp mura	Heavy & high power consumption	Ideal optical & low power consumption

Fig. 7-9 Dual-sided lighting technology comparison.

Indeed, dual-sided display has the potential for a diversity of future public display applications, there are other teams announced dual-sided display by different methods. AUO states CCFL scheme [110], but we consider it will result in low brightness as overcoming serious lamp mura issue. The way by Dankook Univ. is heavy and high power consumption

[109]. Therefore, NCTU demonstrate this dual-sided display performance successfully [Fig. 7-9].

7.1.4 Conclusion

Part I already demonstrated LED device using pulsed-spray conformal phosphor coating with low color deviation [Fig. 7-10]. Part II demonstrated LED lighting module using remote phosphor scheme with high luminance, low color deviation, uniform luminous distribution and compact configuration [Fig. 7-11]. Part III, demonstrated dual-sided display system with ultra slim configuration, attractive appearance, low power consumption and light weight [Fig. 7-12].

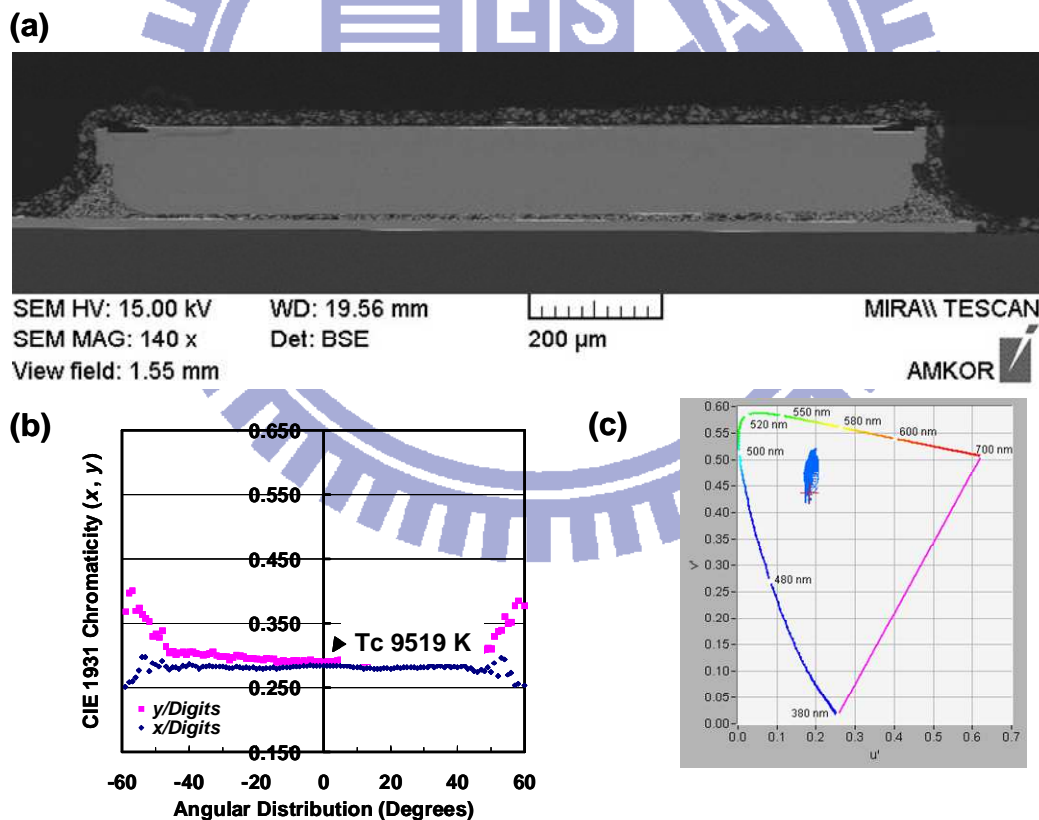


Fig. 7-10 Part I accomplished LED device using pulsed-sprary with low color deviation.

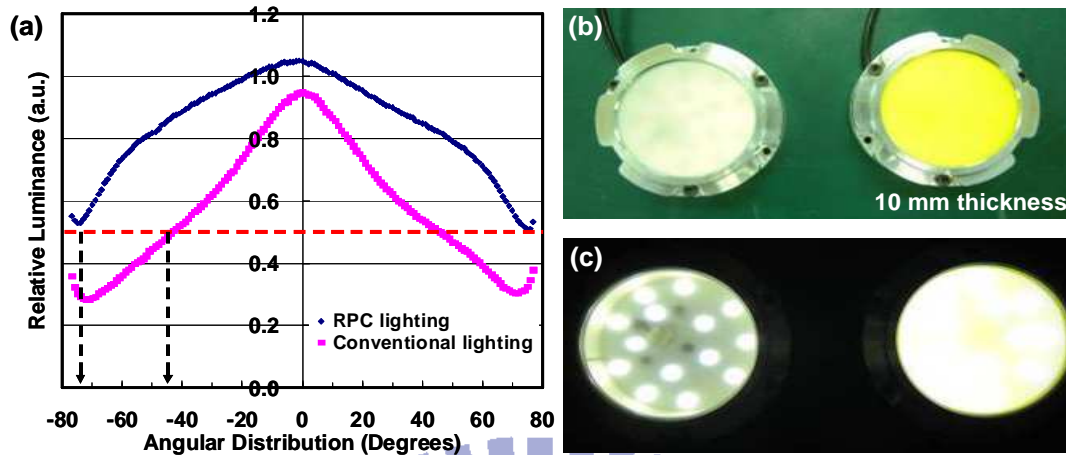


Fig. 7-11 Part II accomplished LED lighting module using remote phosphor scheme with high brightness, low color deviation, uniform luminous distribution and slim configuration.

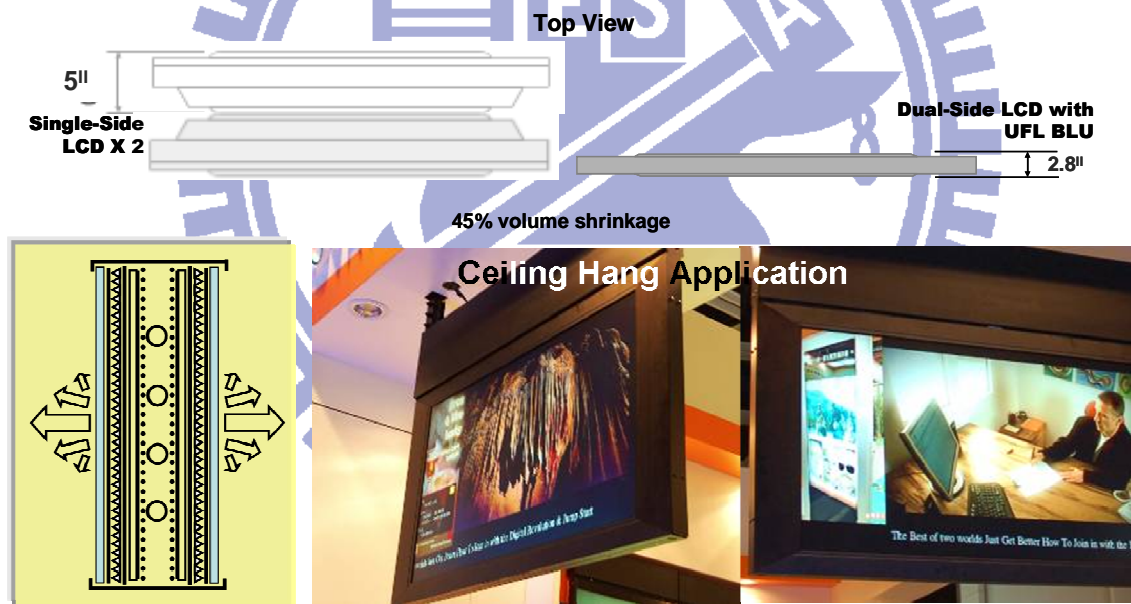


Fig. 7-12 Part III accomplished dual-sided display system using UV-excited fluorescent light (UFL) with high brightness, high color saturation, slim configuration and attractive appearance.

Figure 7-13 summarizes the three stages accomplishment of this investigation. In the part on the device, the proposed CPC scheme that involves the novel pulsed-spray coating method improve luminous efficiency by 8% and dramatically decrease color deviation by 70% in a 3inch COB array sample. This process involves mechanical deposition without a chemical

reaction. In the part on the lighting module, a 7inch lighting module is realized using the proposed RPC scheme. The sample improves brightness by 7% and luminous efficiency by 13%; it also greatly reduces the thickness by 79%. In the finally part, a 42inch dual-sided display system based on UFL lighting by the RPC scheme is demonstrated. Relative to a traditional display system, the brightness is improved by 8%, the power consumption is reduced by 30%, and the size (includes the system thickness and weight) is reduced by almost half.

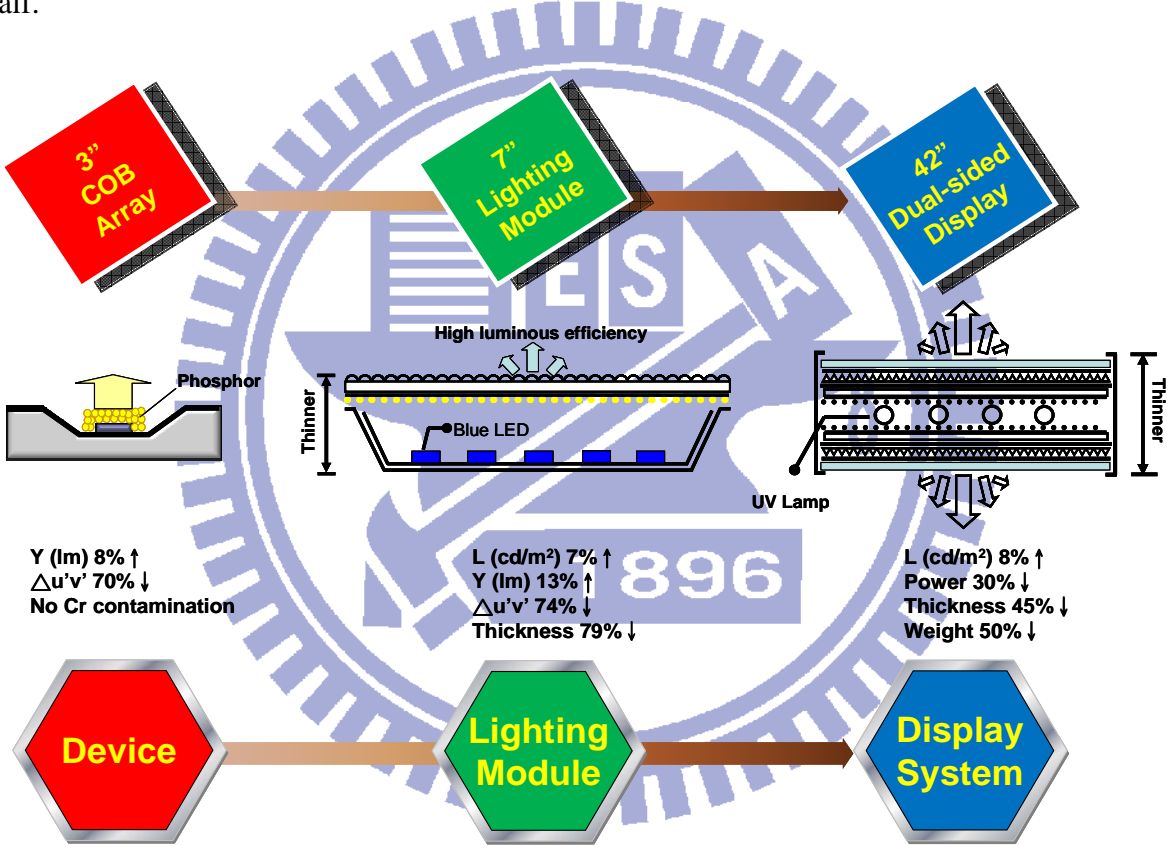


Fig. 7-13 The accomplishment of objectives in this investigation.

Accordingly, this investigation optimizes the RPC scheme with high brightness, low color deviation, high luminous uniformity including slim configuration; meanwhile, this study achieves the world's first dual-sided display system using RPC scheme with perfect optics performance, low power consumption, productive process including an attractive configuration.



Fig. 7-14 The applications meet the requirement of asymmetry dual-sided display.

7.2 Future Works

This thesis presented many results concerning the application of conformal and remote phosphor coating methods to forming planar lighting modules. In part I, we achieved LED devices using pulsed-spray conformal phosphor with low color deviation. However, the dependence of temperature on this pulsed-spray phosphor film should be investigated. To conduct the lifetime test under a condition of high temperature (60°C) and high humid (90% RH) continually is necessary. After test, the luminance decay and the adhesion strength of phosphor layer will be compared with conventional dispensing coating and ensured the proposed pulsed-spray system can satisfy for commercial application.

After that, the intension of this work is to develop an optical mechanism in a dual-sided display that uniformly. However, dual-sided display suffers application limitation including in particular conditions [Fig. 7-14]. Since the illumination is different between indoor and outdoor [Fig. 7-15], the preferred dual-sided display is asymmetric illumination. For the reason that symmetrical dual-sided display is just a starting point, future works will address display systems with asymmetrical illumination by exploiting a transfective method [Fig. 7-16(c)]. Further, the light source will be altered from UV lamp to blue LED light source to reduce pollution considerably and save energy [Fig. 7-16(d)].

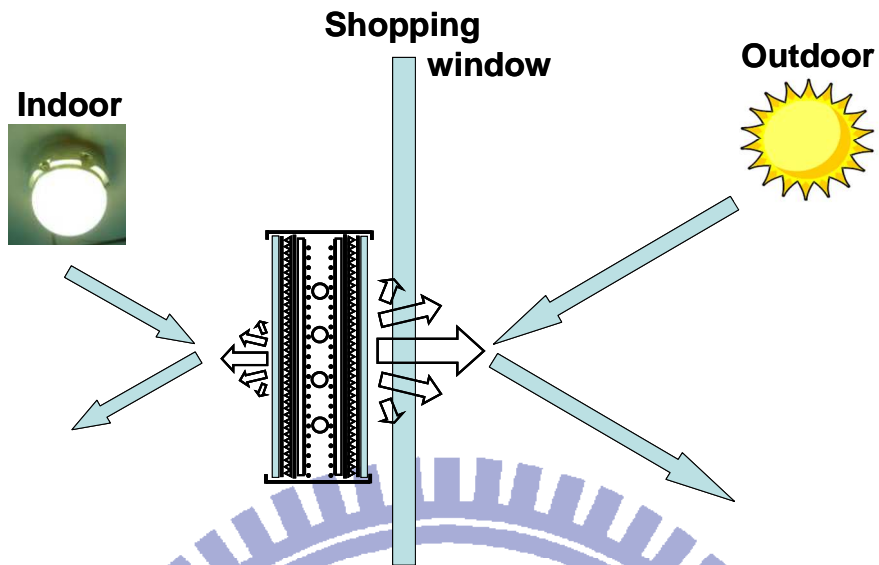


Fig. 7-15 The environmental illumination affects the demand of display luminance.

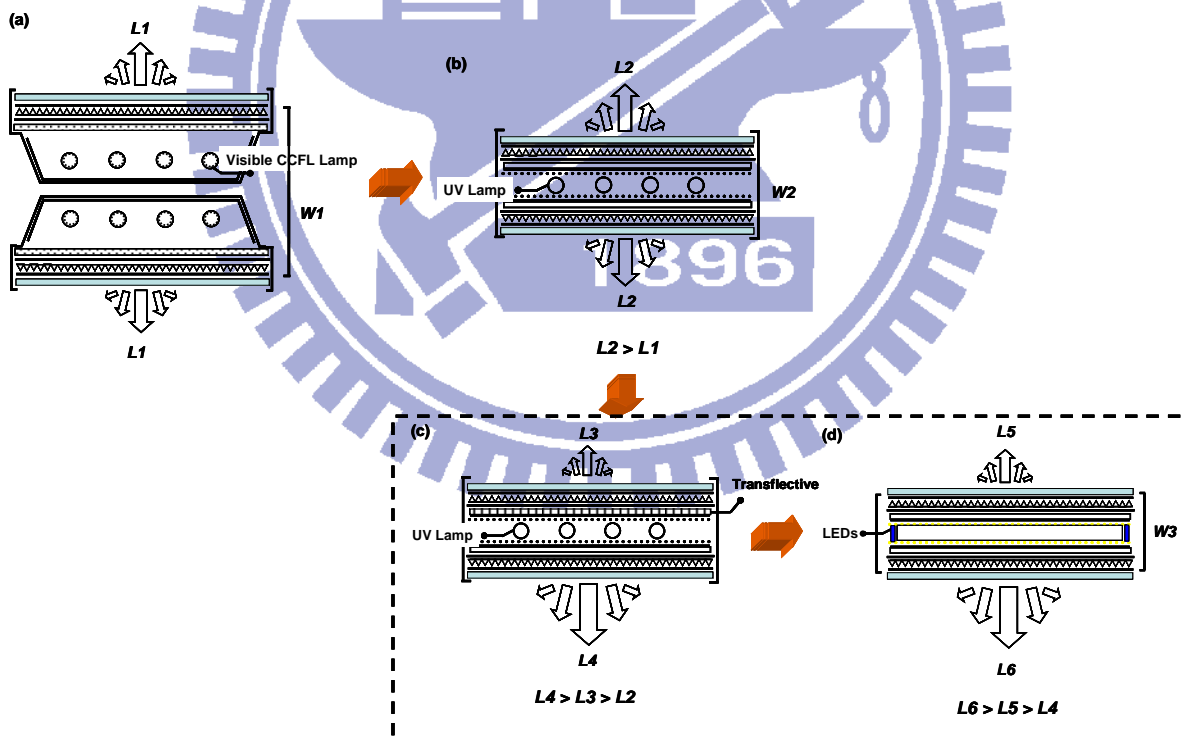
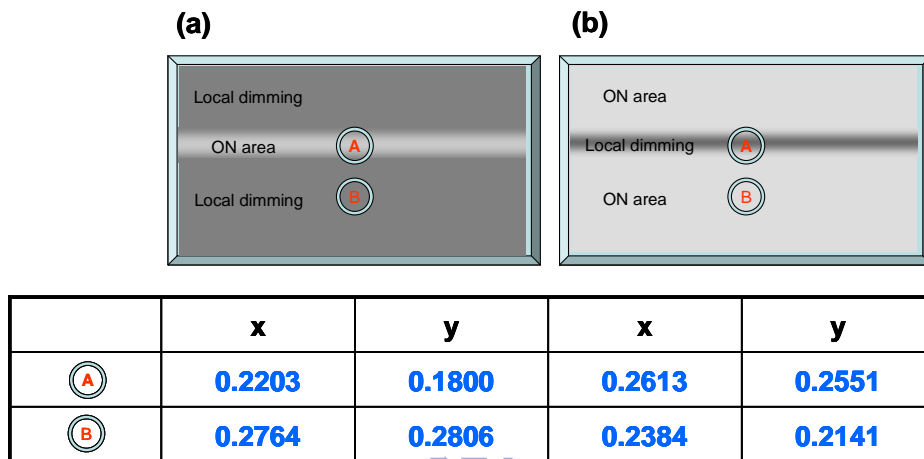


Fig. 7-16 The future works of RPC scheme in dual-sided display system. From picture (a) to (b), it illustrates the current accomplishment; whereas, from picture (b) to (c) to (d), these suggest proposal of asymmetry illumination and blue LED light source in future works.



* RP film / BS-912 / BEF-III

Fig. 7-17 To verify the color variation of RPC scheme using TFT-LCD display system with local dimming function. (a) Small area ON pattern, and (b) small area dimming pattern.

To improve display optical contrast and reduce backlighting power consumption, current TFT-LCD displays utilize backlighting dimming function to control local area luminance complying with the gray scale of display content. As Fig. 7-17 shows, experimental result exhibits serious color deviation when RPC backlighting applied to a TFT-LCD display with local dimming function. Point A and B indicate the measured point of color indices on display surface. This problem will impact the applications of RPC backlighting and require further investigation.

Professor W. A. Crossland of Cambridge Univ. presents results obtained by combing UFL with a color-filter-less to increase the luminous efficiency of TFT-LCD display [120-122]. As shown in [Fig. 7-18(b)], method (b) presented by Prof. Crossland increased luminance of method (a) by 30%. High energy UV light destroys liquid crystals of TFT-LCD panel as longer-time operation. In the future work, the UV light source may be replaced by blue LEDs using in the RPC approach, as presented in Fig. 7-18(c). In addition, methods of omnidirectional reflection [116], short wave-pass filters [117] or a remote phosphor with ring structure [118] are other luminous improvement solutions that might be integrated into

proposed RPC lighting system.

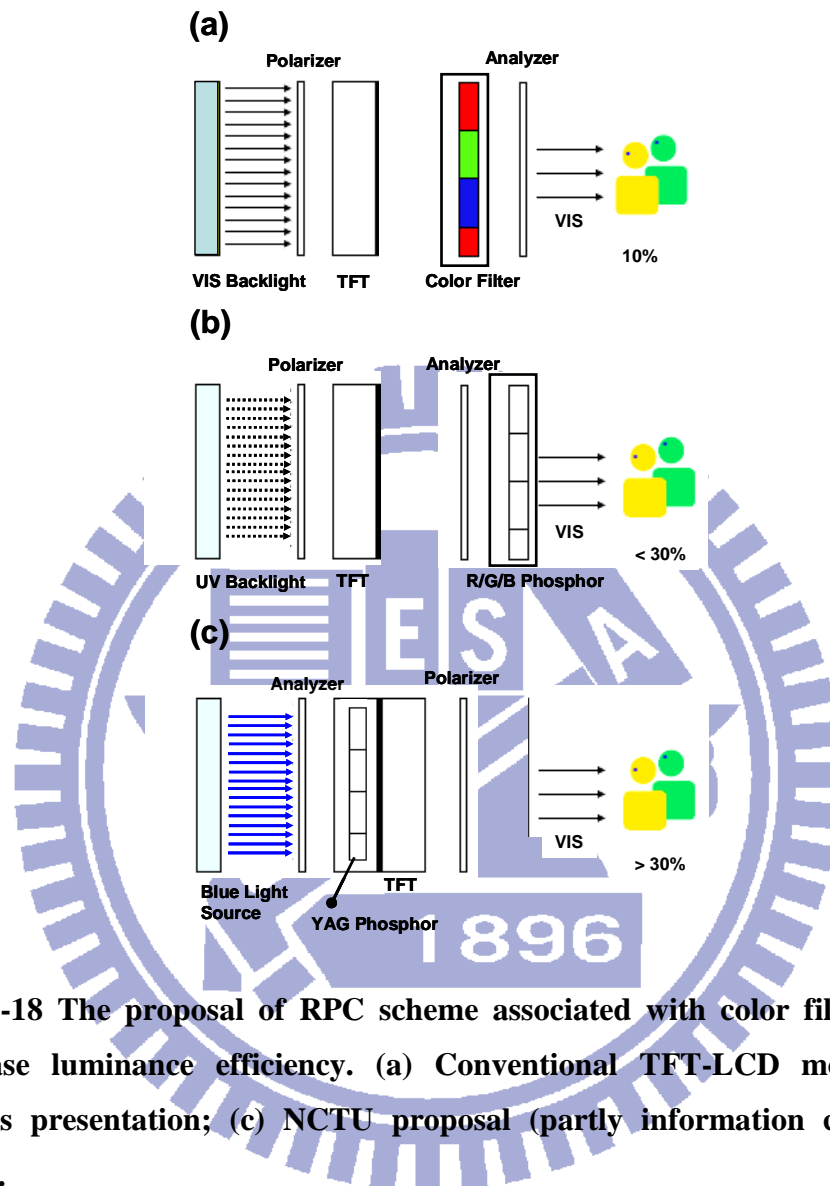


Fig. 7-18 The proposal of RPC scheme associated with color filter less to increase luminance efficiency. (a) Conventional TFT-LCD module; (b) Philips presentation; (c) NCTU proposal (partly information cited from [122]).

Consistent with OIDA prediction [119], TFT-LCD display has 50-65 lm/W efficiency when apply 100 lm/W efficiency wLEDs device [Fig. 7-19]. In contrary, the proposed RPC backlighting can achieve 60-80 lm/W efficiency based on the same blue LEDs in this investigation. Afterwards, the new proposal [Fig. 7-18(c)] can raise the efficiency to 105-120 lm/W on account of color-filter-less [Fig. 7-19]. Accordingly, when the wLEDs device has 200 lm/W efficiency by year 2020 [Table 7-1], RPC backlighting with 160-190 lm/W efficiency is assumed to be achieved using color-filter-less and other announced solutions

[116-119] in the near future.

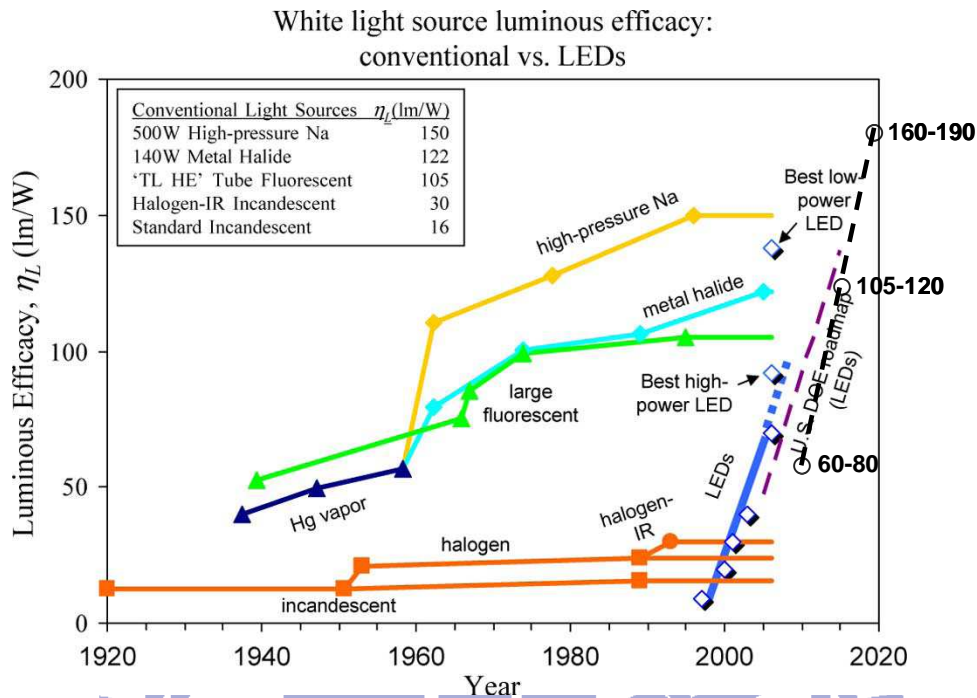


Fig. 7-19 Evolution of luminous efficacy performance of white light sources. Commercially available high-power LED performance is indicated by the points along the solid blue curve. The U.S. Department of Energy (DOE) projections is indicated by the dashed purple line [125]. The efficiency prediction of RPC backlighting in this investigation is indicated by back dash line.

Table 7-1 The efficiency prediction of RPC backlighting.

Year	LED Device Efficiency (lm/W)	Conventional Backlighting (lm/W)	RPC Backlighting (lm/W)
2010	100	50-65	60-80
2015	130	65-85	105-120
2020	200	100-130	160-190

References

- [1] G. H. Tsuei, J. W. Pen, W. S. Sun, “Simulating the illumination and the efficiency of the LED and fluorescent lights used in indoor lighting design”, *Opt. Express*, Vol. 16, No. 23, 2008.
- [2] “Color Quality of White LEDs”, U.S. Department of Energy, Energy Efficiency and Renewable Energy, PNNL-SA-5007, Jan. 2008.
- [3] N. Ohta and A. Robertson, “Colorimetry: Fundamentals and Application”, John Wiley & Sons Ltd, The Atrium, Southern Gate, Chichester, West Sussex PO198SQ, England, 2005.
- [4] W. J. Smith, “Modern Optical Engineering”, 4th Ed., McGraw-Hill Companies, 2008.
- [5] P. Duygulu, “Radiometry Measuring Light”, Bilkent University, 2006.
- [6] 陳君彥, “顯示器色彩學”講義, 工研院光電所, Oct. 07, 2005.
- [7] <http://www.RadiantImaging.com>
- [8] 李孝貽, “液晶影像顯示光學初階”講義, 明新科技大學, Aug. 10, 2004.
- [9] Pochi Yeh, “Fundamentals of Thin Film Optics”, NCTU, Hsinchu, Taiwan, Dec. 14, 2007.
- [10] G. R. Fowles, “Introduction to Modern Optics”, 2nd Ed., Dover Publication, Mineola, New York, USA, 1989.
- [11] E. Hecht, “Optics”, 3rd Ed., Addison Wesley Longman Inc., 1998.
- [12] S. O. Kasap, “Optoelectronics and Photonics: Principles and Practices”, Pearson Prentice Hall, 2001.
- [13] C. H. Hung, C. H. Tien, “Phosphor-converted LED modeling by bidirectional photometric data”, *Opt. Express*, Vol. 18, No. 103, 2010.
- [14] E. Veach, “Robust Monte Carlo Methods for Light Transport Simulation”, Ph.D. Dissertation, Stanford University, USA, 1998.
- [15] http://en.wikipedia.org/wiki/Bidirectional_scattering_distribution_function
- [16] C. H. Tien, C. H. Hung, “An interactive model of diffuse illumination from bidirectional photometric data”, *Opt. Express*, Vol. 17, No. 2, 2009.
- [17] http://en.wikipedia.org/wiki/Full_width_at_half_maximum
- [18] Prof. Alan Hedge, “Glare and Visual Performance: Glare”, Cornell University, Jan. 2010.
- [19] “Applications Note: Haze”, Hunterlab, Vol. 9, No. 6, 2008.
- [20] Y. Ohno, “CIE Fundamentals for Color Measurements”, IS&T NIP16 Conference, Vancouver, Canada, Oct. 16- 20, 2000.
- [21] J. Schanda, “Colorimetry: Understanding the CIE System”, 2007, John Wiley & Sons. Ltd.
- [22] E. F. Schubert, “Light Emitting Diodes”, Cambridge University Press, Cambridge, 2003.

- [23] <http://www.soslightbulbs.com/colortemperaturechart.aspx>
- [24] J. Smith, "Calculating Color Temperature using the TAOS TCS3414CS Digital Color Sensor", Dec. 2008.
- [25] 盧慶儒, "次世代 LCD 背光源件發展趨勢: 多色 LED 背光畫質豔麗", DIGITIMES, Mar. 2006.
- [26] G. Harbers, C. Hoelen, "High Performance LCD Backlighting using High Intensity Red, Green and Blue Light Emitting Diodes" in SID Symp. Dig. Tech. Papers, 2001.
- [27] S. S. Kim, B. H. Berkeley, T. Kim, "Invited Paper: Advancements for Highest-Performance LCD-TV" in SID Symp. Dig. Tech. Papers, 2001, pp. 1938-1941.
- [28] J. S. Li, C. C. Lai, C. F. Hsu, T. Y. Chang and W. C. Wang, "Color Reproduction Method of Adobe RGB Images on Wide Color Gamut Display" in SID Symp. Dig. Tech. Papers, 2009, pp. 1227-1230.
- [29] Y. Uchida, T. Taguchi, "Lighting theory and luminous characteristics of white light-emitting diodes", Opt. Eng., 44(12), 124003 (Dec. 2005).
- [30] http://en.wikipedia.org/wiki/Color_rendering_index
- [31] K. Kakinuma, "Technology of Wide Color Gamut Backlight with Light-Emitting Diode for Liquid Crystal Display Television", Jpn. J. Appl. Phys., Vol. 45, No. 5B, 2006, pp. 4330-4334.
- [32] Dr. P. Bodrogi, S. Bruckner and Prof. T. Q. Khanh, "Re-defining the Color Rendering Index", CIE, Book of Abstracts, 27-29 May 2009, Budapest, Hungary.
- [33] "Colour Rendering of White LED Light Sources", CIE Technical Report, CIE 177:2007.
- [34] "Method of Measuring and Specifying Colour Rendering Properties of Light Sources", CIE Technical Report, CIE 13.3-1995.
- [35] "Application Note: Color Rendering", NICHIA, SIS-KSE3578, Aug. 2004.
- [36] "LED Measurement Series: Color Rendering Index and LEDs", U.S. Department of Energy, Energy Efficiency and Renewable Energy, PNNL-SA-56891, Jan. 2008.
- [37] Y. Ohno, "Color Rendering and Luminous Efficiency of White LED Spectra", Fourth International Conference on Solid State Lighting, Proc. of SPIE, Vol. 5530, Bellingham, WA, 2004.
- [38] Prof. Marc Fontoynt, lecture of "Field and laboratory testing of SSL: user preferences for homes, shops and museums Opportunities", National Engineering School of State Public Works-Lyon, France.
- [39] E. F. Schubert, J. K. Kim, H. Luo and J. Q. Xi, "Solid-state lighting- a benevolent technology", Institute of Physics Publishing, Rep. Prog. Phys. 69 (2006), pp. 3069-3099.
- [40] F. M. Steranka, M. Krames, G. Mueller, R. Mueller-Mach, T. Trottier et al, "High Power LEDs- Technology Status and Market Applications," phys. stat. sol. (a) 194, No. 2, 380-388 (2002).
- [41] M. O. Holcomb, R. Mueller-Mach, G. Mueller, D. Collins, R. M. Fletcher, D. A. Steigerwald, S. Eberle, Y. K. Lim, P. S. Martin, M. Krames, "The LED Lightbulb:

Are we there yet? Progress and Challenges for Solid State Illumination,” Lasers and Electro-Optics, 2003 CLEO’03 Conference on 1-6 June 2003.

- [42] Z. Liu, S. Liu, K. Wang, and X. Luo, “Optical Analysis of Color Distribution in White LEDs with Various Packaging Methods,” IEEE Photon. Technol. Lett., Vol. 20, No. 24, 2027-2029 Dec. 15, 2008.
- [43] J. H. Yum, S. Y. Seo, S. Lee, Y. E. Sung, “Comparison of $Y_3Al_5O_{12}:Ce_{0.05}$ Phosphor Coating Methods for White Light Emitting Diode on Gallium Nitride,” Proc. of SPIE, Vol. 4445, 60-68 (2001).
- [44] B. Hou, H. Rao, and J. Li, “Methods of Increasing Efficiency of Phosphor-Converted LED Realized by Conformal Phosphor Coating,” J. Display Technol., Vol. 5, No. 2, 57-60 Feb. 2009.
- [45] R. Mueller-March, G. O. Mueller, M. R. Krames, and T. Trottier, “High-Power Phosphor-Converted Light-Emitting Diodes Based on III-Nitrides”, IEEE J. Selected Topics Quantum Electron, VOL. 8, NO. 2, March/APRIL 2002.
- [46] A. Borbely, S. G. Johnson, “Performance of phosphor-coated light-emitting diode optics in ray-trace simulation”, Opt. Eng., 44(11), 11308 (Nov. 2005).
- [47] B. Hou, H. Rao, and J. Li, “Phosphor Coating Technique with Slurry Method in Application of White LED,” Solid State Lighting and Solar Energy, Technologies, Proc. of SPIE, Vol. 6841, 684106, (2007).
- [48] N. T. Tran and F. G. Shi, “Studies of Phosphor Concentration and Thickness for Phosphor-Based White Light-Emitting-Diodes,” J. Lightw. Technol., Vol. 26, No. 21, 3556-3559 Nov. 1, 2008.
- [49] J. K. Kim, H. Luo, E. F. Schubert, J. Cho, C. Sone and Y. Park, “Strongly Enhanced Phosphor Efficiency in GaInN White Light-Emitting Diodes Using Remote Phosphor Configuration and Diffuse Reflector Cup”, Jpn. J. Appl. Phys., Vol. 44, No. 21, (2005).
- [50] S. C. Allen and A. J. Steckl, “A nearly idea phosphor-converted white light-emitting diode”, Appl. Phys. Lett., vol. 92, 143309 (2008).
- [51] C. Hoelen, H. Borel, J. de Graaf, M. Keuper, M. Landhorst, C. Mutter, L. Waumans, and R. Wegh, “Remote phosphor LED modules for general illumination- towards 200 lm/W general lighting LED light sources”, Eighth International Conference on Solid State Lighting, Proc. of SPIE, vol. 7058, 70580M, (2008).
- [52] Y. Ito, T. Tsukahara, S. Masuda, T. Yoshida, N. Nada, T. Igarashi, T. Kusunoki, and J. Ohsako, “Optical Design of Phosphor Sheet Structure in LED Backlight System”, in SID Sym. Dig. Tech. Papers, vol. 39, pp. 862-865, (2008).
- [53] N. Narendran, Y. Gu, J. P. Freyssinier-Nova, and Y. Zhu, “Extracting phosphor-scattered photons to improve white LED efficiency”, phys. stat. sol. (a) 202, No. 6 (2005).
- [54] Y. Zhu and N. Narendran, “Optimizing the Performance of Remote Phosphor LEDs”, J. Light & Vis. Env., Vol. 32, No. 2, (2008).
- [55] H. Luo, J. K. Kim, E. F. Schubert, J. Cho, C. Sone and Y. Park, “Analysis of high-power packages for phosphor-based white-light-emitting diodes”, Appl. Phys. Lett., vol. 86, 243505 (2005).

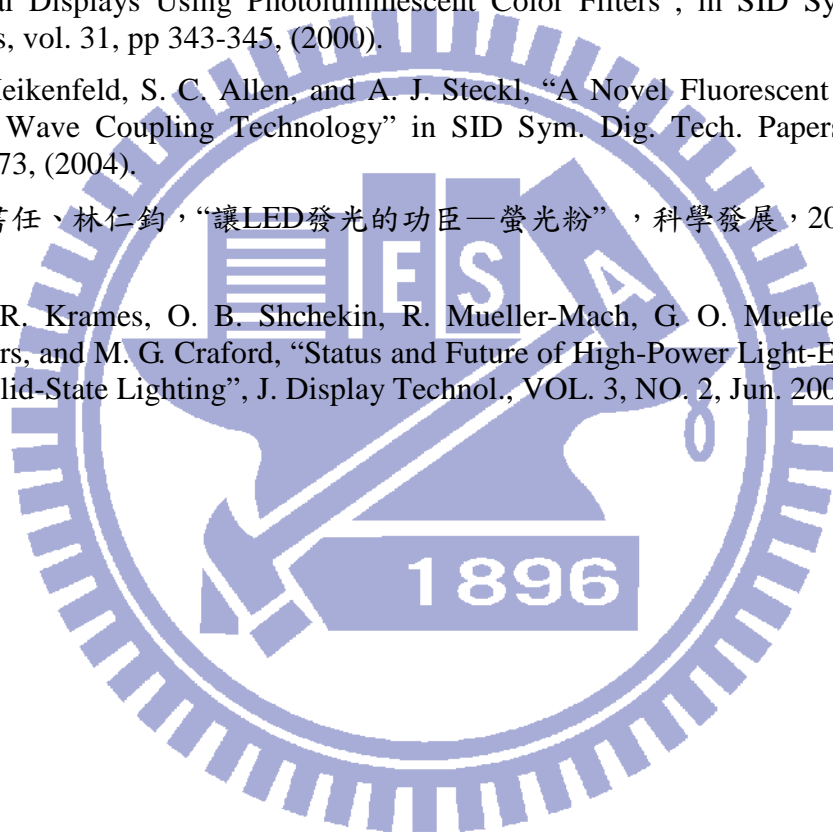
- [56] D. Y. Kang, E. Wu, D. M. Wang, "Modeling white light-emitting diodes with phosphor layer", *Appl. Phys. Lett.*, Vol. 89, 231102 (2006).
- [57] S. C. Allen, and A. J. Steckl, "ELiXIR- Solid-State Luminaire With Enhanced Light Extraction by Internal Reflection", *J. Display Technol.*, VOL. 3, NO. 2, Jun. 2007.
- [58] N. Narendran, "Improved Performance White LED", Fifth International Conference on Solid State Lighting, Proc. of SPIE, Vol. 5941, Bellingham, WA, 2005.
- [59] H. Wu, N. Narendran, Y. Gu, and A. Bierman, "Improving the Performance of Mixed-Color System by Using Scattered Photon Extraction Technique", Seventh International Conference on Solid State Lighting, Proc. of SPIE, Vol. 6669, 666905, (2007)
- [60] Z. Liu, S. Liu, K. Wang, and X. Luo, "Optical Analysis of Phosphor's Location for High-Power Light-Emitting Diodes", *IEEE Transactions on Device and Materials Reliability*, VOL. 9, NO. 1, Mar. 2009.
- [61] H. Luo, J. K. Kim, Y. A. Xi, E. F. Schubert, J. Cho, C. Sone, and Y. Park, "Trapped whispering-gallery optical modes in white light-emitting diode lamps with remote phosphor", *Appl. Phys. Lett.*, Vol. 89, 041125 (2006).
- [62] K. M. Moon, S. H. An, H. K. Kim, J. H. Chae, Y. J. Park, "Phosphor concentration and geometry for high power white light emitting diodes", *Light Emitting Diodes: Materials, Devices, and Applications for Solid State Lighting XIV*, Proc. of SPIE, Vol. 7617, 2010.
- [63] W. Schwedler, F. Nguyen, "Invited Paper: LED Backlighting for LCD TVs", in *SID Sym. Dig. Tech. Papers*, vol. 41, pp. 1091-1096, (2010).
- [64] J. Gourlay, I. Miller, "High Efficiency Hybrid Backlight for Large-area LCD TV", in *SID Sym. Dig. Tech. Papers*, vol. 41, pp. 1097-1099, (2010).
- [65] C. C. Kang, J. F. Lin, Y. C. Wu, S. C. Yeh, T. R. Chen, "Late-News Poster: High Efficiency Uniform LED Surface Light Source", in *SID Sym. Dig. Tech. Papers*, vol. 41, pp. 1418-1421, (2010).
- [66] R. S. West, H. Konijn, W. Sillevis-Smitt, S. Kuppens, N. Pfeffer, Y. Martynov, Y. Takaaki, S. Eberle, G. Harbers, T. W. Tan, L. E. Chan, "High Brightness Direct LED Backlight for LCD-TV", in *SID Sym. Dig. Tech. Papers*, vol. 34, pp. 1262-1265, (2003).
- [67] 張奇偉, "基礎光學"講義, 工研院光電所, Sep. 2005.
- [68] "Vikuiti™ Brightness Enhancement Film (BEF) II", 3M IPC, 2002.
- [69] "Vikuiti™ Dual Brightness Enhancement Film (DBEF)", 3M IPC, 2001.
- [70] R. Withnall, J. Silver, G. R. Fern, and A. L. Lipman, "Experimental and Theoretical Luminous Efficiency of Phosphors used for Producing White Light from Blue-emitting LEDs", in *SID Sym. Dig. Tech. Papers*, vol. 38, pp. 515-518, (2007).
- [71] 葉耀宗、董建岳、劉偉仁、張學明、陳政民, "螢光粉特性探討", 工研院材化所, 工業材料雜誌 258 期, Jun. 2008.
- [72] C. R. Ronda, "Luminescence: From Theory to Applications", 2008 Wiley-Vch Verlag GmbH & Co., KGaA, Weinheim.

- [73] 葉耀宗, “發光二極體之光轉換材料”, 化工技術第 13 卷第 12 期, Dec. 2005.
- [74] C. Sommer, J. R. Krenn, P. Pachler, M. Schweighart, S. Tasch, and F. P. Wenzl, “The Effect of the Phosphor Particle Sizes on the Angular Homogeneity of Phosphor-Converted High Power White LED Light Sources”, IEEE J. Selected Topics Quantum Electron., Vol. 15, No. 4, July/August 2009.
- [75] N. T. Tran, J. P. You, and F. G. Shi, “Effect of Phosphor Particle Size on Luminous Efficacy of Phosphor-Converted White LED,” J. Lightw. Technol., Vol. 27, No. 22, Nov. 2009.
- [76] G. Blasse and A. Bril, “A investigation of some Ce^{3+} activated phosphors”, J. Chem. Phys. Vol. 47(12), pp.5139-5145, (1967).
- [77] H. T. Huang, C. C. Tsai, Y. P. Huang, J. Chen, J. Lin, and W. C. Chang, "Phosphor Conformal Coating by a Novel Spray Method for White Light-emitting Diodes as Applied to Liquid-crystal Backlight Module", XXIX International Display Research Conference, Eurodisplay 2009, Sep. 14th-17th, 2009, Rome, Italy (IDRC 2009).
- [78] H. T. Huang, C. C. Tsai, and Y. P. Huang, "Conformal Phosphor Coating Using Pulsed Spray to Reduce Color Deviation of White LEDs", Opt. Express, Vol. 18, No. 102, pp. A201-A206, Jun. 2010.
- [79] S. Nakamura and G. Fasol (eds.), The Blue Laser Diodes, GaN Based Light Emitters and Lasers, Springer, Berlin, pp. 216-221, (1997).
- [80] M. Anandam, “Progress of LED backlights for LCDs”, J. of the SID 16/2, pp. 287-310, (2008).
- [81] C. H. Tien, C. H. Hung, B. W. Xiao, , H. T. Huang, Y. P. Huang, , and C. C. Tsai, “Planar Lighting by Blue LEDs Array with Remote Phosphor”, Light-Emitting Diodes: Material, Devices, and Applications for Solid State Lighting XIV conference, Proc. of SPIE, vol. 7617, 761707, (2010).
- [82] B. W. Xiao, C. H. Hung, H. T. Huang, Y. P. Huang, C. H. Tien, C. C. Tsai, H. P. D. Shieh, J. Chen, J. Lin, and W. C. Chang, “Optical Properties of Visible-light Excited Phosphor Sheet (VEPS) System”, in SID Sym. Dig. Tech. Papers, vol. 40, pp. 1034-1037, (2009).
- [83] S. C. Allen, “Illumination for the 21st Century: High Efficiency Phosphor-Converted Light-Emitting Diodes for Solid-State Lighting”, Doctorate of Ph.D., University of Cincinnati, 2007.
- [84] W. C. Chang, H. T. Huang, C. C. Tsai, Y. P. Huang and H. P. D. Shieh, "Remote Phosphor for Future LED Backlight Applications", SID Symposium Digest, vol. 41, No.66.2, pp. 862-865, 2010.
- [85] H. T. Huang, C. C. Tsai, Y. P. Huang, J. Lin and W. C. Chang, "Remote Phosphor with Blue Light-emitting Diodes Array on Board as Applied to Liquid-crystal Backlight Module", 9th International Meeting on Information Display, Oct. 12th-16th, 2009/KINTEX, Seoul, Korea (IMID 2009).
- [86] H. T. Huang, C. C. Tsai, Y. P. Huang, J. Lin and W. C. Chang, "Remote Phosphor with Blue Light-emitting Diodes Array on Board for a Liquid-crystal Backlight Module", 11th Asian Symposium on Information Display, Oct. 7th-10th, 2009, Guangzhou, China (ASID'09).

- [87] B. W. Xiao, C. H. Hung, H. T. Huang, J. Chen, J. Lin, W. C. Chang, Y. P. Huang, C. H. Tien, C. C. Tsai, and H. P. D. Shieh, "Optical Simulation and Analysis of Visible-light Excited Phosphor Sheet (VEPS) System", International Display Manufacture Conference, April 27-30, 2009 (IDMC'09).
- [88] B. W. Xiao, C. H. Hung, H. T. Huang, J. Chen, Y. P. Huang, C. H. Tien, C. C. Tsai, and H. P. D. Shieh, "LEDs-based Flat Lighting Device for LCD Backlight Applications", International Conference on Optics and Photonics in Taiwan, December 4-6, 2008 (OPT'08).
- [89] M. Bass, E. W. V. Stryland, D. R. Williams, W. L. Wolfe (eds.), Handbook of Optics, vol. 2, McGraw-Hill, New York, pp. 26.2- 26.4, (1995).
- [90] B. W. Xiao, "Development of Thin Format Light-Emitted Flat Lighting Systems for LCD Applications", A Thesis of Master Degree, NCTU, Jun. 2009.
- [91] F. X. Sillion and C. Puech, Radiosity and Global Illumination, Morgan Kaufmann Publisher Inc., San Francisco, (1994).
- [92] D. Feng, Y. Yan, X. Yang, G. Jin and S. Fan, "Novel Integrated Light-Guide Plates for Liquid Crystal Display Backlight", J. Opt. A: Pure Appl. Opt., vol. 7, 111-117 (2005).
- [93] Y. H. Lu and C. H. Tien, "Novel Direct-LED-Backlight Unit Using Grooved Hexagonal Light-Guide Plate", in SID Sym. Dig. Tech. Papers, vol. 37, pp. 1513-1516, (2006).
- [94] R. Tsuchiya, Y. Kawasaki, S. Ikebe, T. Shiba, and J. Kinoshita, "Thin Side-Lit, Hollow-cavity Flat LED Lighting Panel for Ultra-Uniform LCD Backlight Applications", in SID Sym. Dig. Tech. Papers, vol. 39, pp. 874-877, (2008).
- [95] S. S. Choi, H. C. Bae, W. J. Kin, J. C. Choi, B. C. Yang, E. J. Kang, and T. S. Jang, "Ultra-Slim TV Module Technology", in SID Symp. Dig. Tech. Papers, vol. 40, pp. 720-722, (2009).
- [96] J. Park, S. Lim, "Design of a Thin Multiple-Lamp Backlight System by Optical Simulation", in SID Symp. Dig. Tech. Papers, vol. 32, pp. 690-693, (2001).
- [97] S. C. Chung, C. R. Ou, H. Y. Lin, B. Horng, C. C. Lin, and H. H. Lo, "Novel Beam Shaping Structure for the CCFL Based Direct Backlight System", IDW 04 DIGEST, pp.667-669, (2004).
- [98] A. Nagasawa, K. Fujisawa, "An Ultra Slim Backlight System using Optical-Patterned Film", in SID Symp. Dig. Tech. Papers, vol. 36, pp. 570-573, (2005).
- [99] C. C. Hu, T. L. Su, W. M. Pai, and W. C. Lan, "New Concepts of LCD-TV Backlight Design with Variable Lamp Pitch", in SID Symp. Dig. Tech. Papers, vol. 37, pp. 1428-1431, (2006).
- [100] C. H. Tien, Y. H. Lu and Y. J. Yao, "Tandem Light-Guides With Micro-Line-Prism Arrays for Field-Sequential-Color Scanning Backlight Module", J. Display Technol., Volume 4, Issue 2, pp. 147-152, Jun. 2008.
- [101] G. W. Han, M. J. Jin, H. J. Park, S. S. Jung, J. M. Moon, and I. B. Kang, "Computer Simulation Based Optical Efficiency Maximization for a Direct-Type LED Backlight Unit", in SID Symp. Dig. Tech. Papers, vol. 39, pp. 1591-1593, (2008).

- [102] N. Kijima, Y. Shimomura, T. Kurushima, H. Watanabe, S. Shimooka, M. Mikami and K. Uheda, "New Green and Red Phosphors for White LEDs", *J. Light & Vis. Env.*, Vol.32, No.2, 2008, pp. 202-207.
- [103] H. T. Huang, C. C. Tsai, and Y. P. Huang, "A Direct-View Backlight With UV Excited Trichromatic Phosphor Conversion Film", *J. Display Technol.*, Vol. 6, No. 4, 128-134 Apr. 2010.
- [104] H. T. Huang, C. H. Hung, Y. P. Huang, C. H. Tien, C. C. Tsai, H. P. D. Shieh, J. Lin, J. Chen, P. Chen, and W. C. Chang, "UV Excited Flat Lighting (UFL) System for LCD-TV Backlight Application", in *SID Sym. Dig. Tech. Papers*, vol. 39, pp. 862-865, (2008).
- [105] S. Zhang, "Vacuum-Ultraviolet/Visible Conversion Phosphors for Plasma Display Panels", *IEEE Transactions on Plasma Science*, VOL. 34, NO. 2, APRIL 2006.
- [106] A. Watanabe, S. Naoki, M. Tamatani, F. Yanagisawa, K. Terashima, "Luminescent Material for Mercury Discharge Lamp Including Phosphor and a Continuous Protective Layer", U.S. Pat. No. 5,604,396, 1997.
- [107] Y. Muramo, M. Kimura, A. Dempo, S. Nouda, Y. Fukawa, "Application of UV-LED to the LCD Backlight", in *SID Sym. Dig. Tech. Papers*, vol. 41, pp. 982-984, (2010).
- [108] http://www.kismart.com.tw/double_sided.html
- [109] S. Hwang, H. Kim, C. Kim and S. Lim, "High Luminance Uniformity Flat Fluorescent Lamp for Dual View LCD Backlight Application," in *SID Sym. Dig. Tech. Papers*, Vol. 40, (2009).
- [110] Y. S. Tsai, "Backlight Module," U.S. Patent 6 995 815, Feb. 7, 2006.
- [111] H. T. Huang, C. C. Tsai, and Y. P. Huang, "Dual-Sided Slim LCD Display System with UV Excited Flat Backlight", in *SID Sym. Dig. Tech. Papers*, Vol. 40, pp. 1030-1033, (2009).
- [112] H. T. Huang, C. C. Tsai, and Y. P. Huang, "Ultraviolet excitation of remote phosphor with symmetrical illumination used in dual-sided liquid-crystal display", *Opt. Lett.*, Vol. 35, No. 15, pp. 2547-2549, Aug. 2010.
- [113] F. P. Incropera, and D. P. DeWitt, *Fundamentals of Heat and Mass Transfer*, Fourth Edition, John Wiley, 1996.
- [114] B. Li, D. Zhang, Y. Huang, Z. Ni, and S. Zhuang, "A new structure of multi-layer phosphor package of white LED with high efficiency", *Chinese Opt. Lett.*, Vol. 8, No. 2, Feb. 2010.
- [115] J. P. You, N. T. Tran and F. G. Shi, "Light extraction enhanced white light-emitting diodes with multi-layered phosphor configuration", *Opt. Express*, Vol. 18, No. 5, Mar. 2010.
- [116] J. C. Su, C. L. Lu, and C. W. Chu, "Design and fabrication of white light emitting diodes with an omnidirectional reflector", *Applied Opt.*, Vol. 48, No. 26, Sep. 2009.
- [117] S. H. Cho, J. R. Oh, Y. H. Lee, Y. R. Do, "Efficiency enhancement in white phosphor-on-cup light-emitting diodes using short wave-pass filters", *Light-Emitting Diodes: Materials, Devices, and Applications for Solid State Lighting XIV*, Proc. of SPIE Vol. 7617, 2010.

- [118] M. T. Lin, S. P. Ying, M. Y. Lin, K. Y. Tai, S. C. Tai, C. H. Liu, J. C. Chen, and C. C. Sun, "Ring Remote Phosphor Structure for Phosphor-Converted White LEDs", IEEE Photon. Technol. Lett., VOL. 22, NO. 8, Apr. 2010.
- [119] J. Y. Tsao, Ed., 2002, OIDA, <http://lighting.sandia.gov/lightingdocs/>
- [120] A. C. Newport, A. Vecht, P. A. Bayley and W. A. Crossland, "Optimised Photoluminescent Phosphors for UV-excited Light Emitting Systems", in SID Sym. Dig. Tech. Papers, vol. 29, (1998).
- [121] W. A. Crossland, I. D. Springle and A. B. Davey, "Liquid-crystal-modulated photoluminescent displays (PLLCDs)", J. of the SID 6/2, pp 117-124, 1998.
- [122] S. L. Njo, R. V. Asselt, D. J. Broer, and C. M. R. de Witz, "Light-Efficient Liquid Crystal Displays Using Photoluminescent Color Filters", in SID Sym. Dig. Tech. Papers, vol. 31, pp 343-345, (2000).
- [123] J. Heikenfeld, S. C. Allen, and A. J. Steckl, "A Novel Fluorescent Display Using Light Wave Coupling Technology" in SID Sym. Dig. Tech. Papers, Vol. 35, pp. 470-473, (2004).
- [124] 王書任、林仁鈞，"讓LED發光的功臣—螢光粉"，科學發展，2009年3月，435期。
- [125] M. R. Krames, O. B. Shchekin, R. Mueller-Mach, G. O. Mueller, L. Zhou, G. Harbers, and M. G. Craford, "Status and Future of High-Power Light-Emitting Diodes for Solid-State Lighting", J. Display Technol., VOL. 3, NO. 2, Jun. 2007.





Publication List

Journal Papers

1. **Hsin-Tao Huang**, Chuang-Chuang Tsai, and Yi-Pai Huang, "Conformal Phosphor Coating Using Pulsed Spray to Reduce Color Deviation of White LEDs", *Opt. Express*, Vol. 18, No. 102, pp. A201-A206, 21 June 2010 (SCI, IF=3.477).
2. **Hsin-Tao Huang**, Chuang-Chuang Tsai, and Yi-Pai Huang, "Ultraviolet excitation of remote phosphor with symmetrical illumination used in dual-sided liquid-crystal display", *Opt. Lett.*, Vol. 35, No. 15, pp. 2547-2549, August 1, 2010 (SCI, IF=3.299).
3. **Hsin-Tao Huang**, Chuang-Chuang Tsai, and Yi-Pai Huang, "A Direct-View Backlight With UV Excited Trichromatic Phosphor Conversion Film", *IEEE/OSA J. Display Technol.*, VOL. 6, NO. 4, pp. 128-134, APRIL 2010 (SCI, IF=1.928).
4. **Hsin-Tao Huang**, Yi-Pai Huang, and Chuang-Chuang Tsai, "Planar Lighting Using Array of LEDs to Excite Yellow Remote Phosphor Film", *IEEE/OSA J. Display Technol.*, VOL. 7, NO. 1, pp. 44-51, JANUARY 2011 (SCI, IF=1.928).

International Conference Papers

1. (Oral, Invited Paper) Wen-Chi Chang, **Hsin-Tao Huang**, Chuang-Chuang Tsai, Yi-Pai Huang and Han-Ping D. Shieh, "Remote Phosphor for Future LED Backlight Applications", *SID Symposium Digest*, vol. 41, No.66.2, pp. 862-865, May 23-30, 2010, Seattle, WA, US (SID'10).
2. (Oral) Chung-Hao Tien, Chien-Hsiang Hung, Bo-Wen Xiao, **Hsin-Tao Huang**, Yi-Pai Huang and Chuang-Chuang Tsai, "Planar Lighting by Blue LEDs Array with Remote Phosphor", *Proc. SPIE*, Vol. 7617, 761707, 2010, San Francisco, CA, USA.
3. (Oral) **Hsin-Tao Huang**, Chuang-Chuang Tsai, and Yi-Pai Huang, "Dual-Sided Slim LCD Display System with UV Excited Flat Backlight", *SID Symposium Digest*, vol. 40, No.68.3, pp. 1030-1033, May 31- June 5, 2009, San Antonio, TX, US (SID'09).
4. (Oral) Bo-Wen Xiao, Chien-Hsiang Hung, **Hsin-Tao Huang**, Yi-Pai Huang, Chung-Hao Tien, Chuang-Chuang Tsai, Han-Ping D. Shieh, Jerry Chen, Jeremy Lin, and Wen-Chi Chang, "Optical Properties of Visible-light Excited Phosphor Sheet (VEPS) System", *SID Symposium Digest*, vol. 40, No.68.4, pp. 1034-1037, May 31- June 5, 2009, San Antonio, TX, US (SID'09).
5. (Oral) **Hsin-Tao Huang**, Chuang-Chuang Tsai, Yi-Pai Huang, Jerry Chen, Jeremy Lin, and Wen-Chi Chang, "Phosphor Conformal Coating by a Novel Spray Method for White Light-emitting Diodes as Applied to Liquid-crystal Backlight Module", *XXIX International Display Research Conference, Eurodisplay 2009*, Sep. 14th-17th, 2009, Rome, Italy (IDRC 2009).
6. (Oral) **Hsin-Tao Huang**, Chuang-Chuang Tsai, Yi-Pai Huang, Jeremy Lin and Wen-Chi Chang, "Remote Phosphor with Blue Light-emitting Diodes Array on Board as Applied to Liquid-crystal Backlight Module", *9th International Meeting on Information Display*, Oct. 12th-16th, 2009/KINTEX, Seoul, Korea (IMID 2009).

7. (Oral) **Hsin-Tao Huang**, Chuang-Chuang Tsai, Yi-Pai Huang, Jeremy Lin and Wen-Chi Chang, "Remote Phosphor with Blue Light-emitting Diodes Array on Board for a Liquid-crystal Backlight Module", 11th *Asian Symposium on Information Display*, Oct. 7th-10th, 2009, Guangzhou, China (ASID'09).
8. (Distinguished Poster Award) Bo-Wen Xiao, Chien-Hsiang Hung, **Hsin-Tao Huang**, Jerry Chen, Jeremy Lin, Wen-Chi Chang, Yi-Pai Huang, Chung-Hao Tien, Chuang-Chuang Tsai, and Han-Ping D. Shieh, "Optical Simulation and Analysis of Visible-light Excited Phosphor Sheet (VEPS) System", *International Display Manufacture Conference*, April 27-30, 2009 (IDMC'09).
9. (Oral) **Hsin-Tao Huang**, Chien-Hsiang Hung, Yi-Pai Huang, Chung-Hao Tien, Chuang-Chuang Tsai, Han-Ping D. Shieh, "UV Excited Flat Lighting (UFL) System for LCD-TV Backlight Application", *SID Symposium Digest*, vol. 39, No.57.1, pp. 862-865, May 18-23, 2008, Los Angeles, CA, US (SID'08).
10. (Oral) Bo-Wen Xiao, Chien-Hsiang Hung, **Hsin-Tao Huang**, Jerry Chen, Yi-Pai Huang, Chung-Hao Tien, Chuang-Chuang Tsai, and Han-Ping D. Shieh, "LEDs-based Flat Lighting Device for LCD Backlight Applications", *International Conference on Optics and Photonics in Taiwan*, December 4-6, 2008 (OPT'08).

US Patents

1. **Hsin-Tao Huang**, Deng-Kuen Shiau, Chun-Chi Hsu, Chun-Chung Hsiao and Mao-Wei Lin, "Display Panel and a Light Source Used therein", U.S. Pub. No. 2010/0134999, (Jun. 3, 2010).
2. Chun-Chung Hsiao, Yi-Sing Peng, Sung-Po Chen, **Hsin-Tao Huang**, "Flat Panel Display and Backlight Module Thereof", U.S. Pub. No. 2009/0231831, (Sep. 17, 2009).
3. **Hsin-Tao Huang**, Chun-Chung Hsiao, "Light Source Module with Wavelength Converting Structure and Method of forming the same", U.S. Pub. No. 2009/0194774 (Aug. 6, 2009).
4. Chun-Chung Hsiao, **Hsin-Tao Huang**, "Patterned Wavelength Converting Structure", U.S. Patent No. 7,832,885, (Nov. 16, 2010).
5. **Hsin-Tao Huang**, Chun-Chung Hsiao, "Lighting Module with Wavelength Converting Structure and Manufacturing Method for the same", U.S. Pub. No. 2009/0196015, (Aug. 6, 2009).
6. **Hsin-Tao Huang**, Chun-Chung Hsiao, "Method of Forming Light-Scattering Dots inside the Diffusion Plate and Light Guide Plate by Laser Engraving", U.S. Pub. No. 2009/0067178, (Mar. 12, 2009).
7. **Hsin-Tao Huang**, Hsiu-Mei Fang, "Display Device, A Front Frame Used therein, and a Method of Manufacture thereof", U.S. Pub. No. 2008/0266771, (Oct. 30, 2008).
8. **Hsin-Tao Huang**, Deng-Kuen Shiau, Chun-Chi Hsu, Chun-Chung Hsiao and Mao-Wei Lin, "Display Panel and a Light Source Used therein", U.S. Pub. No. 2008/0225506, (Sep. 18, 2008).
9. **Hsin-Tao Huang**, "Connecting Structure Used in a Liquid Crystal Display Panel", U.S. Patent No. 7,384,688, (Jun. 10, 2008).
10. **Hsin-Tao Huang**, Chun-Chien Chu, "Backlight Module for a Liquid Crystal Display Device", U.S. Patent No. 7,086,775, (Aug. 8, 2006).

11. **Hsin-Tao Huang**, Chun-Chien Chu, “Backlight Module of Liquid Crystal Display Device”, [U.S. Patent No. 7,207,707](#), (Apr. 24, 2007).
12. **Hsin-Tao Huang**, “Method for Inspection Defects on a Display Panel”, U.S. Pub. No. 2005/0151558, (Jul. 14 2005).

Taiwan Patents

1. **黃信道**, 蕭淳中, 陳松柏, 彭意興, 蔡秉翰, “數位電子看板/Digital Electrical Billboard”, [TW M382552](#), 2010/06/11.
2. **黃信道**, “一種液晶顯示模組/Liquid Crystal Display Module”, [TW I310856](#), 2009/06/11.
3. **黃信道**, 蕭淳中, 陳松柏, 彭意興, 蔡秉翰, “薄型液晶顯示器/Thin Liquid Crystal Display”, [TW M357817](#), 2009/05/21.
4. **黃信道**, 陳明倫, 方秀美, 廖經桓, 許博淳, 陳秋君, “背光模組結構/Backlight Module Structure”, [TW 200921209](#), 2009/05/16.
5. 張加欣, 田尻智久, **黃信道**, 蕭淳中, “背光模組及其光源結構/Backlight Module and Light Structure Using the Same”, [TW 200848864](#), 2008/12/16.
6. **黃信道**, 方秀美, “顯示裝置,其使用之顯示面板框體及其製造方法/A Display Apparatus, A Front Frame Used Therein, and A Method of Manufacture Thereof”, [TW 200843609](#), 2008/11/01.
7. **黃信道**, 蕭淳中, “使用雷射內雕之擴散板與導光板結構/Diffusion Plate and Light Guide Plate Structure Using Laser Engraving”, [TW M343817](#), 2008/11/01.
8. 蕭淳中, 彭意興, 陳松柏, **黃信道**, “可供多面顯示之平面顯示器及其背光模組/A Flat Panel Display Capable of Multi-Sided Viewings and Its Back Light Module”, [TW M341857](#), 2008/10/01.
9. **黃信道**, 蕭淳中, “具有共享之波長轉換結構之光源模組/Light Source Module with Shared Wavelength Converting Structure”, [TW M341811](#), 2008/10/01.
10. 蕭淳中, **黃信道**, “圖案化波長轉換結構/Patterned Wavelength Converting Structure”, [TW M341800](#), 2008/10/01.
11. **黃信道**, 蕭登昆, 徐俊琪, 蕭淳中, 林茂煒, “顯示面板及其使用之光源裝置/A Display Panel and A Light Source Used Therein”, [TW 200837447](#), 2008/09/16.
12. **黃信道**, 蕭淳中, “包含波長轉換結構之照明模組/Lighting Module with Wavelength Converting Structure”, [TW M338317](#), 2008/08/11.
13. **黃信道**, “層狀結構之導電膠材/Conductive Material with A Laminated Structure”, [TW I299502](#), 2008/08/01.
14. **黃信道**, “顯示面板缺陷的檢測方法/Method for Inspecting Defects on A Display Panel”, [TW I281079](#), 2007/05/11.
15. **黃信道**, 朱俊傑, “液晶顯示裝置用之背光模組/Back Light Module of Liquid Crystal Display”, [TW I257511](#), 2006/07/01.
16. **黃信道**, 朱俊傑, “背光模組/Back-Light Module”, [TW I226494](#), 2005/01/11.

Awards

2009/04/27 Distinguished Poster Award in *International Display Manufacture Conference*, (IDMC'09), Taipei, Taiwan.

2010/05/23 Invited Paper in 48th *SID International Symposium*, Seattle, Washington, USA

2010/10/29 國立交通大學 99 年度秋季師生榮獲重要學術獎表揚

2010/12/11 Technology Research Scholarship of *CTCI Foundation* (財團法人中技社九十九年度科技研究獎)



Curriculum Vitae

Personal Information

Name: Hsin-tao Huang

Birthday day: 06/09/1969

Addr.: Chupei City, Hsinchu County, Taiwan

TEL: 0928-551232

E-mail: stevenhuang.eo96g@nctu.edu.tw

Education

JUL./2007-JAN./2011 Received Ph.D. degree in the *Institute of Electro-Optical Engineering at National Chiao Tung University*, Hsinchu, Taiwan.

JUL./1994-JUL./1996 Received MS degree in the *Department of Materials Science and Engineering at National Cheng Kung University*, Tainan, Taiwan.

JUL./1988-JUL./1991 Graduated in the *Department of Materials Engineering at National Taipei University of Technology*, Taipei, Taiwan.

Experience

JUL./2007-JAN./2011 He joined *KISmart Corporation* as Sr. manager in CTO Office and dedicated to technology mining regarding the integration of color, optics, material, & mechanical engineering in both of "Flat Display" & "LED Lighting" field. He achieved the development of low color deviation LED devices using conformal phosphor coating (CPC) by pulsed-spray method and high luminous efficiency light engine using remote phosphor coating (RPC). Moreover, he achieved the public information display system using dual-sided UV-excited fluorescent lighting (UFL) scheme.

FEB./2000-JUL./2007 He joined *Quanda Display Inc. (QDI)* at the very beginning stage and served as Sr. manager to involve in the complete TFT-LCD products cycle of Notebook, monitor and TV display. He experienced the department of process engineering, product engineering, project management and product development in this period. In Feb. 2006, QDI merged into *AU Optronics Corp. (AUO)*, he was appointed by the head of AUO to join the technology center and lead a project to study the new optical system & integrated optical materials.

JUL./1996-FAB./2000 He enrolled in *Electronics Research & Service Organization (ERSO), Industrial Technology Research Institute (ITRI)* as researcher. He joined the TFT-LCD

display team to develop chip on glass (COG) bonding, flip chip bonding, and tape carrier package (TCP) schemes using material of anisotropic conductive adhesive (ACF). In middle 1998, he joined the IC package team to develop advanced wafer level package and chip scale package (CSP) scheme.

